The Pennsylvania State University

The Graduate School

Eberly College of Science

UNDERSTANDING THE BIOCHEMISTRY AND PHYSIOLOGY OF GAMMA CARBONIC ANHYDRASES IN *METHANOSARCINA THERMOPHILA*

A Thesis in

Biochemistry, Microbiology, and Molecular Biology

by

Sabrina Anastasia Zimmerman

Submitted in Partial Fulfillment
of the Requirements
for the Degree of

Doctor of Philosophy
August 2007

The thesis of Sabrina Anastasia Zimmerman was reviewed and approved* by the following:

James G. Ferry
Stanley Person Professor and Director, Center for Microbial Structural Biology
Thesis Advisor
Chair of Committee

Sarah Ades
Assistant Professor of Biochemistry and Molecular Biology

J. Martin Bollinger, Jr.
Associate Professor of Biochemistry and Molecular Biology
Associate Professor of Chemistry

Squire Booker
Associate Professor of Biochemistry and Molecular Biology

Juliette Lecomte
Associate Professor of Chemistry

Ming Tien
Professor of Biochemistry

Robert A. Schlegel
Professor of Biochemistry and Molecular Biology
Head of the Department of Biochemistry, Microbiology and Molecular Biology

*Signatures are on file in the Graduate School

ABSTRACT

To date, there are five independently evolved classes (α-, β-, γ-, δ-, and ζ-) of carbonic anhydrases (CAs) participating in many physiological functions. Although the γ-class is widely distributed, only one CA (Cam from a methanoarchaeon *Methanosarcina thermophila*) has been characterized while no physiological function has yet been documented. The work presented in this thesis contributes to the general understanding of the biochemistry of CAs by kinetically investigating Cam, the prototypic γ-class CA. In these studies, Cam was shown to utilize a hydrogen bond network analogously to the hydrogen bond network described for the α- and β-class CAs that involves Cam active site residues Gln75 and Asn73. In addition, Cam residue Asn202 may orient and polarize the incoming carbon dioxide molecule much like the backbone amide of α-class residue Thr199. Therefore, the α-, β-, and γ-class CA, Cam, each independently evolved variations of a fundamental functions that are essential for catalysis. This thesis also presents the initial characterization of the newly identified second γ-class isozyme, CamH, thus significantly increasing the understanding of the γ-class. CamH possesses several properties significantly different from Cam. Contrary to Cam, CamH does not possess a signal peptide, suggesting CamH is cytosolic whereas Cam is located at the membrane. Preliminary kinetic analyses reveal the rate of CO_2 hydration in CamH ($k_{cat}/K_m = 10^4\ M^{-1}s^{-1}$) is two-fold lower than observed in Cam ($k_{cat}/K_m = 10^6\ M^{-1}s^{-1}$). Despite the kinetic differences, both CamH and Cam are up-regulated during aceticlastic methanogenesis. Therefore, a model was proposed based on this information outlining roles for Cam and CamH in acetate uptake in *Methanosarcina* species.

TABLE OF CONTENTS

LIST OF FIGURES

LIST OF TABLES

LIST OF ABBREVIATIONS

CA	Carbonic Anhydrase
HCAII	Human Carbonic Anhydrase isozyme II
Cam	Carbonic Anhydrase from *Methanosarcina thermophila*
CDCA	Cd-Containing Carbonic Anhydrase
Zn	Zinc
Cd	Cadmium
TWCA1	*Thalassiosira weissflogii* Carbonic Anhydrase 1
DIC	Dissolved Inorganic Carbon
RuBisCO	Ribulose-1,5-bisphosphate carboxylase/oxygenase
EXAFS	Extended X-ray Absorption Fine Structure
PSR	Proton Shuttle Residue
Co	Cobalt
CA-RP(s)	Carbonic Anhydrase-Related Protein(s)
CamH	Cam Homolog
PVDF	polyvinylidene difluoride
SEC	Size Exclusion Chromatography
PEP	Phosphoenolpyruvate
HAC	Acetate
TMA	Trimethylamine
MetOH	Methanol

ACKNOWLEDGEMENTS

Most importantly I thank Dr. Ferry, my thesis advisor, for his unwavering confidence in me and my potential. Dr. Ferry always presented the opportunities that allowed personal and professional growth. My experience in Dr. Ferry's laboratory here at Pennsylvania State University, has strengthened my fascination with science and refueled my passion to contribute to science both as a mentor and as a student. I thank the remainder members of my thesis committee (Drs. Sarah Ades, Martin J. Bollinger, Jr., Squire Booker, Juliette Lecomte, and Ming Tien) for their commitment to the betterment of my thesis and the BMMB department. I would also like to thank my family, in particular my mother, Charlotte, and late aunt, Patricia, who encouraged me to dream beyond my means and do. I thank my father, Harry, who encouraged me both to work harder, but to enjoy life when I could. Ultimately, this accomplishment was the culmination of love given by my family and my close friends, supporting me through the maniac process that is science. Thank You.

Chapter 1

The Biochemistry, Physiology, and Phylogeny of Carbonic Anhydrases

1.1 Introduction to Carbonic Anhydrases

The reversible hydration of carbon dioxide to bicarbonate (Eq. **1**) facilitates many diverse biological functions [1, 2] which are catalyzed by an unrelated family of metalloenzymes termed carbonic anhydrases (CA), present in all three domains of life [3-5].

$$CO_2 + H_2O \rightleftarrows HCO_3^- + H^+ \qquad \text{(Equation } \mathbf{1}\text{)}$$

At present, there are five identified CA classes (α-, β-, γ-, δ-, ζ-) possessing no sequence homology among them [3-12], indicative of independent evolution. In addition, crystal structures for three CA classes (α-, β- and γ-) reveal no structural homology (Figure 1) [13-15]. An organism can possess one to several CAs belonging to one or many CA classes in which each CA carries out distinct physiological or pathological functions.

The five classes can be divided into eukaryotic and prokaryotic CAs. The eukaryotic CAs generally include the α-class and several members of the "plant-type" β-class CAs. The α-class are monomeric zinc enzymes found mostly in mammals with few examples in the *Bacteria* domain [1, 13, 16-22]. The "plant-type" β-class CAs are also zinc enzymes that range from dimers to octamers [7, 8, 23-29]. The prokaryotic CAs incorporate the bacterial members of the "plant-type" β-class, the remaining two β-

subclasses ("cab-type" and "carboxysome"), and the γ-, δ-, and ζ- classes. The "cab-type" β-subclass is distributed in the *Bacteria* and *Archaea* domains [4, 30]. However, the "carboxysome" β-subclass, formerly annotated as ε-class,[24, 31] seems unique to bacterial carboxysomes. Both sub-classes exist as a dimer of dimers; however, in the "carboxysome" CAs, only one dimer possesses a CA active site while the corresponding site in the adjacent dimer remains inactive. Putative γ-class CAs, based on sequence homology, have been identified in the Bacteria and Archaea domains; however, only the γ-class prototypic CA (Cam), isolated from the methanoarchaeon *Methanosarcina thermophila*, has been extensively characterized [6, 15, 32-36]. Cam is a trimeric iron metalloenzyme *in vivo*, although it retains robust activity with cobalt and zinc *in vitro* [32, 34]. Little is known about the newly discovered δ- and ζ-classes of CAs. Prototypes of both classes were isolated from marine diatoms [37, 38]. The δ-class CA is a zinc enzyme while the ζ-class contains cadmium [10, 38-41].

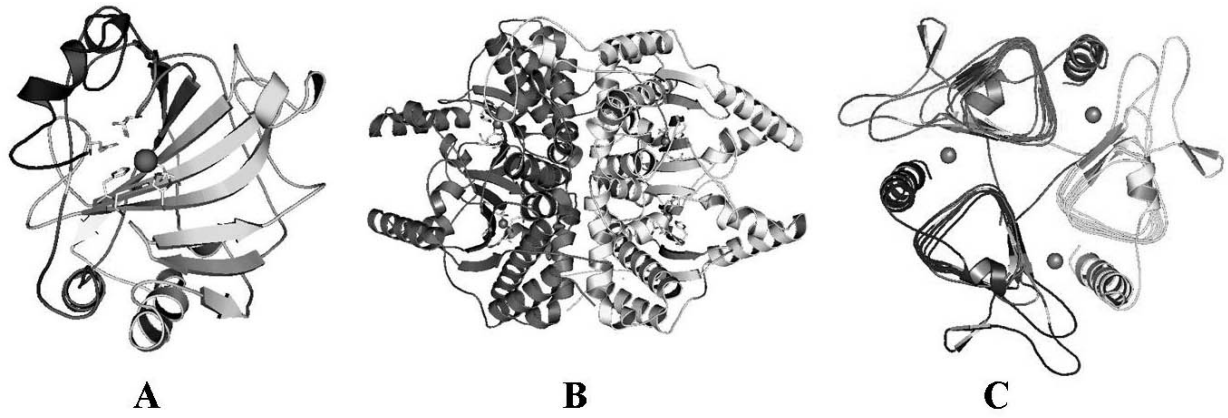

Figure 1: Representative crystal structures from α-, β-.and γ-class CAs.

A) α-class carbonic anhydrase from human erythrocytes, HCAII (1CA2), is monomeric with a single active site containing a zinc metal. B) β-class carbonic anhydrase from chloroplasts from *Porphyridium purpureum* (1DDZ) is an octamer with eight active sites, each containing a zinc metal. Represented here is a dimer of dimers for simplicity. C) The prototypic γ-class carbonic anhydrase, Cam, (1THJ) from *Methanosarcina thermophila* is trimeric with three active sites that contain iron *in vivo.* Displayed using OpenSource Pymol version 0.97 2004.

1.2 General Catalytic Mechanism

Although independently evolved, kinetic analyses reveal that three characterized CA classes (α-, β- and γ-) share the same two-step ping-pong mechanism (Eq. **1.2- 1.5**) [7, 18, 23, 25, 27, 32, 35, 42-52]. Each step is kinetically distinct; the first step (Eq. **1.2** and Eq. **1.3**), CO_2 hydration, is described by the kinetic parameter k_{cat}/K_m, whereas the second step (Eq. **1.4** and Eq. **1.5**), proton transfer, is reflected by k_{cat} [3, 43, 47, 48, 53]. During CO_2 hydration, the CO_2 molecule associates with a hydrophobic region adjacent to the active site of the α- and β- CAs [14, 45, 48, 54-57]. No defined CO_2 binding site has been characterized in the prototypic γ-class CA (Cam). Current data support that two

Cam active site residues transiently tether CO_2 in the active site at the onset of catalysis [36, 58]. Regardless, once CO_2 enters the active site, the lone pair electrons of the metal-bound hydroxide nucleophically attack the incoming CO_2 molecule (Eq. **1.2**). The now metal-bound HCO_3^- undergoes various intermediates including a bidentate bound HCO_3^- which is eventually displaced from the metal by an incoming water molecule (Eq. **1.3**).

$$E\text{–}M^{2+}\text{–}OH^- + CO_2 \rightleftarrows E\text{–}M^{2+}\text{–}HCO_3^- \quad \text{(Equation } \mathbf{1.2}\text{)}$$

$$E\text{–}M^{2+}\text{–}HCO_3^- + H_2O \rightleftarrows E\text{–}M^{2+}\text{–}H_2O + HCO_3^- \quad \text{(Equation } \mathbf{1.3}\text{)}$$

$$E\text{–}M^{2+}\text{–}H_2O \rightleftarrows H^+\text{–}E\text{–}M^{2+}\text{–}OH^- \quad \text{(Equation } \mathbf{1.4}\text{)}$$

$$H^+\text{–}E\text{–}M^{2+}\text{–}OH^- + B \rightleftarrows E\text{–}M^{2+}\text{–}OH^- + BH^+ \quad \text{(Equation } \mathbf{1.5}\text{)}$$

The second catalytic step regenerates the metal-bound hydroxide *via* a proton transfer event consisting of an intramolecular (Eq. **1.4**) and intermolecular component (Eq. **1.5**) [47, 48]. During proton transfer, a proton is extracted from the metal-bound water (Eq. **1.4**) by a residue, with a pK_a ~ 7, in the active site (intramolecular). Initially, it was unclear if the proton was transferred from this amino acid directly to water or to an intermediary, like a buffer molecule. Calculations [3] determined the fastest that an ionizable group possessing a pK_a = ~7 can transfer a proton directly to water is approximately 10^3 s^{-1}. However, many CAs exhibit turnover rates approaching 10^6 s^{-1}, suggesting, at least in these CAs, the proton is transferred directly to a buffer molecule [47]. Solvent hydrogen isotope effects were observed during chemical equilibrium [51]

experiments in the with α-class CA, HCAII (k_{cat} ~10^6 s^{-1}) confirming that an proton was transferred from the zinc bound water or a neighboring active site residue directly to a buffer molecule (Eq. **1.5**). It was also determined that in buffer limiting conditions transfer of the proton from the active site moiety to the buffer, referred as intermolecular proton transfer, is rate-limiting [19]. However, when buffer is in excess, the transfer of the proton from the zinc bound water to the active site moiety, termed intramolecular proton transfer (Eq. **1.4**), becomes rate-limiting [51, 59]. Further, the intramolecular proton transfer step is rate-limiting for CAs exhibiting a k_{cat}/K_m greater than 10^4 $M^{-1}s^{-1}$. Thus, these "fast" CAs require a designated active site residue, known as a proton shuttle residue (PSR), to extract and shuttle the proton out to buffer [35, 51, 59].

Catalytically essential residues involved in both catalytic steps have been characterized in the α-, β-, and γ-class CAs (Eq. **1.2**- **1.5**). In the well-characterized α-class CAs, a hydrogen bond network constructed by residues Glu106 and Thr199, and the metal-bound hydroxide plays an essential role in CO_2 hydration [60-65]. This hydrogen bond network optimally positions the lone pair electrons and further lowers the pK_a of the metal-bound hydroxide [46, 62, 64]. In addition, the backbone amide of Thr199 hydrogen bonds and stabilizes the various intermediates of HCO_3^- and aids in product removal [46, 62].

No analogous hydrogen bond network has been characterized in the β-class. However, a strictly conserved aspartate is proposed to hydrogen bond to an equally conserved arginine that may function to orient the metal-bound hydroxide for catalysis [4, 66], much like α-class residues Thr199 and Glu106. In addition, recent kinetic

studies of site-directed variants of the well-conserved glutamine in "plant-type" β-class CAs, Gln151 in *Pisum sativum* and Gln158 in *Arabidopsis thaliana* [50], suggest this glutamine hydrogen bonds with HCO_3^- to stabilize transition states and aid in HCO_3^- removal, similarly to the backbone amide of α-class residue Thr199 [25, 50]. No corresponding functional residue has been characterized in the "cab-type" β-class CA although His23 in Cab has been postulated [4, 52].

Interestingly, a hydrogen bond network, analogous to the α-class hydrogen bond network, has been characterized in the prototypic γ-class CA, Cam [36, 64]. The γ-class hydrogen bond network involving conserved residues Gln75 and Asn73 orients and increases the nucleophilicity of the metal-bound hydroxide. Evidence also suggests that a third Cam active site residue, Asn202, stabilizes the HCO_3^- transition states, much like the backbone amide of Thr199 and the "plant-type" β-class glutamine [36]. In all proposed putative γ-class CA homologs [4, 5, 67, 68] Gln75 and Asn73 are strictly conserved. The majority of these homologs also possess Asn202.

These characterized α-, β-and γ-class CAs exhibit catalytic efficiencies (k_{cat}/K_m) greater than 10^4 $M^{-1}s^{-1}$; thus a proton shuttle residue (PSR) has been characterized that extracts a proton from metal-bound water and shuttles it to buffer. In α-class CA, HCAII, residue His64 was identified by NMR [51] to possess a side chain could sustain proton transfer [42]. Site-directed mutagenesis to replace His64 with an alanine had drastic effects on the kinetic parameter, k_{cat}, while the substitution had minimal effects on k_{cat}/K_m [42]. The Ala64 variant could be rescued to near wildtype k_{cat} values when assayed in the presence of a strong exogenous proton acceptor, 1, 2-dimethylimidazole

[42, 47, 51, 69, 70], further supporting the role of His64 in proton transfer. In β-class CAs, there is evidence that strictly conserved aspartate may play a role in proton transfer [23, 66]; however, the details of proton transfer still remain unclear. The essential PSR is Glu84 in γ-class CA, Cam [35], characterized in a fashion similar to His64 in HCAII. Therefore, although structurally diverse, the active site architecture provides certain conserved catalytic functions for active site residues in the convergently evolved α-, β-, and γ- classes.

To date, only qualitative measurements have been used to assay CA activity in the prototypic members of the newly discovered δ- and ζ-class with the exception of a ^{18}O exchange experiment conducted on whole cell preparations of the marine diatom, *Thalassiosira weissflogii* [10-12, 38, 40, 41]. Both the δ- and ζ- class can be expressed simultaneously under certain conditions [10]. Therefore, the kinetic parameters determined from this study cannot be assigned to either class. Until rigorous kinetic or structural investigations are conducted there can be no speculation as to which residues are catalytically involved. Based on existent data from the α-, β-, and γ-class CAs, catalytically relevant residues most likely are present in the δ- and ζ-class CAs that may function in a hydrogen bond network to orient and lower the pK_a of the metal bound hydroxide, and aid in product removal. Also if these prototypes are "fast" CAs, a PSR may be present to aid in regeneration of the catalytic moiety.

1.3 α-Class Carbonic Anhydrases

Prior to 1933, two main theories existed explaining the details of CO_2 transport in blood [1, 2]. According to the bicarbonate theory, CO_2 travels in the form of HCO_3^- in blood from the muscle to the lungs where blood protein(s) dehydrate the HCO_3^- into CO_2 which then is expired from the lungs. The second theory, or direct combination theory, hypothesized that the CO_2 becomes reversibly bound to blood protein(s), possibly a heme-protein, and then carried to the lungs and released upon arrival. Evidence existed supporting both theories. In 1933, Stadie et al. [2] and Meldrum et al. [1] simultaneously discovered a non-heme-protein present in large quantities in muscle and red blood cells responsible for reversible CO_2 hydration, and named it carbonic anhydrase [1, 71].

CA activity was observed in two distinct ways. Meldrum et al. monitored CA activity via the "boat" technique. The "boat" is a two chamber sealed glass boat in which one chamber contains CA in phosphate buffer while the second chamber contains $NaHCO_3$. The submerged "boat" equilibrates in a temperature controlled water bath. Upon equilibration, the contents of the chambers were mixed and the evolution of CO_2 was monitored via an attached manometer [1]. Alternatively, the Stadie laboratory monitored the pH change via an pH electrode upon addition of solubilized CO_2 to a solution containing the crudely purified blood CA as solubilized CO_2 was hydrated to HCO_3^- and H^+ [2]. It was later determined by Zn precipitation by sodium quinaldinate and mercury thiocyanate from pure CA preparations that CA was a Zn metalloenzyme [72].

It was discovered three decades later that the CA characterized from erythrocytes in the 1930s was, in fact, two co-purified isozymes, isozymes B and C, which were later renamed to CAI and CAII, respectively [53] (Table **1.1**). To date, there are 16 identified mammalian isozymes, four plant α-class CAs and three bacterial α-class CAs. The current identified isozymes are generally separated into two groups, eukaryotic and prokaryotic (Table **1.1**). The eukaryotic group can be further separated into isozymes that are cytosolic, transmembrane, and mitochondrial. Table **1.1** summarizes the distribution and function (in some cases proposed) of existing α-class CAs. The α-class CAs are wide spread in eukaryotes and modestly represented in prokaryotes; however, no known α-class isozyme has been identified in the Archaea domain.

Table **1.1**: Distribution and function of identified α-class isozymes.

Information was combined from [3, 16, 17, 21, 22, 53, 73-78]

Distribution	Isozyme	Tissue Location	Cellular Location	Function
Mammals				
	CA1	blood, spleen, placenta, colon lymph node infant brain	cytosolic	respiration, ion transport
	CA2	brain, spleen, kidney, heart, placenta, multiple sclerosis, bone, retina, uterus tumor, colon tumor	cytosolic	respiration, bone development, acid/base regulation, vision, pyrimidine synthesis
	CA3	skeletal muscle, kidney, lung, mammary gland, alveolar rabdomyosarcoma, liver	cytosolic	anti-oxidant, CO_2 diffusion
	CA4	kidney, heart, macrophage, colon tumor, fetal heart	membrane bound	bone development, vision, bile production
	CA5A	liver, spleen, mitochondria	cytosolic	gluconeogenesis, ureogenesis
	CA5B	mitochondria, brain	cytosolic	fatty acid synthesis, ureogenesis, insulin secretion
	CA6	Saliva, skin	secreted	pH homeostasis
	CA7	brain, liver, lung,		
	CA-RP 8	tumors, embryo, colon, lung liver, mammary gland	Cytosolic (interface of tumor progression)	tumorgenesis, cerebellar degeneration
	CA-RP 9	testis, brain tumor, myotubes	transmembrane	tumorgenesis, development
	CA-RP 10	brain, embryo, eye, testis, lymph node	transmembrane	development
	CA-RP 11	brain, neuroepithelim, sarcoma, tonsil, pregnant uterus, B cells	***a***	tumorgenesis, development
	CA12	colon, ovarian cancer, pancreas, kidney, colon tumor, colon mucosa	transmembrane	tumorgenesis, ureogenesis,
	CA13	myotubes, melanoma	***a***	***a***
	CA14	Liver spleen, retina, muscle heart, prostate, mammary gland, kidney, embryo, brain, lung, melanocytes	transmembrane	signal transduction, *tumor suppressor*
	car 15	kidney	putative transmembrane	***a***
Plants				
Dioscorea cayenensis,	CAH (Discorin)	tuber	***a***	anti-oxidiant
C. reinhardii, A. thaliana, Oryza sativa	CAH1	chloroplast	periplasmic	photosynthesis
C. reinhardii, A. thaliana	CAH2	chloroplast	***a***	***a***
C. reinhardii	CAH3	chloroplast thylakoid	membrane associated	photosynthesis
Eubacteria				
Helicobacter pylori	CAH		*extracellular*	*pH homeostasis*
Salmonella typhimurium	CAH		*extracellular*	***a***
Neisseria gonorrhoeae	ORF2		*extracellular*	CO_2 acquisition

a Information was either not known or unclear.

1.3.0.1 Carbonic Anhydrase-Related Proteins (CA-RPs)

CA activity varies among the α-class isozymes. However, mammalian isozymes, CAVIII, CAIX (formerly MN), CAX, and CAXI exhibit no or slight CA activity. Sequence and structural comparisons of these isozymes with HCAII, the most CA active α-class isozyme, revealed overall conserved structure with regard to active α-class CAs; however, key differences exist in the active sites, especially with respect to catalytically essential residues [53]. As a result, these α-class isozymes have been termed Carbonic Anhydrase-Related Proteins, or CA-RPs, and thus renamed CA-RPVIII, CA-RPIX, etc. Hypothetically CA-RPs (CAH-RPs) have been identified in *Caenorhabditis elegans*, yam *Dioscorium cayenesis*, extracellular regions of receptor protein tyrosine phosphotases β and γ (RTPβ and γ), as well as in several pox viruses [21] based on the sequence homology to aforementioned characterized CA-RPs. Commonly, many CA-RPs possess amino acid substitutions or lack one or more of the three histidines essential for Zn binding, and thus for efficient CA activity [20].

Recently CA-RPs VIII, IX, X, and XI was found to be expressed in neuronal cells [17] and associated with carcinomas [17, 78, 79]. To date, evidence suggests CA-RPs do not appear to function as CAs *in vivo*; however, these isozymes seem to provide essential biological functions [17, 78, 79]. In tumors, it seems CA-RPs play a role in hypoxia and tumorgenesis [17, 78, 79]. CA-RPs has been shown to be widely distributed during organogenesis in mice embryonic development [77, 80]. Partial gene deletion of CA-RP VIII in mice resulted in a developmental deformity and in a "waddle" phenotype [76].

Sequences of acatalytic CA-RPs maintain a prominent invariability amongst those identified [53]. These isozymes may have evolved new functions that require retention of structure but allow for the loss of CA activity. It has been suggested that CA-RPs may act as transcription factors or activators. Thus, much is not understood about how these CA-RPs evolved or the selective pressures that deemed CA activity superfluous.

1.3.1 General Overview of the α-Class Protein Structure

Structural investigations of solved crystal structures, including a bacterial example [81], reveal an overall conserved structure amongst α-class isozymes (Figure **1.2**). All characterized α-class CAs are shown to be monomeric ranging from 22-34 kDa molecular mass. The structure is dominated by a central 10 stranded β-sheet with three α-helices, which can vary in length. However, the β-sheet is largely conserved and divides the enzyme into two sections [3, 53]. The upper section contains the active site and the N-terminal region of the protein while the bottom section is largely hydrophobic (Figure **1.2)**. As per convention, all numbering of the amino acids in the isozymes refers to the amino acid number of HCAI [82]. The active site is roughly cone-shaped, being ~15Å wide and ~15Å deep situated in the upper portion of the enzyme [13, 42, 48, 54, 69, 81, 83-86]. The Zn ion is located at the bottom of this conical cavity positioned in the middle of the β-sheet. Three histidine residues (His94, His96, His119) and a water coordinate the Zn ion tetrahedrally [3, 53], with the exception of CA-RPs. The Zn is further stabilized by indirect ligands, Gln92, Asn244, and Glu117, that

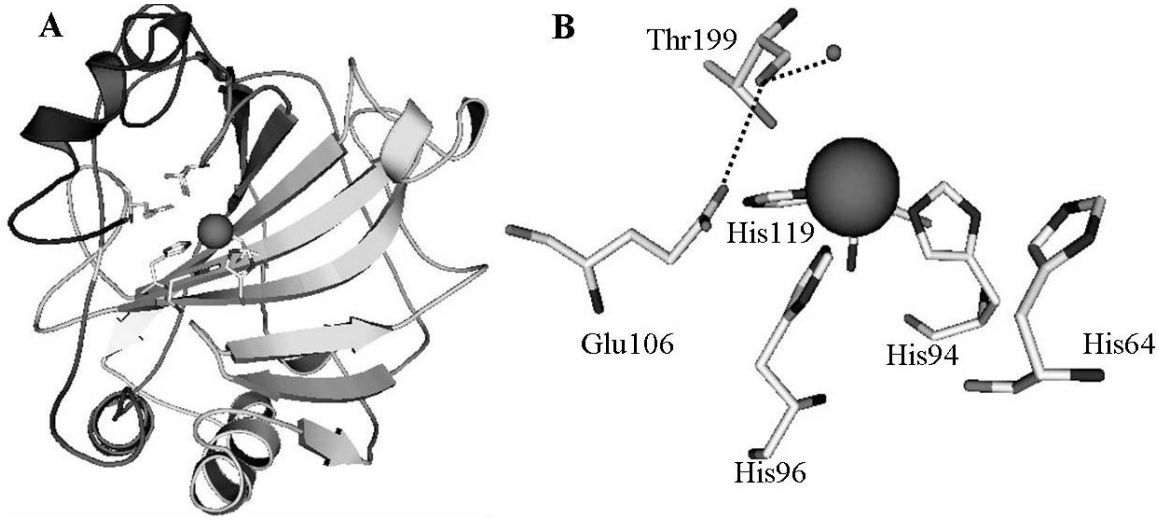

Figure 1.2**: Representative overall structure and active site of the α-class isozymes**.

A) Ribbon diagram of α-class CA overall structure including the conserved active site residues. B) The α-class active site depicting conserved metal ligands (His94, His96, His119) and catalytic essential residues Thr199 and Glu106, as well as PSR His64 shown in the "in" position. The dotted lines represent hydrogen bonds. The large sphere represents the Zn ion whereas the small sphere represents the metal chelating water. Crystal representation are displayed using OpenSource Pymol version 0.97 2004.

hydrogen bond to the primary chelating histidines, His94, His96, and His119, respectively [87]. Data suggest that these indirect ligands play a role in the affinity and selectivity of Zn in the α-class CAs [87, 88]. Thr199, shown to be essential in CO_2 hydration, hydrogen bonds with the Zn-bound hydroxide to orient the catalytic moiety as well as lower the pK_a of the attacking group [46, 60-62, 70, 89, 90].

This strictly conserved residue is found on a loop containing residues 197-206 that connects strand 7 to strand 8 in the central β-sheet [53]. Also this loop contains Thr200, which has been postulated to aid in proton transfer [42, 51, 65]; however, this residue is not conserved amongst the isozymes [53, 67].

The hydrophobic pocket adjacent to the Zn, in the lower portion, is also conserved. Evidence suggests this area may be the substrate binding site [53, 91] which functions to enhance CO_2 reactivity by desolvating the substrate and direct the now, activated CO_2 towards the Zn-bound hydroxide [64, 92]. Some variability occurs amongst the isozymes at residue 131, which is located on an α-helix that traverses this pocket. The residue residing at position 131 determines how this α-helix is positioned relative to the Zn [53, 54]. Position 131 also is the main determinant of what conformation this region assumes. For example, substitution of a valine for a tyrosine at 131 influences whether this region is an α-helix or an extended loop.

The proton shuttle residue, commonly at position 64 in α-class isozymes, influences the turnover rate for the isozymes. For those "fast" α-class CAs, His64 acts as a PSR relaying a proton from the active site via intervening waters to buffer [42, 86]. The efficiency of proton transfer and, therefore, the high turnover rate, is attributed to the ability of His64 to swing towards the active site to receive the extracted proton, then move away from the active site to relay the proton to a buffer molecule [42, 43, 48, 63, 69, 93, 94]. Residue 65 plays a small but crucial role in proton transfer [93]. Proton transfer differs amongst the isozymes due to steric interference by residue 65. For example, in isozyme CAV, a Phe65 impedes proton transfer from His64 due to its bulky functional group [74]. Isozyme CAIII exhibits a drastically diminished k_{cat} (10^3 s^{-1}) compared to that of HCAII (10^6 s^{-1}) primarily due to Leu64 and lack of any other suitable PSR [94]. The k_{cat} of CAIII can be rescued to HCAII values by substituting a histidine for the leucine [75].

1.4 β-Class Carbonic Anhydrases

CA activity was first observed in chloroplasts in three leaf species [95]. Initially, CAs were prevalent in higher plants, mostly associated with the chloroplasts in both C_3 and C_4 plants and mesophyll cells in C_4 plants [53]. It has been proposed that CAs maintain a supply of CO_2 in C_3 and C_4 plants for use by RuBisCO (Ribulose-1,5-bisphosphate carboxylase/oxygenase) in chloroplasts and aid in providing HCO_3^- for Phosphoenolpyruvate (PEP) carboxylase. Sequence comparison of these isolated plant CAs compared to α-class CAs' sequences revealed these plant CAs represented a distinct CA class termed the β-class [53]. At first, it was thought that the α-class CAs only occurred in mammals and the newly identified β-class was solely comprised of plant species; however, β-class CAs later were identified in *Bacteria* and *Archaea* [8, 30, 52]. Distinct structural differences in the active site architecture among characterized β-class CA lead to the β-class being further separated into three sub-classes: plant-type, cab-type, and carboxysome.

Originally represented by plant CAs, the "plant-type" incorporates those β-class CAs where the fourth ligand chelating the active site Zn is the strictly conserved aspartate in addition to the primary metal ligands (Cys-His-Cys motif) represented universally in all β-class CAs. The "plant-type" sub-class is currently represented by CAs from *Pisum sativum*, *Arabidopsis thaliana, Escherichia coli*, *Haemophilus influenzae*, *Mycobacterium tuberculosis* and *Porphyridium purpureum* [7, 8, 14, 23, 29]. These CAs are pH dependent, showing increasing CA activity as the pH increases. The conserved

aspartate may only coordinate to the metal at the neutral pH in which these proteins were crystallized and thus, be considered an artifact [8, 56].

The β-class CA, Cab, isolated from the thermophilic methanogen, *Methanobacterium thermoautotrophicum,* is the founding member of the "cab-type" sub-class [30, 52, 66]. The fourth Zn-ligand is a water molecule, not the conserved aspartate as in the "plant-type" sub-class [7, 27, 28, 52, 96]. Other representatives of the "cab-type" sub-class include CAs from *Spinacea oleracea*, *Chlamydomonas reinhardtii*, *A. thaliana*, and an acatalytic CA from *M. tuberculosis*.

Initially classified as the prototypic and sole member of the ε-class, the CA, CsoCA, was isolated from a cellular organelle called the carboxysome from *Halothiobacillus neaepolitanus* [31]. Later, in lieu of substantial structural similarities with the β-class, CsoCA was reclassified as the prototypic member of the third β-sub-class termed "carboxysome" [24]. This sub-class, like the "cab-type" also adopts a water molecule as the fourth ligand to the Zn ion. CsoCA is a dimer; however, this sub-class differs from the other sub-classes in that there is only one catalytic active site, while the other remains dormant [24]. This dormant active site lacks a metal ligand, a cysteine, and therefore does not bind Zn. The complete loss of the second active site does not appear to offer any obvious advantage. Possibly, this defunct active site may be a coincidental evolutionary consequence as a result of domain rearrangement to allow CsoCA to associate with other proteins. This has not been investigated and remains speculation. No other member has been identified to belong to this sub-class as of yet.

1.4.1 General Overview of β-Class Active Sites

Only seven β-class CAs have been crystallized to date [7, 8, 14, 24, 28, 29, 56] (Figure **1.3**). The β-class CAs range from homodimers to homooctamers with a dimer as the basic unit of oligomerization. In general, the overall structure is similar amongst the three sub-class of β-CAs. The monomers of the sub-classes are generally comprised of an conserved α/β fold described by a central parallel β-sheet bordered by four to five major α-helices [4, 7, 8, 14, 24, 27, 28, 55, 56, 66]. Each monomer contains one functional active site with the exception of the carboxysome class [24, 31]. The Zn ion is coordinated by two cysteines and a histidine; however, the fourth zinc ligand varies between the subclasses in crystal structures. Also conserved in all three subclasses are two active site residues, arginine and aspartate (Figure **1.3**) [4, 7, 8, 14, 24, 27, 28, 55, 56, 66]. It is postulated that the strictly conserved aspartate may act as the PSR in β-class CAs [25, 27, 59, 66]. It is unclear how the arginine is involved in catalysis; however, substitution of the arginine with an alanine results in a drastic loss in k_{cat} and k_{cat}/K_m, supporting an essential catalytic role [8, 23, 25, 27, 66]. The active site differences among the three sub-classes may allude to differences in catalytic mechanism between the three β-class sub-classes or may have evolved to better perform designated physiological functions.

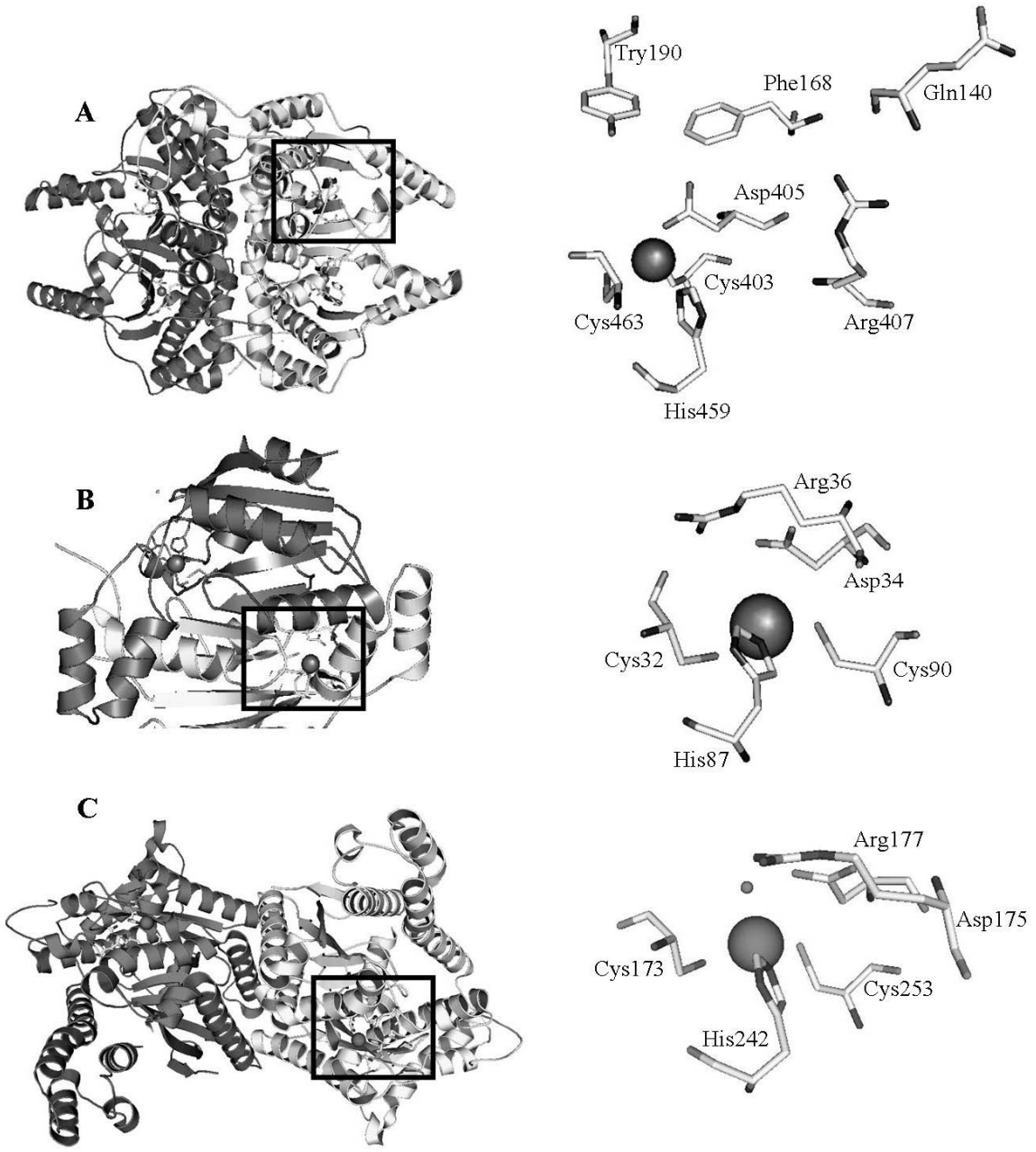

Figure 1.3**: A representative from each β-subclass showing the overall structure as well as the active sites.**

A) "Plant-Type" β-CA *Porphyridium purpureum* tetramer. The active site includes strictly conserved "plant-type" glutamine, tyrosine, and phenylalanine in addition to the aspartate and arginine. B) "Cab-Type" β-CA, Cab, from *Methanobacterium thermoautotrophicum*. C) "Carboxysome-Type" β-CA, CsoSCA, from *Halothiobacillus neapolitanus.* Displayed using OpenSource Pymol version 0.97 2004.

Existing "plant-type" CAs are tetramers with the exception of *P. sativum* CA, which exists as an octamer [14, 56]. The fourth ligand in the "plant-type" β-class CAs is the conserved active site aspartate (Figure **1.3**) [8, 55, 56]. The "plant-type" subclass active site possesses three additional active site residues, a glutamine, a phenylalanine, and a tyrosine [8, 14, 55, 56] that are strictly conserved among the "plant-type" CAs but absent in the "cab-type" and "carboxysome" subclasses (Figure **1.3**). Only the glutamine in *P. sativum* and *A. thaliana* has been shown to be involved in catalysis [50]. These three residues construct a small hydrophilic channel [14] large enough for a water molecule to enter the narrow active site suggesting the "plant-type" active site may rearrange to accommodate the transition states and product release [14]. Recently, an allosteric HCO_3^- binding site has been shown in the bacterial CAs from *E. coli* and *H. influenzae* [29]. The acatalytic site is 8 Å from the Zn ion located perpendicular to the central β-sheet. At least in these "plant-type" β-class CAs, HCO_3^- may regulate activity in *in vivo*.

In the "cab-type" and "carboxysome" subclasses, the fourth ligand is a water molecule (Figure **1.3**) [7, 15, 24, 30]. The "cab-type" includes tetramer and dimer representatives [7, 27, 28] whereas the sole characterized member of the "carboxysome" sub-class is a dimer with only one functional active site [24, 31]. Due to the lack of the conserved glutamine, tyrosine, and phenylalanine residues found in the "plant-type" CAs, the active sites of both the "cab-type" and "carboxysome" sub-classes appear less narrow and more elastic [7, 15, 24]. Structural investigations utilizing inhibitors have not been conducted with the "cab-type" and "carboxysome" CAs. This limits the

understanding of how the active site architecture aids in these CAs performance of their respective physiological functions.

1.5 γ-Class Carbonic Anhydrases

Methanogens are able to produce methane via three main pathways (Table **2**); the reduction of the methyl group either from methanol or methylated amines, reduction of carbon dioxide, and acetate fermentation [97]. The only genera capable of acetoclastic methanogenesis are *Methanosarcina* and *Methanosaeta* (formly *Methanotrix*) [98]. In addition, some members of the *Methanosarcina* spp. can produce methane from all of the three main methanogenesis pathways [97] unlike methanogens from other methane-producing genera. During acetoclastic methanogenesis, CH_3COO^- is transported into the cell by an unknown process [97] where the carbon-carbon bond is cleaved, resulting in a methyl (CH_3) group and a carboxylate (COO^-). The COO^- group is oxidized to CO_2, releasing two electrons. The electrons then reduce the CH_3 group to CH_4, the end product. Compared to the other pathways of methanogenesis, acetoclastic methanogenesis is not as energetically favorable (Table **1.2**). Although methanogens utilizing acetate have an increased doubling time compared to other carbon sources, growth remains vigorous. It is not well understood what processes allow robust growth on acetate; however, mechanistic investigations of acetate metabolism in acetate-grown *Methanosarcina barkeri* implicate the presence of CA may remove CO_2, avoiding accumulation of by-products, and thus driving the overall reaction [99].

Table **1**. **2**: Three main methanogenic reactions.

$CH_3COO^- + H^+ \rightarrow CH_4 + CO_2$	$\Delta G^{o`} =$ **-36 kJ/mol CH_4**
$4\ CH_3OH \rightarrow 3\ CH_4 + CO_2 + 2\ H_2O$	$\Delta G^{o`} =$ **-106 kJ/mol CH_4**
$4\ H_2 + CO_2 \rightarrow CH_4 + 2\ H_2O$	$\Delta G^{o`} =$ **-131 kJ/mol CH_4**

CA activity was first observed in the crude lysate of the metabolically diverse methanogen *Methanosarcina barkeri* [99] during acetate-growth. Monitoring CA activity via the electrometric method, Karrasch et al. [99] determined that CA activity was dependent on the presence of acetate. *M. barkeri* cultures grown on methanol or CO_2/H_2 possessed no CA activity. However, once these cultures were transferred to acetate media, CA activity was induced, strongly suggesting CA played a role in acetate metabolism. Growth ceased when the CA specific inhibitor, dansylamide, was added to *M. barkeri* acetate-grown cultures, implicating the CA plays a crucial role in acetoclastic methanogenesis. CA activity was also shown to be independent of pH and CO_2 concentrations, dismissing the hypothesis that the CA functioned in pH homeostasis or acquisition of CO_2 [99]. In addition, inhibition profiles of CA activity utilizing a membrane permeable CA inhibitor, cyanide, and semi-membrane permeable CA-specific inhibitor, acetozolamide, localized the CA in *M. barkeri* to the cytoplasm possibly associated with the membrane [99]. Therefore, it was concluded that *M. barkeri* CA functions to remove CO_2 waste and/or facilitate cellular entry of acetate.

1.5.1 The prototypic γ-Class CA, Cam

As observed with *M. barkeri*, CA activity was induced upon the metabolic switch from methanol to acetate in *M. thermophila* [6, 100]. Alber et al. originally purified this CA, termed Cam (Carbonic Anhydrase from *Methanosarcina thermophila*), from acetate-grown *M. thermophila* cultures; they also cloned and sequenced the encoding gene [6]. Cam represents the prototypic member of the newly identified γ-class because the lack of structural and sequential homology of Cam to α- and β-class CAs [6, 15, 33, 58]. Cam possesses a 34 amino acid N-terminal signal peptide characteristic of a secretory protein, suggesting that Cam is directed to the membrane. Preliminary electron microscopy data also localized Cam to the membrane; however, the sidedness has not been determined (unpublished results from Birgit Alber). Cam is a homotrimer, approximately 74 kDa with a novel left-handed β-helical fold (Figure **1.4**). Cam maintains three active sites at the interfaces between subunits. Over-expression of heterologous Cam under various metal concentration and competition experiments [34] provide strong evidence that Cam is an iron enzyme *in vivo*. Cam, however, retains robust activity with both Zn and Co *in vitro* [32, 35]. The metal is chelated by three histidines, two histidines (His81 and His121) provided by one subunit with the third (His117) provided by the adjacent subunit [15, 58]. Crystal structures of the Zn- substituted and Co-substituted Cam have been solved. In Zn-Cam , in addition to the metal ligands, the metal is chelated by two waters; one water is the catalytic water whilst the other is a coordinating water [15, 58]. Co-Cam has a third ligating water in addition to the metal ligands and those waters observed in Zn-Cam (Figure **1.4**). Although no crystal structure has been solved for Fe-Cam, it has

been postulated that Fe-Cam exhibits similar geometry as Co-Cam. Therefore, it is presumed that the Fe ion is ligated by three metal ligands and three waters.

Kinetic characterization of Cam substantiates a two-step ping-pong mechanism [32] (Eq. **1.2- 1.5**). A pH profile of k_{cat}/K_m indicates that two ionizable groups are involved in CO_2 hydration [32]. One pK_a (~6.8) is assigned to the catalytic metal bound water. Water bound to a metal in the absence of enzyme has a pK_a of ~9.0 [89]. Therefore, in addition to the metal, active site residue(s) in the near vicinity of the metal bound water further perturb the pK_a of the catalytic water increasing its nucleophilcity, most likely via a hydrogen bond network as first described in α-class CAs. Gln75, strictly conserved in all putative γ-class homologs, was confirmed to be the primary player in a hydrogen bond network in Cam via kinetic analyses of Gln75 variants [36]. Further, pH profiles of Gln75 variants showed a loss of the ~6.8 pK_a or a marked increase indistinct from the second pK_a at ~8.3 [36]. It was concluded that Cam utilized a hydrogen bond network comprised of Gln75 and Asn73 that orients and perturbs the pK_a of the catalytic metal bound hydroxide. It is unknown what group(s) is responsible for the second pK_a (~8.3). Recently, it has been proposed that the second pK_a (~8.3) represents the coordinating water that is hydrogen bonded to active site residue Glu62. Cam crystal structures [15, 58] and kinetic analyses of Glu62 variants [35] indicate Glu62 participates in the CO_2 hydration step, although details are unclear.

Proton transfer, described by k_{cat}, is dependent on one ionizable group (~6.3) [32] referred to as the PSR. Cam possesses an acidic loop originating 6 Å from the metal bound water and extending out into buffer [15, 35]. Kinetic analyses of variants of the series of glutamates (Glu62, Glu84, Glu88, Glu89) located on this loop revealed Glu84 to

be the primary PSR. An alanine variant of residue 84 showed a drastic decrease in k_{cat} whereas k_{cat}/K_m remained relatively unaffected [35]. In addition, a conservative substitution of a histidine for Glu84 results in a loss of the pK_a ~6.3, supporting of Glu84 being the responsible group for an ionization at this pK_a [15, 35].

Structural analyses of Cam (see section **1.5.1.1**) also identified active site residue Asn202 [15, 58] as possibly relevant to catalysis. Little to no CA activity was observed for Asn202 variants, suggesting Asn202 plays a key catalytic role. Asn202 is proposed to hydrogen bond with the metal bound HCO_3^-, thus stabilizing the transition state [36, 58]; however, what role Asn202 plays is unknown [36].

1.5.1.1 Structural Characteristics of Cam

Both Co-and Zn-reconstituted Cam crystal structures have been solved. These represent the only structural examples of the γ-class [15, 58]. Both structures show that Cam is a trimer. Each monomer is comprised of seven complete turns of a left-handed parallel β-helix[15] with two α-helices. A short α-helix caps each monomer; this helix may aid to avoid aggregation of this overall hydrophobic protein [15]. A second C-terminal α-helix forms anti-parallel to the β-helix [15, 101], interacting with the active site (Figure **1.4**). A cross-section of each monomer reveals an equilateral triangle, much like a Toblerone chocolate bar [15, 58, 101], in which the interior is hydrophobic. Upon trimerization, roughly 25% of each monomer is hidden [15]. The trimer is stabilized by hydrophobic interactions, salt bridges and hydrogen bonds. Arg59

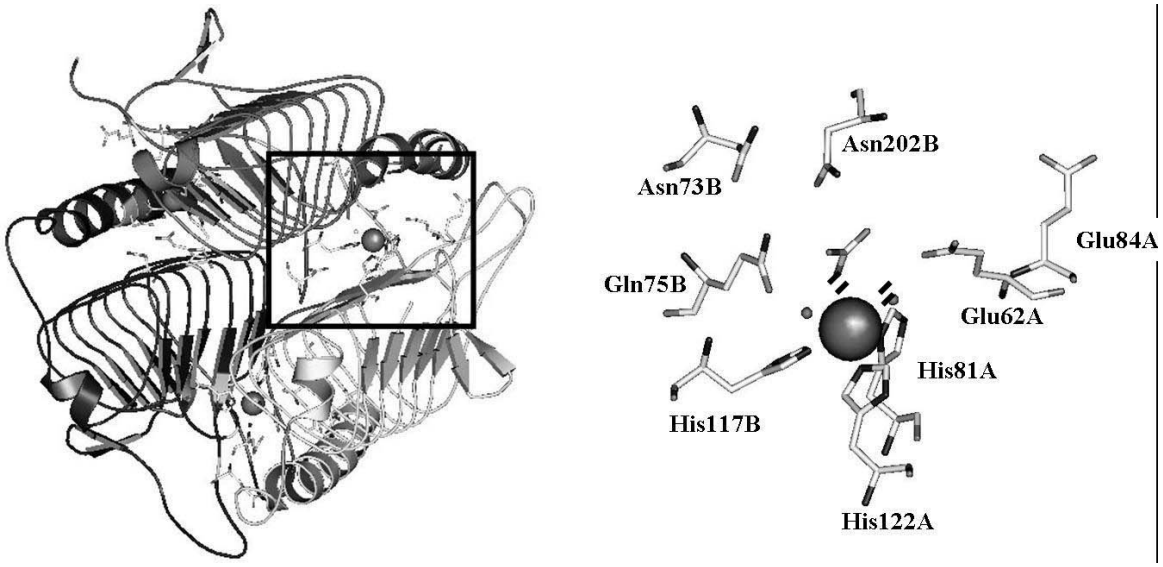

Figure 1.4**: Overall structure of the prototypic γ-class CA, Cam.**

Letters "A" and "B" refer to the contributing monomer. The dashed lines refer to those waters that are comparable in both Zn- and Co-Cam. The large sphere refers to the metal whereas the small sphere refers to coordinating waters. The active site is shown complexed with a bicarbonate molecule chelated to the metal at the position where the catalytic water otherwise would reside. Displayed using OpenSource Pymol version 0.97 2004.

was shown to play a key role in trimerization and stabilization of the holoenzyme [102]. A salt bridge exists between Arg59 and Asp61 on the same monomer. In addition, Arg59 forms a separate salt bridge with Asp76 on the adjacent monomer [15, 101, 102]. Removal of the positive charge at position 59 abolishes these salt bridges leading to increased aggregation and instability of the trimer at high and low temperatures [102]. These residues are strictly conserved amongst all putative γ-class homologs [4, 5, 67, 68].

The active site occurs at the interface between two monomers, with each monomer contributing residues to the active site architecture (Figure **1.4**). The Zn is pentacoordinate with a trigonal bipyramidal geometry, whereas the Co metal is hexacoordinate with a octahedral geometry [58]. Both metals are ligated by three

histidines, two from one monomer (His81 and His121) and the third histidine (His117) from the adjacent monomer (Figure **1.4**). Zn is further ligated by two waters; one catalytic water and one coordinating water [58], whereas the Co in Co-Cam is ligated with three water molecules, one catalytic water and two coordinating waters [58]. A crystal structure has not been solved for Fe-Cam, although EXAFS data are consistent with the Fe being hexacoordinate, suggesting a similar geometry as the Co-Cam [34]. The orientation of the catalytic water in Co-Cam is slightly different than that of the catalytic water in the Zn-Cam, however, both catalytic waters are within hydrogen bonding distance to the catalytic essential residues Gln75 and Asn202 (Figure **1.4**) [58].

No apparent CO_2 binding site was observed in the crystal structures. It is speculated that the hydrophobic patch composed of aromatic residues Leu83, Met135, Phe138, Phe140, Ile157, Val172 and Phe132 may be involved [58]. In an alternative scenario, the incoming CO_2 may be tethered by hydrogen bonds to Gln75 and Asn202 [36]. No data exists for either hypothesis and thus, the details of CO_2 binding remain speculative.

1.5.2 Putative γ-Class Homologs

Initial alignments of putative γ-class homologs with the prototypic Cam sequence are based on structural similarities [4, 5, 33, 67, 68]. A sequence is considered a putative homolog if it includes a heptapeptide repeat, characteristic of the left-hand β-helix, and the three metal ligands His81, His117 and His121. Based on these criteria, putative γ-class CA homologs appeared to be distributed throughout all three domains of life. The

most promising γ-class CA candidates were the putative homologs from *Synechococcus* (CcmM), *E. coli* (CaiE and YrdA) , *Pseudomonas aeruginosa* (Fbp), *Coxiella brunette* (Cox), and several candidates in *A. thaliana* (At1γCA1, At1γCA2, At5γCA3, At5gCAL1, At3γCAL2) [67, 68]. Current alignments [68] require putative homologs to contain additional structurally important residues Arg59, Asp61, and Asp76 or equivalent substitutions. Previously assigned homologs, CcmM, CaiE, YrdA, Fbp, Cox, At1γCA1, At1γCA2, At5γCA3, At5gCAL1, and At3γCAL2 were retained within this alignment as well as an additional putative γ-class homolog from the methanogen *Methanococcus jannaschi* (Y304).

Additionally, these sequences also possess Gln75 and Asn73 with the exception of CcmM which replaces Asn73 with an isoleucine [67, 68]. Only one of these homologs, *M. jannaschi* Y304, possesses the additional Cam catalytic relevant residues, Asn202, Glu62, and Glu84 [68]. In the remaining homologs, no neighboring residues at these positions appear able to substitute for Asn202 and/or Glu62; however, without crystal structures, this remains speculation. The presence or lack of these conserved catalytic residues could delineate which putative γ-class homologs possess CA activity, and, therefore, are true CAs, from those sequences that are not active CAs and may be γ-class CA-RPs. However, the importance of these residues in catalysis may be unique to the γ-class CAs of methanogens and not general characteristics of the γ-class. The more γ-class CAs identified and characterized, the more information will be available to determine what traits are distinctive for γ-class CA. Any differences between confirmed γ-class CAs may be related to that CA's physiological role.

1.5.2.1 γ-Class-Like Proteins

Several previously identified γ-class homologs from *A. thaliana* [67, 68] have been heterologously expressed and purified. Sequence investigations reveal these putative homologs, Atγ1CA1, Atγ1CA2 and Atγ5CA3, are lacking residues Asn202, Glu62 and Glu84 shown to be key in catalysis in the prototypic γ-class CA, Cam [103]. Structural models of At1γCA1 show the His ligands, Arg59, Asp76, and Gln75 are well conserved. Although, the model suggests residues Tyr207, and Asp88, also conserved in At1γCA2 and At5γCA3, may replace Cam residues Asn202 and Glu62, respectively [103]. Recombinant proteins of these three homologs exhibit no CA activity when assayed under a variety of conditions [103-105]. Lack of observable activity may be due to inefficient assay conditions or lack of catalytically relevant residues. If the latter, these homologs may represent γ-class CA-RPs.

Unlike other identified putative γ-class CAs [67, 68], a newly identified putative γ-class CA discovered in the marine alga, *Emiliania huxleyi* [106] lacks conserved residues Gln75, Asn202, Glu62 and metal ligands His81, His117, and His122. This homolog, γ-EhCA2, was heterologously expressed, purified, and shown to exhibit CA activity [107]. However, γ-EhCA2 only shares 15% sequence homology with the prototypic γ-class Cam. Based on the amino acid sequence, γ-EhCA2 does possess the conserved overall β-helix structure and structural relevant residues Arg59, Asp61, and Asp76 [107]. Soto et al. discuss that the lack of homology with Cam may reflect

characteristics that are unique to the eukaryotic γ-class CAs [107]. Alternatively, γ-EhCA2 may represent a new class of CAs or a sub-class of the γ-class CAs.

1.6 δ-Class Carbonic Anhydrase

Phytoplankton, such as diatoms, efficiently sequester the inorganic carbon in aquatic environments utilizing C_3 biochemistry [108], which requires CO_2 as the substrate for RuBisCO during photosynthesis. However, the majority of dissolved inorganic carbon (DIC) in marine environments exists as HCO_3^- [109]. Diatoms either convert HCO_3^- extracellularly via an external CA or directly uptake HCO_3^- via a specific transporter, then converting it to CO_2 with an internal CA [109, 110]. Morel et al. observed increased intracellular CA activity when cultures of the marine diatom, *Thalassiosira weissflogii*, were grown under a low partial pressure of CO_2 [11]. Phosphorimaging of cellular lysate of cultures grown in the presence of ^{65}Zn confirmed the majority of cellular Zn was associated with CA activity. Growth under limiting ^{65}Zn concentrations drastically lowered CA activity [11]. This CA, termed TWCA1 [12], was cloned using cDNA and heterologously expressed.

Sequence comparisons of TWCA1 with α-, β-, and γ-class CAs sequences revealed no sequence homology, thus establishing a new CA class, the δ-class [12, 39, 41]. The *twca1* cDNA encodes a 34 kDa protein that is processed *in vivo* to a 27 kDa CA active protein [12]. Though the 72 amino acid region upstream of the cleavage site shares few properties characteristic of a chloroplast signal peptide, it is thought this region directs the mature TWCA1 protein to the chloroplast [12]. There is strong

evidence that Zn is the physiological metal for TWCA1 [11]; however, Co has been shown to associate with TWCA1 when Zn is absent [41]. To date, only qualitative CA activity has been reported for this enzyme [11, 12, 41]. TWCA1 has yet to be kinetically characterized.

1.6.1 The δ-class CA Active Site

TWCA1 is thought to occur as a dimer, but little data exist to lend further insight into the overall structure and oligomerization of TWCA1. The active site, however, has been investigated [37]. Comparing the EXAFS data with those of bovine α-class CA and spinach β-class CA indicated that the TWCA1 active site resembles more closely that of the α-class. The best EXAFS curve fit supports a zinc ion coordinated by three histidines and an oxygen, most likely contributed by a bound water. In TWCA1, the geometry of the Zn seems to be similar with the metal in α-class CA determined by Zn K near-edge spectra comparisons [37]. Further structural analysis of TWCA1 may reveal more similarities between not only the α-class CAs and CAs in general.

1.7 ζ-Class Carbonic Anhydrases

Because of exceptionally nutrient limiting conditions, the open sea is the most extreme environment on Earth [111]. The distribution of many biologically relevant metals, such as zinc (Zn), is comparable to that of major nutrients, phosphate, nitrate and silicate, distributed throughout the water column [10]. Previously thought to be toxic to

organisms, cadmium (Cd) concentrations have also correlated well with phosphate distribution [112, 113]. Biochemically, Cd has been used to characterize the active site environment of metalloenzymes due to Cd spectroscopic properties [3]. When TWCA1 is substituted with Cd, the δ-class CA exhibits decreased CA activity relative to wild-type TWCA1 [39, 41]. Interestingly, the addition of Cd to growth medium enhances growth of the marine diatom, *T. weissflogii* [39]. These findings coupled with Cd distribution in the ocean prompted scientists to ask whether Cd played any biological role in the marine environment either as a surrogate metal for Zn-CAs when Zn is limiting, or in a Cd-specific CA [10].

Initial investigation of cellular lysate from *T. weissflogii*, using native PAGE and an in-gel CA assay, revealed that two distinct active CA bands are present [10, 40, 113]. Cultures of *T. weissflogii* were then grown in the presence of labeled ^{65}Zn or ^{109}Cd [10]. Cellular lysate from each respective radio-labeled culture was separated on a native-PAGE gel. Phosphorimaging and the in-gel CA assay determined that the high molecular weight CA active band contained ^{109}Cd while the lower molecular weight band contained ^{65}Zn. The ^{65}Zn band was assigned to the intracellular δ-class CA, TWCA1. The ^{109}Cd band represented the now prototypic member of the ζ-class, CDCA1. This is the first example of a physiologically relevant biological role for Cd in Nature [38, 40]. Further, CDCA1 expression increased under Zn and CO_2 limiting conditions supports the hypothesis that CDCA1 may function to concentrate CO_2 during photosynthesis, *T. weissflogii* when Zn becomes limiting in the environment [113]. The ability to acquire inorganic carbon in Zn-limited environments, like the ocean, may have given diatoms the competitive advantages needed to become the primary producers they are today [114].

1.7.1 The ζ-Class CA Active Site

To date, no crystal structure has been solved for any ζ-class CA. However, EXFAS data of CDCA1, when compared to standards, describe a metal apparently tetrahedrally coordinated by two or more thiolates [10, 38, 40, 115]. The spectra are consistent with the metal being ligated in a Cys-His-Cys motif, much like the β-class CAs, with a water molecule acting as the fourth ligand. In fact, sequence alignments of CDCA homologs and "plant-type"β-class CAs not only reveal a common metal ligation motif, but show the strictly conserved β-class residues, arginine and aspartate, are also well-conserved in CDCA-like sequences. This perceived active site homology between the independent evolved classes may speak to the physiological function these CAs provide in their host organism. Data exist supporting a role concentrating CO_2 for some "plant-type" β-class and the prototypic ζ-class CAs for the large photosynthetic enzyme complex, RuBisCO [10, 23, 25, 38, 114]. Therefore, the active site architecture represented by "plant-type" and CDCA and CDCA-like CAs may be better adapted to interact with RuBisCO. This is an example amongst the five independently evolved CA classes where some catalytic functions are conserved despite the lack of sequence homology.

1.7.2 ζ-Class Homologs and Distribution

Although CDCA1 is the only characterized member of the ζ-class, a putative homolog was identified in *T. pseudomonana*. Little differences exist between the

nucleotide sequence of *T. weissflogii* CDCA1 and this putative *T. pseudomonana* homolog. In *T. weissflogii*, *cdca1* encodes a three repeat gene, bearing an overall 85% identity to each other which transcribes into a ~69kDa monopeptide [114]. Conversely, the ortholog in *T. pseudomonana* exists as a single repeat [114] encoding a putative protein ~26kDa which corresponds to a single repeat of the *T. weissflogii* CDCA1 [38, 40]. Therefore, it is possible that one repeat is sufficient for an active Cd-CA.

Potential *cdca* genes were identified by nested PCR using degenerate primers designed from the *T. weissflogii* and *T. pseudomonana* sequences [114]. Pure cultures of a variety of marine diatoms and marine environmental isolates were investigated. Several *cdca*-like sequences were found to exist in a wide range of diatoms, green algae, and a coccolithophore. Two of the diatoms (*Thalassiosira oceania* and *Phaeodactylum tricornutum*) identified to possess *cdca*-like sequence experienced enhanced growth in the presence of Cd. However, no *cdca*-like sequences were detected in other phytoplankton species, most likely due to the bias inherent in the degenerate primers.

Phylogenetic analysis of these *cdca*-like sequences from pure cultures generated a distance tree comprised of three groups. The Tw group clustered the majority of the *Thalassiosira* spp. genes. The remainder of the *Thalassiosira* sequences including that of *T. oceania* and *T. pseudomonana* were grouped in the Tp clade. The remainder of the diatom sequences group to form the Np clade. It is noteworthy that the *cdca*-like sequences did not separate according to the morphological differences in the diatoms, i.e. pennate *vs*. centric diatoms. Ultimately, there is strong evidence supporting a novel biological role for Cd in Nature, as well as the wide-spread distribution of the ζ-class CAs.

1.8 A Comparative Approach to Understanding Carbonic Anhydrases

Since the discovery of the α-class (CA) [1, 2] the majority of CA research has been primarily conducted with α-class isozymes from mammalian tissue. Until recently, CAs were not considered to be wide spread in prokaryotes except in those phototrophic microorganisms that experience CO_2 limiting conditions. It is now known CAs are ubiquitous in nature, providing a wide range of physiological functions. The insights gained investigating the biochemistry and physiology of the mammalian α-class CAs has significantly contributed to research stratagem development conducted on the more recently discovered CA classes. This is best exemplified in experiments conducted with eukaryotic marine organisms [116].

Current structural, biochemical, and physiological information of all CAs reveals there are striking similarities amongst the independently evolved classes. Hydrogen bond networks that prime the metal for catalysis have been characterized in three of the five classes. Fast CAs, those with turnover rates greater than 10^4 s^{-1}, require a PSR within 8Å of the Zn ion with the capability of alternate conformations. Most remarkable is the discovery that the drastically variable active sites of the α-, β- and γ-class CAs, when overlaid, reveal the metal ligands and those residues involved in the hydrogen bond network superimpose, demonstrating a conservation of the general architecture. This comparative experimental approach to CA research has been key to begin to understand how CAs, reinvented five times, appear to differ superficially but actually have great underlying similarities.

Using this comparative approach, this thesis biochemically investigates the prototypic member of the γ-class (Cam from a methane-producing *Methanosarcina* species). Although the γ-class is widely distributed in prokaryotes, only one CA has been kinetically characterized and no physiological function has been confirmed for any γ-class CAs. The overarching goal of this thesis is to increase the understanding of the general characteristics of γ-class CA and those unique to archaeal γ-class CA. In addition, this thesis presents data on the initial biochemical characterization of the CA active γ-class isozyme, CamH, also found in *Methanosarcina* species. CamH portrays properties significantly different from Cam, lending a valuable comparative approach towards understanding the biochemistry and physiology of the γ-class. Also included is an initial investigation, using biochemical and genetic approaches, of the physiological function of Cam during acetoclastic methanogenesis in *M. acetivorans*. Ultimately, this research contributes to the biochemical and physiological understanding of the γ-class and, in general, all CA classes.

1.9 References

1. Meldrum, N.N. and F.J.W. Roughton, *Carbonic anhydrase. Its preparation and properties.* Journal of Physiology, 1933. **80**: p. 113-141.
2. Stadie, W.C. and H. O'Brien, *The Catalysis of the Hydration of Carbon Dioxide and Dehydration of Carbonic Acid by an Enzyme Isolated from Red Blood Cells.* Journal of Biological Chemistry, 1933. **103**(2): p. 521-529.

3. Dodgson, S., et al., *The Carbonic Anhydrases*. 1991, New York: Plenum Press. 379.

4. Smith, K.S., et al., *Carbonic anhydrases is an ancient enzyme widespread in prokaryotes.* Proceedings of the National Academy of Sciences, 1999. **96**(26): p. 15184-15189.

5. Tripp, B., K. Smith, and J.G. Ferry, *Carbonic anhydrase: New insights for an ancient enzyme.* The Journal of Biological Chemistry, 2001. **276**(52): p. 48615-48618.

6. Alber, B.E. and J.G. Ferry, *A carbonic anhydrase from the archaeon Methanosarcina thermophila.* Proceedings of the National Academy of Sciences, 1994. **91**(15): p. 6909-6913.

7. Covarrubias, A.S., et al., *Structure and function of carbonic anhydrase from Mycobacterium tuberculosis.* The Journal of Biological Chemistry, 2005. **280**(19): p. 18782-18789.

8. Cronk, J., et al., *Crystal structure of E. coli beta-carbonic anhydrase, an enzyme with an unusual pH-dependent activity.* Protein Science, 2001. **5**: p. 911-22.

9. Elleby, B., et al., *Characterization of carbonic anhydrase from Neisseria gonorrhoeaea.* European Journal of Biochemistry, 2001. **268**: p. 1613-1619.

10. Lane, T.W. and F.M.M. Morel, *A biological function for cadmium in marine diatoms.* Proceedings of the National Academy of Sciences, 2000. **97**(9): p. 4627-4631.

11. Morel, F.M.M., et al., *Zinc an carbon co-limitation of marine phytoplankton.* Nature, 1994. **369**: p. 740-741.

12. Roberts, S.B., T.W. Lane, and F.M.M. Morel, *Carbonic Anhydrase in the Marine Diatom Thalassiosira weissflogii (Bacillariophyceae).* Journal of Phycology, 1997. **33**: p. 845-850.

13. Saito, R., et al., *Structure of bovine carbonic anhydrase II at 1.95 angstrom resolution.* Acta crystallographica. Section D, Biological crystallography, 2004. **60**: p. 792-795.

14. Kimber, M. and E. Pai, *The active site architecture of Pisum sativum β-carbonic anhydrase is a mirror image of that of α-carbonic anhydrases.* The EMBO Journal, 2000. **19**(7): p. 14-7-1418.

15. Kisker, C., et al., *A left-handed beta-helix revealed by the crystal structure of a carbonic anhydrase from the archaeon Methanosarcina thermophila.* EMBO Journal, 1996. **15**(10): p. 2323-2330.

16. Marcus, E.A., et al., *The periplasmic alpha-carbonic anhydrase activity of Helicobacter pylori is essential for acid acclimation.* Journal of Bacteriology, 2005. **187**(2): p. 729-738.

17. Nishimori, I., et al., *Expression of carbonic anhydrase-related protein VIII, X, XI in the enteric autonomic nervous system.* Biomedical Research, 2003. **14**: p. 70-74.

18. Ren, X. and S. Lindskog, *Kinetics And Mechanism Of Cobalt-Substituted Bovine Muscle Carbonic Anhydrase.* European Journal of Biochemistry, 1987. **106**(6-7): p. 430-430.

19. Ren, X.L. and S. Lindskog, *Buffer Dependence Of CO_2 Hydration Catalyzed By Human Carbonic Anhydrase I.* Biochimica et biophysica acta, 1992. **1120**(1): p. 81-86.

20. Sly, W.S. and H. Py, *Human carbonic anhydrases and carbonic anhydrase deficiences.* Annual Review of Biochemistry, 1995. **64**: p. 375-401.

21. Tashian, R.F., et al., *Carbonic anhydrase (CA)-related proteins (CA-RPs), and transmembrane proteins with CA or CA-RP domains.* EXS, 2000. **90**: p. 105-20.

22. Chirica, L., et al., *The complete sequence, expression in Escherichia coli, purification and some properties of carbonic anhydrase from Neisseria gonorrhoeae.* European Journal of Biochemistry, 1997. **244**: p. 755-760.

23. Johansson, I. and C. Forsman, *Kinetic studies of pea carbonic anhydrase.* European Journal of Biochemistry, 1993. **218**: p. 439-446.

24. Sawaya, M., et al., *The Structure of β-carbonic anhydrase from the carboxysomal shell reveals a distinct subclass with one active site for the price of two.* Journal of Biological Chemistry, 2006. **281**(11): p. 7546-7555.

25. Rowlett, R.S., et al., *Kinetic characterization of wild-type and proton transfer-impaired variants of beta-carbonic anhydrase from Arabidopsis thaliana.* Arch Biochem Biophys, 2002. **404**(2): p. 197-209.

26. Mitra, M., et al., *Identification of a New Chloroplast Carbonic Anhydrase in Chlamydomonas reinhardtii.* Plant Physiology, 2004. **135**: p. 173-182.

27. Rowlett, R.S., et al., *Kinetic And Structural Characterization Of Spinach Carbonic Anhydrase.* Biochemistry, 1994. **33**(47): p. 13967-13976.

28. Strop P, et al., *Crystal structure of the "cab"-type beta class carbonic anhydrase from the archaeon Methanobacterium thermoautotrophicum.* Journal of Biological Chemistry, 2001. **27 6**(13): p. 10299-305.

29. Cronk, J., et al., *Identification of a Novel Noncatalytic bicarbonate binding site in eubacterial β-Carbonic Anhydrase.* Biochemistry, 2006. **45**: p. 4531-4361.

30. Smith, K.S. and J.G. Ferry, *A Plant-Type (β-Class) Carbonic Anhydrase in the Thermophilic Methanoarchaeon Methanobacterium thermoautotrophicum.* Journal of Bacteriology, 1999. **181**(20): p. 6247-6253.

31. So, A.K.C., et al., *A novel evolutionary lineage of carbonic anhydrase (epsilon class) is a component of the carboxysome shell.* Journal of Bacteriology, 2004. **186**(3): p. 623-630.

32. Alber, B.E., et al., *Kinetic and spectroscopic characterization of the γ-class carbonic anhydrase from the methanoarchaeon Methanosarcina thermophila.* Biochemistry, 1999. **38**(40): p. 13119-13128.

33. Alber, B.E. and J. G. Ferry, *Characterization of heterologously produced carbonic anhydrase from Methanosarcina thermophila.* Journal of Bacteriology, 1996. **178**(11): p. 3270-3274.

34. Tripp, B.C., et al., *A role for Iron in an Ancient Carbonic Anhydrase.* Journal of Biological Chemistry, 2004. **279**(8): p. 6683-6687.

35. Tripp, B.C. and J.G. Ferry, *A structure-function study of a proton transport pathway in the gamma-class carbonic anhydrase from Methanosarcina thermophila.* Biochemistry, 2000. **39**(31): p. 9232-9240.

36. Zimmerman, S.A. and J.G. Ferry, *Proposal for a Hydrogen Bond Network in the Active Site of the Prototypic Gamma-Class Carbonic Anhydrase.* Biochemistry, 2006. **45**(16): p. 5149-57.

37. Cox, E.H., et al., *The active site structure of Thalassiosira weissflogii carbonic anhydrase 1.* Biochemistry, 2000. **39**(40): p. 12128-12130.

38. Lane, T.W., et al., *Isolation and Characterization of a Cadmium Carbonic Anhydrase from a Marine Diatom.* Nature, 2005. **42**.

39. Price, N.M. and F.M.M. Morel, *Cadmium and cobalt substitution for zinc in marine diatom.* Nature, 1990. **344**: p. 658-660.

40. Lane, T., et al., *Biochemistry: A cadmium enzyme from a marine diatom.* Nature, 2005. **435**(5 May 2005): p. 42.

41. Lane, T.W. and F.M.M. Morel, *Regulation of carbonic anhydrase expression by zinc, cobalt, and carbon dioxide in the marine diatom Thalassiosira weissflogii.* Plant Physiology, 2000. **123**(1): p. 345-352.

42. Fisher, Z., et al., *Structural and kinetic characterization of active-site histidine as a proton shuttle in catalysis by human carbonic anhydrase II.* Biochemistry, 2005. **44**(4): p. 1097-105.

43. Khalifah, R.G., *The carbon dioxide hydration activity of carbonic anhydrase I. Stop-flow kinetic studies on the native human isoenzymes B and C.* Journal of Biological Chemistry, 1971. **246**(8): p. 2561-2573.

44. Kogut, K.A. and R.S. Rowlett, *A Comparison Of The Mechanism Of Action Of Native And Co^{2+}-Substituted Carbonic Anhydrase-II.* Journal of Biological Chemistry, 1987. **194**: p. 17-BIOL.

45. Krebs JF, et al., *Kinetic and spectroscopic studies of hydrophilic amino acid substitutions in the hydrophobic pocket of human carbonic anhydrase II.* Biochemistry, 1993. **32**(17): p. 4496-505.

46. Liang, Z.W., et al., *Importance of the Conserved Active-Site Residues Tyr7, Glu106 and Thr199 for the Catalytic Function of Human Carbonic Anhydrase II.* European Journal of Biochemistry, 1993. **211**(3): p. 821-827.

47. Lindskog, S. and J.E. Coleman, *The Catalytic Mechanism of Carbonic Anhydrase.* Proceedings of the National Academy of Sciences, 1973. **70**(9): p. 2505-2508.

48. Lindskog, S., *Structure and mechanism of carbonic anhydrase.* Pharmacol. Ther, 1997. **74**(1): p. 1-20.

49. Lindskog, S. and A. Liljas, *Carbonic Anhydrase and the Role of Orientation in Catalysis.* Current Opinion in Structural Biology, 1993. **3**(6): p. 915-920.

50. Rowlett, R.S., et al., *Examination of the role of Gln-158 in the mechanism of CO_2 hydration catalyzed by β-carbonic anhydrase from Arabidopsis thaliana.* Archives of biochemistry and biophysics, 2004. **425**(1): p. 25-32.

51. Silverman D. N. and S.H. Vincent, *Proton transfer in the catalytic mechanism of carbonic anhydrase.* CRC Crit. Rev. Biochem, 1984. **14**: p. 207-255.

52. Smith, K.S., et al., *Structural and kinetic characterization of an archaeal beta-class carbonic anhydrase.* Journal of Bacteriology, 2000. **182**(23): p. 6605-6613.

53. Chegwidden, W.R., N. Carter, and Y.H. Edwards, *The Carbonic Anhydrases: New Horizons*. 200, Basel: Birkhäuser Verlag.

54. Boriack-Sjodin, P.A., et al., *Structural analysis of inhibitor binding to human carbonic anhydrase II.* Protein Sci, 1998. **7**(12): p. 2483-9.

55. Cronk JD, et al., *Crystal structure of E. coli beta-carbonic anhydrase, an enzyme with an unusual pH-dependent activity.* Protein Science, 2001. **5**: p. 911-22.

56. Mitsuhashi, S., et al., *X-ray structure of β-carbonic anhydrase from the red alga, Porphyridium purpureum, reveals a novel catalytic site for CO_2 hydration.* The Journal of Biological Chemistry, 2000. **275**(8): p. 5521-5526.

57. Nair SK and D. Christianson, *Crystallographic studies of azide binding to human carbonic anhydrase II.* European Journal of Biochemistry, 1993. **213**(1): p. 507-15.

58. Iverson, T., et al., *A closer look at the active site of γ-class carbonic anhydrases: High-Resolution crystallographic studies of the carbonic anhydrase from Methanosarcina thermophila.* Biochemistry, 2000. **39**: p. 9222-9231.

59. Tu, C.K., et al., *Chemical rescue of proton transfer in catalysis by carbonic anhydrases in the β- and γ-class.* Biochemistry, 2002. **41**(51): p. 15429-15435.

60. Kiefer, L.L., S.A. Paterno, and C.A. Fierke, *Hydrogen-Bond Network In The Metal-Binding Site Of Carbonic Anhydrase Enhances Zinc Affinity And Catalytic Efficiency.* Biochemistry, 1995. **117**(26): p. 6831-6837.

61. Krebs, J.F. and C.A. Fierke, *Determinants Of Catalytic Activity And Stability Of Carbonic Anhydrase II As Revealed By Random Mutagenesis.* Journal of Biological Chemistry, 1993. **268**(2): p. 948-954.

62. Krebs, J.F., et al., *Structural And Functional Importance Of A Conserved Hydrogen-Bond Network In Human Carbonic Anhydrase II.* Journal of Biological Chemistry, 1993. **268**(36): p. 27458-27466.

63. McCall, K.A., C.C. Huang, and C. A. Fierke, *Function and mechanism of zinc metalloenzymes.* Journal of Nutrition, 2000. **130**(5): p. 1437S-1446S.

64. Merz, K.M., *Insights into the function of the zinc hydroxide-Thr199-Glu106 hydrogen bonding network in carbonic anhydrases.* Journal of Molecular Biology, 1990. **214**: p. 799-802.

65. Thoms, S., *Hydrogen bonds and the catalytic mechanism of human carbonic anhydrase II.* Journal of Theoretical Biology, 2002. **215**(4): p. 399-404.

66. Smith, K.S., C. Ingram-Smith, and J.G. Ferry, *Roles of the conserved aspartate and arginine in the catalytic mechanism of an archaeal beta-class carbonic anhydrase.* Journal of Bacteriology, 2002. **184**(15): p. 4240-4245.

67. Hewett-Emmett, D. and R.E. Tashian, *Functional Diversity, Conservation, and Convergence in the Evolution of the α-, β-, and γ-Carbonic Anhydrase Gene Familes.* Molecular Phylogenetics and Evolution, 1996. **5**(1): p. 50-77.

68. Parisi, G., M. Fornasari, and J. Echave, *Evolutionary Analysis of γ-Carbonic Anhydrase and Structurally Related Proteins.* Molecular Phylogenetics and Evolution, 2000. **14**(3): p. 323-334.

69. Roy, A. and S. Taraphder, *Proton transfer pathways in the mutant His-64-Ala of human carbonic anhydrase II.* Biopolymers, 2006.

70. Zheng, Y.J. and K.M. Merz, *Mechanism of the Human Carbonic Anhydrase-II Catalyzed Hydration of Carbon-Dioxide.* Journal of the American Chemical Society, 1992. **114**(26): p. 10498-10507.

71. Davenport, H.W., *The early days of research on carbonic anhydrase.* Annals of NY Academic Science, 1984. **429**: p. 4-9.

72. Kleilin, D. and T. Mann, *Carbonic Anhydrase. Purification and Nature of the Enzyme.* The Biochemical Journal, 1940. **34**(8): p. 1163-1176.

73. Bataller, L., et al., *Carbonic anhydrase-related protein VIII: autoantigen in paraneoplastic cerebellar degeneration.* Annals of Neurology, 2004. **56**(4): p. 575-9.

74. Boriack-Sjodin, P.A., et al., *Structure determination of murine mitochondrial carbonic anhydrase V at 2.45 angstrom resolution: Implications for catalytic proton transfer and inhibitor design.* Proceedings of the National Academy of Sciences, 1995. **92**: p. 10949-10953.

75. Jewell, D.A., et al., *Enhancement of the catalytic properties of human carbonic anhydrase III by site-directed mutagenesis.* Biochemistry, 1991. **30**(6): p. 1484-1490.

76. Jiao, Y., et al., *Carbonic anhydrase-related protein VIII deficiency is associated with distinctive lifelong gait disorder in waddles mice.* Genetics, 2005. **171**(3): p. 1239-1246.

77. Kallio, H., et al., *Expression of carbonic anhydrases IX and XII during mouse embryonic development.* BMC Developmental Biology, 2006. **6**: p. 22.

78. Morimoto, K., et al., *Overexpression of carbonic anhydrase-related protein XI promotes proliferation and invasion of gastrointestinal stromal tumors.* Virchows Archive, 2005. **447**(1): p. 66-73.

79. Potter C. and A. Harris, *Hypoxia inducible carbonic anhydrase IX marker of tumor hypoxia, survival pathway and therapy target.* Cell Cycle, 2004. **3**(2): p. 164-167.

80. Skaggs L.A., et al., *The deduced amino acid sequence of human carbonic anhydrase-related protein (CARP) is 98% identical to the mouse homologue.* Gene, 1993. **126**(2): p. 291-2.

81. Huan, S., et al., *Crystal structure of carbonic anhydrase from Neisseria gonorrhoeae and its complex with the inhibitor acetozolamide.* Journal of Molecular Biology, 1998. **283**: p. 301-310.

82. Kumar, V. and K.K. Kannan, *Enzyme-substrate interactions. Structure of human carbonic anhydrase I complexed with bicarbonate.* Journal of Molecular Biology, 1994. **241**(2): p. 226-232.

83. Nair, S.K., et al., *Structural basis of inhibitor affinity to variants of human carbonic anhydrase II.* Biochemistry, 1995. **34**(12): p. 3981-9.

84. Håkansson, K., et al., *Structure of Native and Apo Carbonic Anhydrase II and Structure of Some of Its Anion-Ligand Complexes.* Journal of Molecular Biology, 1992. **227**: p. 4.

85. Liljas, A. and M. Laurberg, *A wheel invented three times: The molecular structures of the three carbonic anhydrases.* EMBO Reports, 2000. **1**(1): p. 16-17.

86. Eriksson, A.E., T.A. Jones, and A. Liljas, *Refined structure of human carbonic anhydrase II at 2.0 A resolution.* Proteins, 1988. **3**(3): p. 274-282.

87. McCall, K.A. and C.A. Fierke, *Probing determinants of the metal ion selectivity in carbonic anhydrase using mutagenesis.* Biochemistry, 2004. **43**(13): p. 3979-3986.

88. Hunt, J.A., M. Ahmed, and C.A. Fierke, *Metal binding specificity in carbonic anhydrase is influenced by conserved hydrophobic core residues.* Biochemistry, 1999. **38**(28): p. 9054-9062.

89. Alvarez-Santos, S., A. Gonzalez-Lafont, and J.M. Lluch, *Effect of the hydrogen bond network in carbonic anhydrase II zinc binding site. A theoretical study.* Canadian Journal of Chemistry-Revue Canadienne De Chimie, 1998. **76**(7): p. 1027-1032.

90. Xue, Y.F., et al., *Structural-Analysis of the Zinc Hydroxide-Thr-199-Glu-106 Hydrogen-Bond Network in Human Carbonic Anhydrase-II.* Proteins, 1993. **17**(1): p. 93-106.

91. Liang, J.Y. and W.N. Lipscomb, *Binding of substrate CO_2 to the active site of human carbonic anhydrase II: a molecular dynamics study.* Proceedings of the National Academy of Sciences, 1990. **87**: p. 3675-3679.

92. Merz, K.M., *CO_2 binding to human carbonic anhydrase II.* Journal of American Chemical Society, 1991. **113**: p. 406-411.

93. Scolnick, L.R. and D.W. Christianson, *X-ray crystallographic studies of alanine-65 variants of carbonic anhydrase II reveal the structural basis of compromised proton transfer in catalysis.* Biochemistry, 1996. **35**(51): p. 16429-16434.

94. Silverman, D.N. and S. Lindskog, *The Catalytic Mechanism Of Carbonic Anhydrase. Implications Of A Rate-Limiting Proteolysis Of Water.* Accounts of Chemical Research, 1988. **21**(1): p. 30-36.

95. Neish, A.C., *Studies on Chloroplasts II: Their chemical composition and the distribution of certain metabolites between the chloroplasts and the remainder of the leaf.* Biochemical Journal, 1939. **33**(1): p. 300-308.

96. Bracey, M.H., et al., *Spinach carbonic anhydrase: Investigation of the zinc-binding ligands by site-directed mutagenesis, elemental analysis, and EXAFS.* Biochemistry, 1994. **33**(44): p. 13126-13131.

97. Ferry, J.G., *Methanogenesis: Ecology, Physiology, Biochemistry and Genetics*. 1 ed. Chapman and Hall Microbiology Series, ed. C.A. Reddy, et al. 1993, New York: Chapman and Hall. 536.

98. Jones, W.J., D.P. Nagle Jr, and W.B. Whitman, *methanogens and the Diverstity of Archaebacteria.* Microbiological Reviews, 1987. **51**(1): p. 135-177.

99. Karrasch, M., M. Bott, and R.K. Thauer, *Carbonic anhydrase activity in acetate grown Methanosarcina barkeri.* Archives of microbiology, 1989. **151**(2): p. 137-142.

100. Jablonski, P.E., et al., *Protein Content and enzyme activities in Methanol- and Acetate- Grown Methanosarcina thermophila.* Journal of Bacteriology, 1990. **172**(3): p. 1271-1275.

101. Robert, B., B.L. Doyle, and C.R. Matthews, *Zinc binding drives the folding and association of the homo-trimeric γ–carbonic anhydrase from Methanosarcina thermophila.* Protein Engineering, Design, and Selection, 2004. **17**(3): p. 285-291.

102. Tripp, B.C., C. Tu, and J.G. Ferry, *Role of Arginine 59 in the γ-Class Carbonic Anhydrase.* Biochemistry, 2002. **41**: p. 669-678.

103. Parisi, G., et al., *Gamma Carbonic Anhydrases in Plant Mitochondria.* Plant Molecular Biology, 2004. **55**: p. 193-207.

104. Sunderhaus, S., et al., *Carbonic Anhydrase Subunits form a Matrix-exposed Bomain Attached to the Membrane Arm of Mitochondrial Complex I in Plants.* The Journal of Biological Chemistry, 2006. **281**(10): p. 6482-6488.

105. Perales, M., et al., *Disruption of a Nuclear Gene Encoding a Mitochondrial Gamma Carbonic Anhydrase Reduces Complex I and Supercomplex I+III_2 Levels and Alters Mitochondrial Physiology in Arabidopsis.* Journal of Molecular Biology, 2005. **350**: p. 263-277.

106. Quinn, P., et al., *cDNA Microarrays as a Tool for Identification of Biomineralization Proteins in the Coccolithophorid Emiliania huxleyi (Haptophyta).* Applied and Environmental Microbiology, 2006. **72**(8): p. 5512-5526.

107. Soto, A.R., et al., *Identification and Preliminary Characterization of Two cDNAs Encoding Unique Carbonic Anhydrases from the Marine Alga Emiliania huxleyi.* Applied and Environmental Microbiology, 2006. **72**(8): p. 5500-5511.

108. Korb, R., et al., *Sources of Inorganic Carbon for Photosynthesis by Three Species of Marine Diatom.* Journal of Phycology, 1997. **33**: p. 433-440.

109. Nimer, N., M. Iglesias-Rodriguez, and M. Merrett, *Bicarbonate Utilization by Marine Phytoplankton species.* Journal of Phycology, 1997. **33**: p. 625-633.

110. Tortell, P., J. Reinfelder, and F. M. M. Morel, *Active uptake of bicarbonate by diatoms.* Nature, 1997. **390**: p. 243-244.

111. Morel, F.M.M. and N.M. Price, *The Biogeochemical Cycles of Trace Metals in the Oceans.* Science, 2003. **300**(May 9): p. 944-947.

112. Bruland, K.W., *Oceanographic Distributions of Cadmium, Zinc, Nickel and Copper in the North Pacific.* Earth and Planetary Science Letters, 1980. **47**(2): p. 176-198.

113. Cullen, J., et al., *Modulation of Cadmium uptake in phytoplankton by seawater CO_2 concentration.* Nature, 1999. **402**: p. 165-167.

114. Park, H., B. Song, and F.M.M. Morel, *Diversity of the cadmium-containing carbonic anhydrase in marine diatoms and natural waters.* Environmental Microbiology, 2007. **9**(2): p. 403-413.

115. Lane, T.W., et al., *A cadmium enzyme from a marine diatom.* Nature, 2005. **435**: p. 42.

116. Swenson, E.R., *A comparative approach to carbonic anhydrase: The work of Thomas H. Maren.* Comparative Biochemistry and Physiology. Part A, Molecular and integrative physiology, 2003. **136**(2): p. 229-241.

Chapter 2

Biochemical Characterization of a Proposed Hydrogen Bond Network in γ-class CA, Cam

Work presented in this chapter was previously published as "Proposal for a Hydrogen Bond Network in the Active Site of the Prototypic Gamma Class Carbonic Anhydrase, Cam." Sabrina A. Zimmerman and James G. Ferry, *Biochemistry*. 45: 5148-5157.

2.1 Summary

Crystal structures of Cam lead to proposed roles for 3 active-site residues of the prototypic γ-class carbonic anhydrase. These roles were investigated by kinetic analyses of site-specific amino acid replacement variants of the zinc and cobalt forms of Cam. Gln75 replacement variants showed large decreases in k_{cat}/K_m relative to wild-type. Further, the Gln75 variants showed a loss of the pK_a in pH *vs*. k_{cat}/K_m profiles previously attributed to ionization of the metal-bound water yielding the hydroxyl group attacking CO_2. These results support the previously proposed role for Gln75 in hydrogen bonding with the catalytic hydroxide orienting it for attack. Kinetic analyses of Asn73 variants were consistent with a role in hydrogen bonding with Gln75 to position it for optimal interaction with the catalytic hydroxide. Kinetic analyses of Asn202 variants showed substantial decreases in k_{cat}/K_m relative to wild-type enzyme supporting the previously proposed role in polarizing the CO_2 and facilitating attack from the metal-bound

hydroxide. Based on results presented here, and previous structural analyses, we present a catalytic mechanism involving Gln75, Asn73, and Asn202 that also suggests a role for Glu62 not previously recognized. Further, the results suggest that the γ- β- and α-class carbonic anhydrases each independently evolved a hydrogen bond network essential for catalysis.

2.2 Introduction

Rigorous exploration of the well-characterized α-class CA, HCAII, has identified two residues essential for the CO_2 hydration step, Thr199 and Glu106 [1-5]. The Thr199 hydroxyl hydrogen bonds with the carboxylate oxygen of Glu106. This interaction orients the Thr199 hydroxyl to act as a hydrogen bond acceptor to the zinc-bound hydroxide, optimizing orientation of the lone pair of electrons of the hydroxide for nucleophilic attack on CO_2. The backbone amide of Thr199 hydrogen bonds with the CO_2 molecule, polarizing it for nucleophilic attack and providing an environment that increases the K_d of HCO_3^- to promote product removal [4]. Comparisons of active sites in crystal structures of α, β, and γ-class CAs do not reveal threonines or glutamates that correspond to α-class residues, Thr199 and Glu106. This raises the question whether active site residues exist in β and γ-class CAs that provide the same catalytic function as those α-class residues, therefore, identifying a conserved mechanism amongst CAs.

Superimposition of the active site of β-class CAs from *Arabidopsis thaliana* and *Pisium sativum* on the active site of HCAII [6-8] revealed that *A. thaliana* active site residue, Gln158, and equivalent Gln151 in *P. sativum*, were optimally positioned to

provide the same catalytic function as the backbone amide of Thr199 in HCAII [8]. Kinetic studies of the N158A [8] supports this hypothesis. The prototype of the γ-class, Cam, [9] was first isolated from *Methanosarcina thermophila*, a methanogenic microbe from the Archaea domain [10]. Previous inspection of crystal structures of wild-type Co-Cam and Zn-Cam [11] identified four residues adjacent to the metal in the active site that may perform conserved key roles in catalysis analogous to the α-class HCAII and β-class CAs from *A. thaliana* and *P. sativum*. The carbonyl group of Cam active site residue Gln75 is shown within hydrogen bonding distance to the metal-bound hydroxide and, when HCO_3^- is bound, the metal-bound oxygen of the HCO_3^- [11]. This suggests Gln75 could orient and stabilize the metal-bound hydroxide. However, crystal structures also show Glu62 within hydrogen bond distance to a non-metal oxygen of HCO_3^-; yet, in uncomplexed structures, Glu62 orients towards Glu84 which acts as the primary proton shuttling residue [11, 12]. Though kinetic analyses of Glu62 variants [12] indicate participation in CO_2 hydration, the specific function is unknown. Glu62 is unlikely to act as the primary residue orienting the metal-bound hydroxide since Glu62 is not conserved among the putative γ-class CAs; however, Gln75 is strictly conserved. This lead to the proposal that Gln75 and Asn73 act in a hydrogen bond network with the metal-bound hydroxide analogous to the Zn-hydroxide-Thr199-Glu106 hydrogen bond network characterized in α-class CA, HCAII [11, 13]. Cam crystal structures also show Asn202 within hydrogen bonding distance to a nonmetal-bound oxygen of the HCO_3^- molecule, implying a function corresponding to the backbone amide of the α-class Thr199 and β-class Gln151 in *P. sativum* and Gln158 in *A. thaliana*. Here we present kinetic analyses

of site-specific replacement variants of Cam which show Gln75 and Asn202 are essential in catalysis whereas Asn73 has a minor role. The results suggest roles for these residues analogous to active-site residues in the independently evolved α- and β-classes. Further, a more defined role for Glu62 in Cam is proposed.

2.3 Results

2.3.1 Initial Characterization of Cam Variants

Crystal structures of wild-type Cam complexed with bicarbonate [11] identified active site residues, Gln75, Asn73, and Asn202, (Figure **2.1**), with potential functions corresponding to residues Thr199 and Glu106 in the well-characterized α-class CAs [3, 4, 13-15]. Thus, Cam variants, in which Gln75, Asn73, or Asn202 were individually replaced, were generated to investigate the role of these residues in catalysis (Table **2.1**, Table **2.3**, Table **2.4**). All thirteen variants were expressed in soluble form in *E. coli*, with final yields of 20-50 mg of the purified variant/L of cell culture, similar to the ~50 mg yield of the wild-type protein. Each variant was reconstituted with cobalt or zinc with less than 1% loss of protein yield. Every reconstituted variant eluted as a single symmetrical peak from a Superdex 75 size-exclusion column corresponding to a native molecular mass of approximately 70 kDa, identical to the trimeric wild-type. The metal

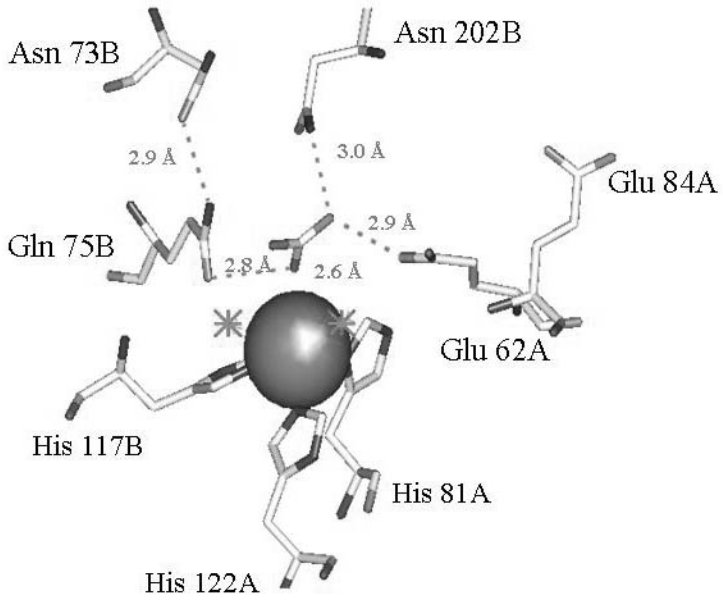

Figure 2.1**: Co-Cam active site complexed with HCO_3^-.**

The figure was displayed with Open-Source Pymol version 0.97 2004. Letters "A" and "B" designate residues contributed by adjacent monomers. The dashed lines represent possible hydrogen bond interactions. Glu84, the proton shuttle residue is shown in the "out" position. The two asterisks on either side of the metal represent the two metal-bound waters.

content determined for each variant (Table **2.1**, Table **2.3**, Table **2.4**) was at least 0.7 metal/monomer, indicative of robust reconstitution. These results suggest that the functional integrity of each variant was similar to wild-type.

Benefiting from its overall $3d^7$ electronic configuration, cobalt was used as a reporter metal to investigate the integrity of the active site in the variants *via* electronic spectroscopy since zinc does not significantly absorb in the UV/Vis range. Intensity and position of the absorbance bands are dependent on the number and type of ligands coordinating the metal as well as the geometry of cobalt in the active site [9]. The visible difference spectra of wild-type Co-Cam *minus* Zn-Cam, and alanine variants, are shown

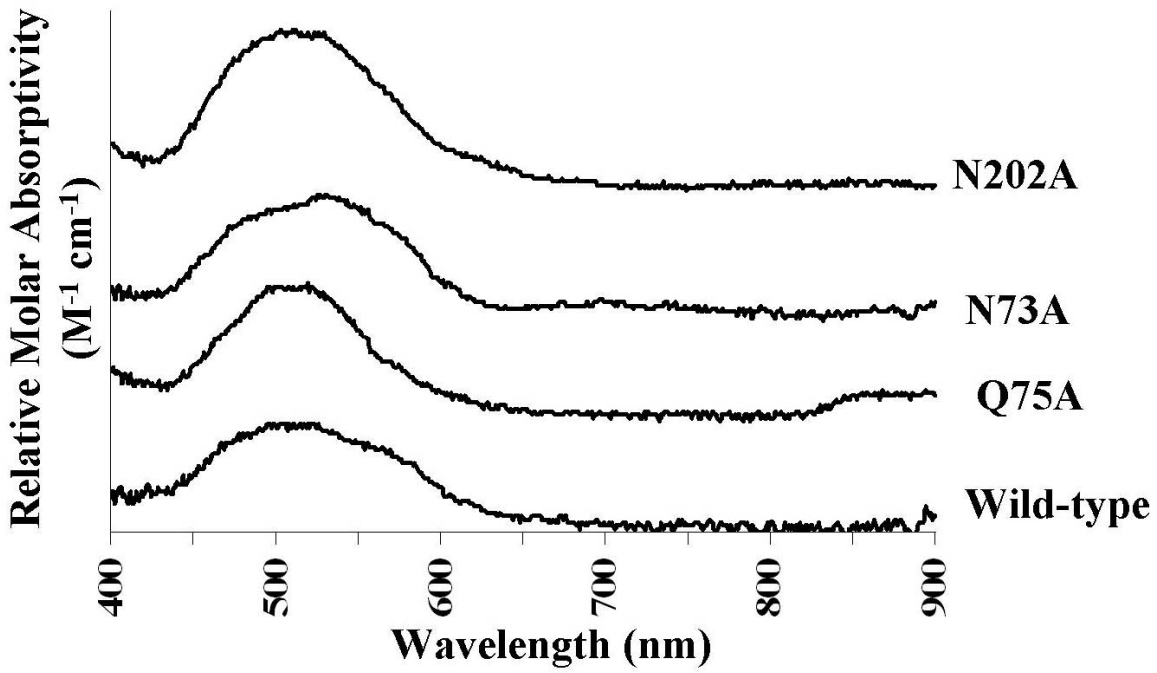

Figure 2.2**: Optical absorption difference spectra of Co- minus Zn-substituted wild-type Cam and variants.**

Conditions were 1.1 mM Cam in 20 mM MOPS, pH 7.0 at 25 °C

in Figure **2.2**. The difference spectrum of wild-type had a low molar absorptivity ($\varepsilon_{515\ nm}$ = 30 M^{-1} cm^{-1}) indicative of a hexacoordinate metal center determined empirically with cobalt standards and consistent with the previously reported structure of Co-Cam [9, 11, 16]. The position of the maximum absorbance band (515 nm) corresponded to an average ligand field of three oxygens, possibly donated by water molecules, and three nitrogens that can be contributed by histidines ligating the metal, consistent with the crystal structure of Cam [9, 11]. The representative difference spectra of variants Co-Q75A, Co-N73A, and Co-N202A were comparable to the wild-type Co-Cam indicating no major alteration of the metal environment. These spectroscopic data further support

that the changes made in the active site of the alanine variants did not interrupt the structural integrity of the active site metal

2.3.2 Kinetic Analyses of Gln75 Variants

Residue Gln75 is positioned to act as a hydrogen bond acceptor to the attacking metal-bound hydroxide as inferred from the distance of the O (ε) atom of Gln75 to the metal-bound oxygen of HCO_3^- in the wild-type Co-Cam structure (**Figure 2.1**). Steady state kinetic parameters of Cam Gln75 variants are shown in Table **2.1**. Conservative replacement of Gln75 with an Asn resulted in ~3% retention of the k_{cat}/K_m value in the Zn-Q75N variant and 0.5% retention in the Co-Q75N variant when compared to the corresponding k_{cat}/K_m value of wild-type Cam. Similarly, the Q75A variants retained ~1% of the wild-type value (Table **2.1**). Replacement of Gln75 with an Asp or Glu almost abolished any detectable k_{cat}/K_m value relative to wild-type. These results support the proposed role for Gln75 stabilizing and positioning the metal-bound hydroxide for attack on CO_2.

Table **2.1**: Michaelis-Menten Steady-State Kinetic Parameters for Wild-type Cam and Variants with Substitutions at Gln75. Assays were Performed using Stopped-Flow Spectroscopy at pH 7.5 and 25° C in 50mM HEPES.

Variant	K_m ($x10^3$ M)	[a] k_{cat}^{eff} ($x\ 10^{-3}\ s^{-1}$)	[a] k_{cat}/K_m^{eff} ($x10^{-6}\ M^{-1}\ s^{-1}$)	[b] Molar metal ratio/monomer
Wild-type Zn-Cam	15.6 ± 0.8	70.2 ± 7.8	4.4 ± 0.5	1.2
Wild-type Co-Cam	15.3 ± 0.9	173.0 ± 4.5	11.7 ± 0.5	0.7
Zn-Q75A	26.7 ± 6.7	1.4 ± 0.2	0.051 ± 0.021	1.3
Co-Q75A	12.0 ± 1.9	0.7 ± 0.1	0.059 ± 0.012	0.7
Zn-Q75N	63.9 ± 18.2	8.29 ± 1.80	0.13 ± 0.07	1.5
Co-Q75N	72.0 ± 13.0	4.8 ± 0.1	0.07 ± 0.02	1.1
Zn-Q75D	36.4 ± 9.8	0.95 ± 0.18	0.026 ± 0.01	1.0
Co-Q75D	15.6 ± 4.1	0.75 ± 0.10	0.048 ± 0.023	0.8
Zn-Q75E	21.6 ± 6.1	0.6 ± 0.1	0.028 ± 0.012	0.8
Co-Q75E	13 ± 2.7	0.57 ± 0.05	0.044 ± 0.013	0.8

[a] Effective k_{cat} and k_{cat}/K_m values were obtained by dividing apparent k_{cat} and k_{cat}/K_m values by the molar ratio of metal/monomer. Thus these adjusted kinetic parameters are based on the amount of protein with active metal centers.

[b] Values for metal ratios per monomer are from one sample of the respective protein preparation.

To further examine the proposed role of Gln75, profiles of pH *vs.* k_{cat} or k_{cat}/K_m of the Q75A and Q75N variants were obtained (Figure **2.3**). Only the Q75N and Q75A variants exhibited enough observable activity to be assayed over a broad pH range. The steady-state parameter k_{cat}/K_m of the Q75N and Q75A variants was pH-dependent. The profiles were best fit to a single pK_a (Eq. **2.6**) differing from the two ionizations that were fit for wild-type Cam (Figure **2.3**, Table **2.2**). This result is consistent with a

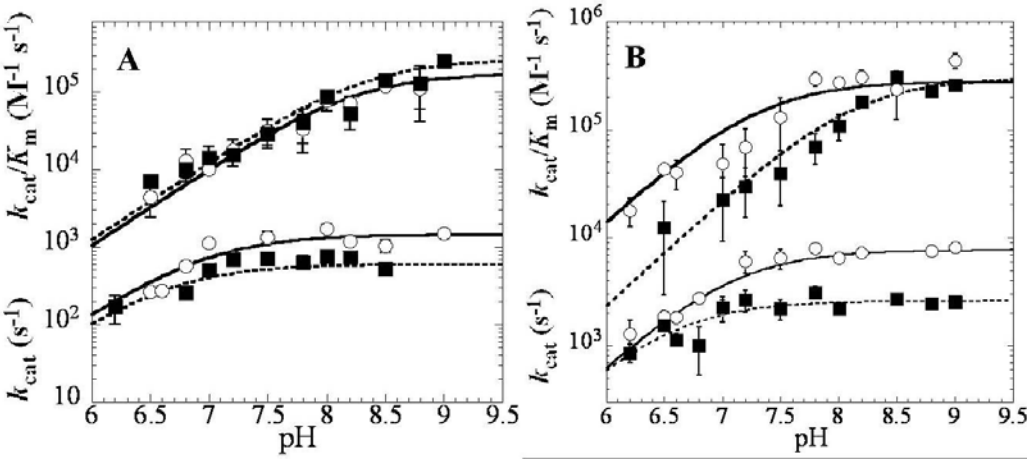

Figure 2.3: pH profiles of steady-state parameters for the Q75A and Q75N Cam variants.

(A) Q75A (■) k_{cat}/K_m^{eff} of Co-Q75A and k_{cat}^{eff} of Co-Q75A and (○) k_{cat}/K_m^{eff} of Zn-Q75A and k_{cat}^{eff} of Zn-Q75A (B) Q75N (■) k_{cat}/K_m^{eff} of Co-Q75N and k_{cat}^{eff} of Co-Q75N (○) k_{cat}/K_m^{eff} of Zn-Q75N and k_{cat}^{eff} of Zn-Q75N.

previous report [16]. The single pK_a (k_{cat}/K_m) values for all the variants were similar to the pK_a^{II} value of wild-type except for the Co-Q75N variant (Table **2.2**). Both metal forms of the Q75N and Q75A variants had k_{cat}/K_m and k_{cat} values at pH 9.0 (Figure **2.3**) that were less than 5% of the previously reported wild-type values [16] except for the Zn-Q75N k_{cat} value that was 13% of the wild-type. These effects on k_{cat}/K_m for the Q75A and Q75N variants further support the proposed role for this residue in the CO_2 hydration step of catalysis. The kinetic parameter, k_{cat}, in wild-type Zn- and Co-Cam, was dependent on a single ionization within ~6.5-6.8 (Figure **2.3** , Table **2.2**).

Table **2.2**: pH-Independent Michaelis-Menten Kinetic Parameters Obtained from the pH Dependence of CO_2 Hydration Catalyzed by Wild-Type Cam, Q75A variant, and Q75N variant.

Parameters [a]	**Wild-type**		**Variant**			
	Zn-Cam	**Co-Cam**	**Zn-Q75N**	**Co-Q75N**	**Zn-Q75A**	**Co-Q75A**
k_{cat} (ms^{-1})	61.2 ± 0.1	104.3 ± 0.2	7.6 ± 0.1	2.66 ± 0.03	1.5 ± 0.6	0.6 ± 0.01
pK_a (k_{cat})	6.8 ± 0.1	6.5 ± 0.1	7.0 ± 0.01	6.5 ± 0.06	6.9 ± 0.04	6.6 ± 0.01
pK_a^{I} (k_{cat}/K_m^{I})	6.9 ± 0.1	6.7 ± 0.1	7.3 ± 0.04	8.1 ± 0.1	8.2 ± 0.08	8.3 ± 0.04
pK_a^{II} (k_{cat}/K_m^{II})	8.2 ± 0.3	8.4 ± 0.2	ND[b]	ND[b]	ND[b]	ND[b]
k_{cat}/K_m^{I} (mM^{-1} s^{-1})	3.3 ± 0.5	5.3 ± 0.5	0.28 ± 0.01	0.30 ± 0.02	0.18 ± 0.02	0.28 ± 0.02
k_{cat}/K_m^{II} (mM^{-1} s^{-1})	6.1 ± 0.5	15.1 ± 1.4	NA[b]	NA[b]	NA[b]	NA[b]

[a] pH-independent kinetic parameters and p*K*a values for CO_2 hydration were determined by fitting pH-dependent k_{cat} and k_{cat}/K_m data obtained over the pH range of 6.2 - 9.0 to **Eq. 4** as described in Materials and Methods.

[b] The kinetic parameter, k_{cat}/K_m, of these variants are dependent on a single pK_a, whereas, in wild-type, k_{cat}/K_m is dependent on two pK_a's.

ND- Not Detected, NA- Not Applicable

2.3.3 Kinetic Analyses of Asn73 Variants

Discovery of Gln75 as important in catalysis encouraged examination of the role of Asn73 which is ideally situated relative to Gln75 to provide a similar role as Glu106 in α-class CAs. As a secondary player in the proposed hydrogen bond network, the O (δ) atom of Asn 73 could potentially act as a hydrogen acceptor to the amide of Gln75 to orient Gln75 for hydrogen bonding with the catalytic metal-bound hydroxide

Table **2.3**: Michaelis-Menten Steady-State Kinetic Parameters for Wild-type Cam and Variants with Substitutions at Asn73. Assays were Performed using Stopped-Flow Spectroscopy at pH 7.5 and 25° C in 50mM HEPES

Variant	K_m ($x10^3$ M)	k_{cat}^{eff} ($x\ 10^{-3}\ s^{-1}$)	k_{cat}/K_m^{eff} ($x10^{-6}\ M^{-1}\ s^{-1}$)	Molar metal ratio/monomer
Wild-type Zn-Cam	15.6 ± 0.8	70.2 ± 7.8	4.4 ± 0.5	1.2
Wild-type Co-Cam	15.3 ± 0.9	173.0 ± 4.5	11.7 ± 0.5	0.7
Zn-N73A	10.9 ± 0.1	20.1 ± 0.8	1.84 ± 0.09	1.0
Co-N73A	17.1 ± 0.3	56.8 ± 0.5	3.33 ± 0.07	0.7
Zn-N73Q	10.5 ± 1.1	19.7 ± 0.9	1.9 ± 0.3	1.0
Co-N73Q	13.9 ± 2.1	28.0 ± 2.0	2.0 ± 0.5	0.8
Zn-N73D	10.4 ± 0.7	44.5 ± 0.5	4.4 ± 0.3	0.8
Co-N73D	15.4 ± 1.4	45.5 ± 2.1	3.0 ± 0.4	1.0

[a] Effective k_{cat} and k_{cat}/K_m values were obtained by dividing apparent k_{cat} and k_{cat}/K_m values by the molar ratio of metal/monomer. Thus these adjusted kinetic parameters are based on the amount of protein with active metal centers.
[b] Values for metal ratios per monomer are from one sample of the respective protein preparation.

(**Figure 2.1**). Steady-state kinetic parameters of Asn73 Cam variants are shown in Table **2.3**. The Zn-N73A and Zn-N73Q variants yielded k_{cat}/K_m values that were ~40% of the corresponding zinc wild-type value, whereas Co-N73A, -Q and -D variants had ~20% of the k_{cat}/K_m values compared to wild-type Co-Cam. An exception to these results was the Zn-N73D variant which retained 100% of the wild-type Zn-Cam k_{cat}/K_m value. At pH 9.0, the Co-N73A and Zn-N73A variants had k_{cat}/K_m and k_{cat} values that were 7% and 10% of the respective wild-type values. These data suggest that Asn73 is not essential for catalysis and is only important for optimal catalysis, possibly by orienting Gln75 for optimal interaction with the metal-bound hydroxide.

2.3.4 Kinetic Analyses of Asn202 Variants

The amide of Asn202 is within hydrogen bonding distance to a nonmetal-bound oxygen of the bicarbonate molecule [11] (**Figure 2.1**), and is similarly positioned to function analogous to the backbone amide of α-class Thr199. The Zn-N202Q, Zn-N202A, and Co-N202A variants had k_{cat}/K_m values at pH 7.5 of 8.7%, 6.0% and 6.1%, respectively, relative to the corresponding wild-type value at pH 7.5 (Table **2.4**). The Co-N202Q, -S, -H and Zn-N202-S and -H variants had k_{cat}/K_m values that were ~3% or less of wild-type values. The CO_2 hydration activities of Co-N202D, Zn-N202E, and Co-N202E variants were too low for a successful fit to the Michaelis-Menten equation (Table **2.4**). The k_{cat} values for all Asn202 variants were equal to or less than 10% of wild-type k_{cat} values. Both metal forms of the Asn202 alanine variants had both k_{cat} and k_{cat}/K_m values at pH 9.0 that were less than or equal to 10% of the respective wild-type values at pH 9.0. The acute decreases in the kinetic constants of the Asn202 variants suggest Asn202 is essential in catalysis and are consistent with the previously proposed role [11] in orienting and polarizing CO_2 for attack by the metal-bound hydroxide.

Table **2.4**: Michaelis-Menten Steady-State Kinetic Parameters for Wild-type Cam and Variants with Substitutions at Asn202. Assays were Performed using Stopped-Flow Spectroscopy at pH 7.5 and 25° C in 50mM HEPES.

Variant	K_m ($x10^3$ M)	[a] k_{cat}^{eff} ($x\ 10^{-3}\ s^{-1}$)	[a] k_{cat}/K_m^{eff} ($x10^{-6}\ M^{-1}\ s^{-1}$)	[b] Molar metal ratio/monomer
Wild-type Zn-Cam	18.2 ± 0.8	76.3 ± 6.8	4.1 ± 1.1	1.0
Wild-type Co-Cam	17.3 ± 0.9	173.0 ± 4.9	11.7 ± 0.5	0.7
Zn-N202A	26.2 ± 3.9	6.6 ± 0.6	0.25 ± 0.06	1.4
Co-N202A	24.6 ± 0.9	17.4 ± 0.4	0.71 ± 0.04	0.8
Zn-N202Q	18.4 ± 0.6	6.7 ± 1.4	0.36 ± 0.21	1.8
Co-N202Q	24.5 ± 1.8	2.60 ± 0.11	0.11 ± 0.01	1.0
Zn-N202S	39.6 ± 5.4	5.1 ± 0.5	0.13 ± 0.03	1.9
Co-N202S	47.3 ± 5.0	12.3 ± 0.9	0.26 ± .005	1.0
Zn-N202H	20.7 ± 14.4	2.7 ± 1.1	0.134 ± 0.145	1.3
Co-N202H	35.8 ± 12.9	15.6 ± 3.8	0.44 ± 0.26	0.99
Zn-N202D	116.2 ± 6.6	9.7 ± 0.5	0.084 ± 0.009	0.98
Co-N202D	ND[c]	ND[c]	ND[c]	0.75
Zn-N202E	ND[c]	ND[c]	ND[c]	0.98
Co-N202E	ND[c]	ND[c]	ND[c]	0.69

[a] Effective k_{cat} and k_{cat}/K_m values were obtained by dividing apparent k_{cat} and k_{cat}/K_m values by the molar ratio of metal/monomer. Thus these adjusted kinetic parameters are based on the amount of protein with active metal centers.

[b] Values for metal ratios per monomer are from one sample of the respective protein preparation.

[c] ND-Not Determinable. Kinetic analyses for these variants yielded activities near the limit of detection precluding reliable k_{cat} and k_{cat}/K_m values determined using the Michaelis-Menten equation.

2.4 Discussion

The crystal structures of three (α, β, and γ) of the five independently evolved classes of CAs reveal diversity in amino acid composition adjacent to the active-site metal [6, 11, 17-23]. However, these three classes have been kinetically described to

participate in a two-step isomechanism involving a catalytic metal-bound hydroxide. This prompted investigations to determine if the γ-class, Cam, shares a common catalytic mechanism. Active site residues, Gln75 and Asn73 of the prototypic γ-class enzyme, Cam, are hypothesized to participate analogously to the α-class hydrogen bond network comprised of Zn-OH^-, Thr199, and Glu106 that aids in orienting the metal-bound hydroxide for attack on CO_2 [3, 4, 11, 13]. The Asn202 of Cam hypothetically polarizes the incoming CO_2 molecule, poising it for attack by the metal-bound hydroxide, akin to the function of the backbone amide of Thr199 [11]. Here, we show that Gln75, Asn73, and Asn202 contribute significantly to the CO_2 hydration step, and propose a catalytic mechanism involving these residues.

2.4.1 Kinetic Analyses of Cam Variants Indicate Roles for Gln75, Asn73, and Asn202 in Catalysis

The decreases in k_{cat}/K_m for the Zn- and Co- Q75A variants indicates Gln75 is essential in the CO_2 hydration step of catalysis, consistent with a role in orienting the metal-bound hydroxide for attack on CO_2. Further, the Zn- and Co-Q75N variants retained less than 3% of the wild-type k_{cat}/K_m Gln75 variants also exhibited a drastic decrease in k_{cat} when compared to wild-type Cam; however, the functionality of Gln75 precludes a role in proton transfer and, therefore, it is unlikely that protein transfer contributes significantly to the decrease in k_{cat}. Although retaining the potential to interact with the metal-bound hydroxide *via* similar amino acid functional group, the widened gap between the carbonyl of the Q75N variants and the metal-bound hydroxide,

due to the loss of one methylene group, may not allow optimal hydrogen bonding between species or proper positioning of the catalytic hydroxide. Interestingly, the carboxylate group of the Q75E variant, which could possibly act as a hydrogen bond acceptor, showed near abolition of k_{cat}/K_m. It is possible that the glutamate has an electronegative charge that disorients the metal-bound hydroxide by repulsion and/or rearranges the active site, impeding catalysis. This scenario may also explain the decreased k_{cat}/K_m value observed in the Q75D variants. Although, gel filtration of the variants and the absorbance spectral data of the Co metal in the active site of variants did not indicate drastic structural changes of the enzyme nor the active site, it is possible that solvent rearrangement did occur as a result of the site specific amino acid replacements that may contribute to the observed reduction in catalysis.

In wild-type Zn- and Co-Cam, k_{cat}/K_m was dependent on two ionizable groups, one at ~6.6-6.8 and a second ~8.0-8.3, in agreement with previous results [24]. The first ionization, ~6.6-6.8, is assigned to the catalytic water [24], while it is unknown what group is responsible for the second pK_a. The pH profiles of k_{cat}/K_m for variants Q75A and Q75N showed a loss of the pK_a at ~6.6-6.8 indicating Gln75 influences ionization of the catalytic water, a result consistent with the previously hypothesized function for Gln75 [13]. It is reported that the pK_a of the catalytic water in the α-class CA, HCAII, increases at least 1 pH unit for Thr199 variants [3, 4]. Thus one possible interpretation for the results is that Gln75 assists the metal in lowering the pK_a of the catalytic water by stabilization of the attacking hydroxide group relative to the water, and loss of the functional group in the Q75A variants results in an increased pK_a of the catalytic water that cannot be resolved from the pK_a at ~8.3. The same explanation can be applied to

interpret the profile of pH *vs.* k_{cat}/K_m for the Co-Q75N variant, although the Zn-Q75N variant showed only a modest increase in the pK_a of the catalytic water and loss of the 8.3 pK_a which is unexplained. This interpretation of these results implies that, of the two metal-bound waters, the catalytic water is within hydrogen bonding distance to Gln75 in both the Zn and Co enzymes consistent with the proposed role for Gln75.

The kinetic parameter k_{cat} in wild-type Zn- and Co-Cam was dependent on a single ionization within ~6.5-6.8. It is unknown what active site species may be responsible for this pK_a, although, it was previously postulated to reflect pK_a of a proton shuttle residue [24]. The pH profiles of k_{cat} for the Q75A and Q75N variants showed retention of this pK_a suggesting that if it reflects a proton shuttle residue replacement of Gln75 does not interfere or influence the pK_a of this residue.

If Asn73 functions in analogy to Glu106 in the α-class enzymes as previously proposed [3, 4, 13], then the requirement for a residue to orient Gln75 in Cam is less strict than for orienting Thr199 in the α-class. This may reflect differences in the active site architecture of Cam and the α-class CAs. Replacement of the α-class Glu106 with alanine or glutamine resulted in much larger decreases in k_{cat} and k_{cat}/K_m than for Asn73 of Cam [3]. The Asn73 variants showed only modest decreases in k_{cat} and k_{cat}/K_m relative to wild-type.

Replacement of Asn73 resulted in a two or three fold decrease in k_{cat}/K_m with the exception of the Zn-N73D variant. One explanation for these results is that the carboxyl of N73D retains the ability to act as a hydrogen bond acceptor at essentially the same distance to Gln75 as in wild-type Cam. While there is no observed affect in catalysis with Zn-N73D, the decrease in k_{cat}/K_m of Co-N73D was comparable to that in other

cobalt substituted Asn73 variants. These discrepancies in k_{cat}/K_m between the Co- and Zn- substituted variants may involve the putative position of the metal-bound catalytic water adjacent to Gln75. Crystal structures reveal that the position of the water adjacent to Gln75 in Co-Cam is unique to that in Zn-Cam [11]. In the Zn-N73 variants, the hydrogen bonding between Gln75 and the catalytic hydroxide may remain intact, although not optimal. Contrary, in Co-N73D, the introduction of a negative charge may position Gln75 beyond favorable interactions with the catalytic hydroxide. Thus, the role of Asn73 may hold greater emphasis to properly angle and position Gln75 in higher coordinated metal centers.

Hakansson's proposal [25] that the backbone amide of Thr199 tethers the incoming CO_2 and destabilizes the HCO_3^- transition state has been substantiated by kinetic and structural data [4, 8, 25]. In β-class CAs from *P. situm* and *A. thaliana,* it has been suggested that Gln151 and Gln158 function comparable to the backbone amide of Thr199 [8, 25]. Cam crystal structures revealed Asn202 is well-positioned to act analogous to these β-class residues as well as the backbone amide of Thr199 in α-class CAs. The 16-fold decrease in k_{cat}/K_m values forAsn202 variants relative to wild-type suggests that Asn202 is important for catalysis. Assuming no structural rearrangements were introduced, the $\Delta\Delta G^{\ddagger}$ of the N202A variant ($-RT\ln(k_{cat}/K_m{}^{variant}/\ k_{cat}/K_m{}^{wildtype})$, estimates that the amide of Asn202 contributes ≅ 0.9 kcal/mol towards stabilization of the transition state. This contribution is comparable to the ≅ 0.8kcal/mol determined for the backbone amide of Thr199 [4]. Thus, the kinetic analyses of the Asn202 variants are

consistent with a role for this residue analogous to the backbone amide of Thr199 in the α-class CAs.

2.4.2 Proposed Catalytic Mechanism of the Prototypic γ-Class Carbonic Anhydrase, Cam.

Cumulating previous results and the results presented here, we propose a mechanism for the prototypic γ-class CA, Cam (Figure **2.4**). Figure **2.4** portrays Zn-Cam, however, the mechanism is also applicable to Co-Cam with the exception of an extra metal-coordinated water. Panel A shows Gln75 and Glu62 engaged in hydrogen bonds with separate waters, consistent with the crystal structure [11]. A proton is extracted from the non-catalytic water coordinated by Glu62, sharing the proton between Glu62 and the previously documented proton shuttle residue, Glu84 [12]. The second pK_a in wild-type Cam at ~8.3 could reflect the ionization of the water within hydrogen bonding distance to Glu 62. Further experiments are needed to test this hypothesis. The metal-bound hydroxide then extracts a proton from the adjacent water hydrogen bonded by Gln75 (Panel B). Now, the catalytic hydroxide hydrogen bonded to Gln75 is primed for nucleophilic attack on the incoming CO_2 molecule while the proton is relayed to Glu84 and ultimately shuttled out to buffer (Panel C). The incoming CO_2 molecule is tethered by hydrogen bonds contributed by the functional group amides of Gln75 and Asn202 (Panel D). The activated CO_2 is attacked by the lone pair of electrons of the metal-bound hydroxide, resulting in a metal-bound HCO_3^- (Panel E). Then, the HCO_3^- swings down, binding in a bidentate fashion to the metal which displaces the coordinated

water previously engaged in a hydrogen bond with Glu62 (Panel F). Observed in structures of both Zn-Cam and Co-Cam, the bidentate bound HCO_3^- displaces the same coordinating water [11]. The proton of the hydroxyl of the bound HCO_3^- shifts (Lindskog transition state) to the oxygen tethered by Asn202 or the hydroxyl rotates *via* the carbon bond (Lipscomb transition state) as described for the α-class CA [1, 26, 27]. An incoming water displaces an oxygen, resulting in a monodentately bound HCO_3^- supported *via* hydrogen bonds with Asn202 and Glu62 (Panel G). Finally, a second water displaces the product from the active site (Panel H).

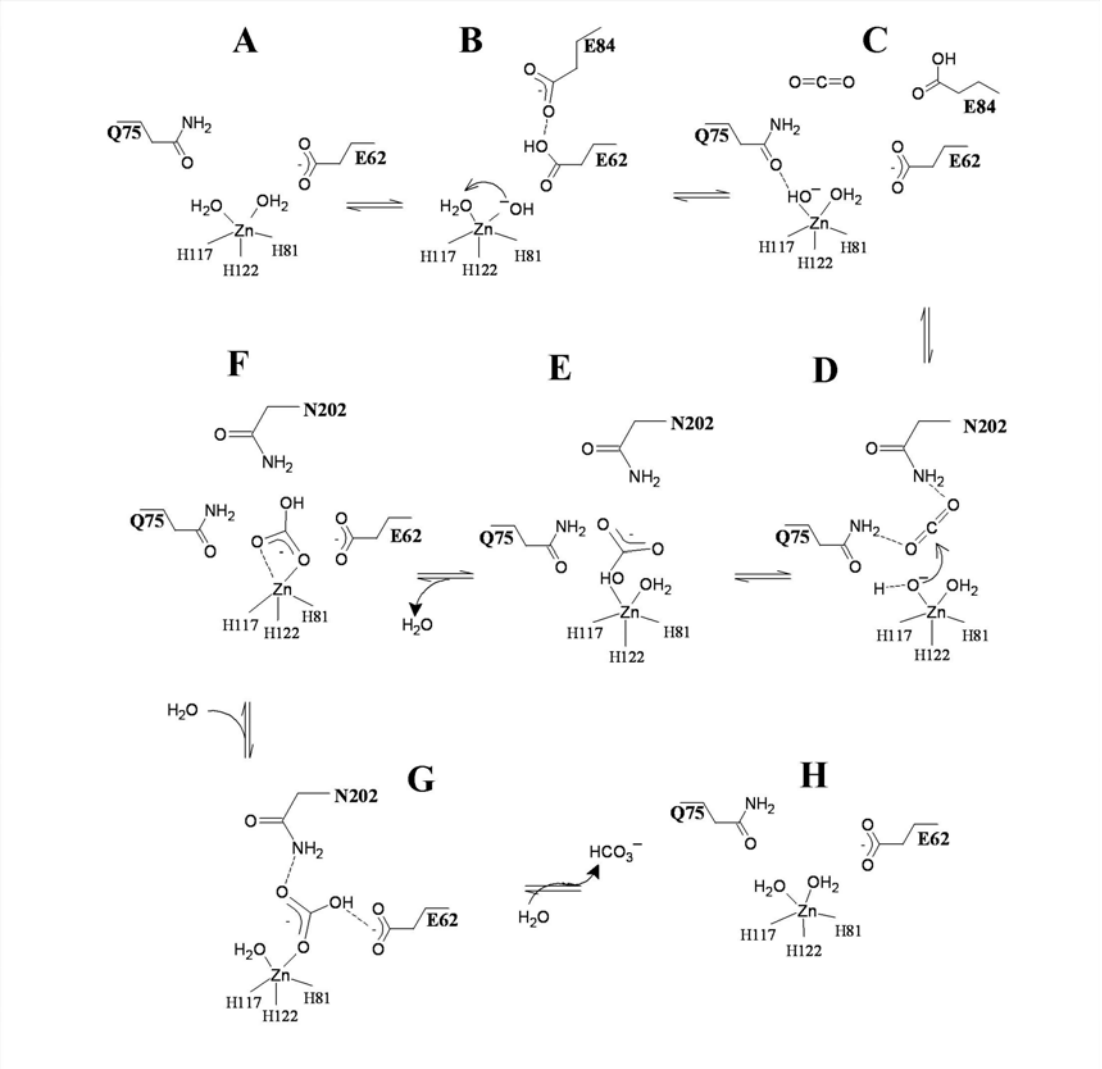

Figure 2.4**: Proposed mechanism for Cam.**

The reaction mechanism is drawn using Zn-Cam as the template. Co-Cam is assumed to have a similar mechanism with an additional coordinating water molecule. (A) Zn^{2+} is coordinated by two water molecules. (B) Glu62 extracting a proton from water, which then extracts a proton from the adjacent water. (C-F) The resulting Zn-OH^- attacks the CO_2 resulting in a bound HCO_3^- that displaces a water molecule. The HCO_3^- undergoes a bidentate transition state where the proton either rotates (Lindskog) or transfers (Lipscomb) to the nonmetal-bound oxygen of the HCO_3^-. (G) As shown in the crystal structures [11], Glu62 hydrogen bonds with hydroxyl HCO_3^- destabilizing it. An incoming water molecule further destabilizes the HCO_3^- by replacing one of the bound oxygens. (H) A second incoming water molecule completely displaces the HCO_3^- resulting in product removal and regeneration of the active site.

This proposed catalytic mechanism portrays a more defined role for residue Glu62. A proton extraction and shuttle function was previously hypothesized based on crystal structure [11, 12]. Although previous kinetic analyses of variants indicate Glu62 as essential for the CO_2 hydration step [12], a more detailed function was not proposed. The mechanism proposed here suggests Glu62 is involved in product removal, contributing to the CO_2 hydration step, and proton transfer, although, it may be difficult to de-convolute each contribution. Structural [11, 12] and kinetic analysis of variants [11, 12] exist that support involvement in both steps. A positive value for $\Delta\Delta G_B$ (k_{cat}) of the double E62A/E84A variant suggests these two residues act in an additive manner during the proton transfer event [12]. Further, Glu84 resides 8 Å from the metal-bound water [11], indicating an intervening residue or water is needed to relay the proton from the metal to buffer. Inspection of Cam crystal structures do not show conserved water(s) that may act as a relay; however, Glu62 is well-positioned in the active site to shuttle protons form the adjacent metal-bound water to Glu84. Indeed in structures of Cam not complexed with HCO_3^-, Glu62 is in a shifted conformation sharing a proton with Glu84 [11].

2.4.3 Superimposition of Cam Active Site and α-class CA Active Site

The active site residues between the α-class CA (HCAII) and the γ-class (Cam) bear no structural identity; except for the metal ligands superimpose (Figure **2.5**). Also, the α-class CA bidentate-bound HCO_3^- shares the approximately same position with the bidentate-bound HCO_3^- in Co-Cam crystal structures [11]. Remarkably, the O (ε) atom

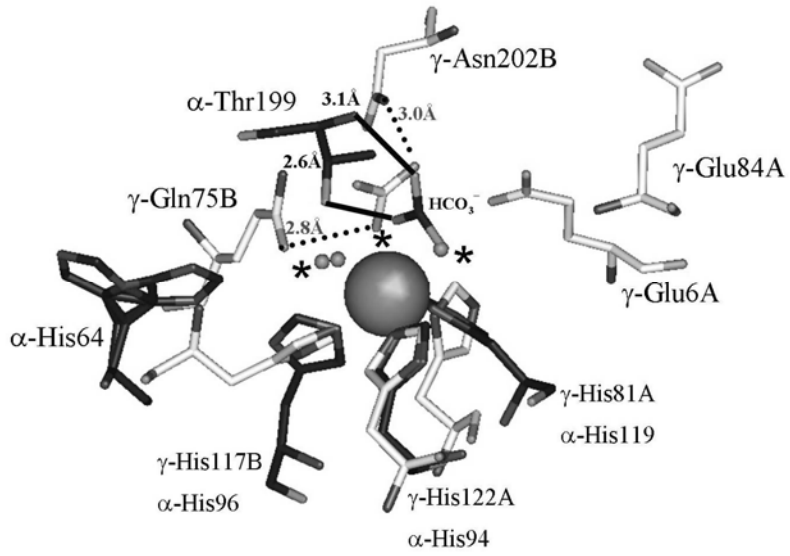

Figure 2.5: Co-Cam active site complexed with HCO_3^- superimposed with Zn-HCAII active site.

The figure was displayed with OpenSource Pymol version 0.97 2004. The HCAII active site members are represented in black and the Cam active site members are represented by white. The α or γ notation refers to residues belonging to α-class CA active site or γ-class CA active site. Letters "A" and "B" designate residues contributed by adjacent Cam monomers. The smaller spheres represent waters of Co-Cam (coordinating) and HCAII (conserved). The asterisks denote those waters that superimpose between the two structures. The dashed lines represent hydrogen bonds from Cam residues to the Cam HCO_3^- molecule which corresponds to the gray distances. The solid lines represent hydrogen bonds from HCAII residues to HCAII HCO_3^- which correspond to the black distances.

of Gln75 and the hydroxyl of Thr199 are similarly situated relative to the respective metal- bound HCO_3^-, as is the amide of Asn202 and the backbone amide of Thr199. These comparative analyses further strengthen the proposed roles for Gln75 and Asn202 in Cam. [28-30].

2.5 Conclusions

This manuscript investigates roles for three active site residues, Gln75, Asn73, and Asn202, in the prototypic γ-class carbonic anhydrase, Cam, that were previously identified in crystal structures of that enzyme. Kinetic analysis of variants of these three residues revealed that Gln75 and Asn202 are important in catalysis and Asn73 plays a supportive role that enhances catalysis. The manuscript also provides a more complete catalytic mechanism constructed using the kinetic data presented in this manuscript as well as previously reported structural data. This proposed mechanism also illustrates a possible role for residue Glu62 not previously realized. As well, the manuscript lends to the mounting evidence that although the five classes of carbonic anhydrases evolved independently, at least for α-, β-, and γ-class carbonic anhydrases, evidences shows these carbonic anhydrases utilize a hydrogen bond network essential for catalysis.

2.6 Materials and Methods

Mutagenesis and Expression. Plasmid pBA1416NB, derived from plasmid pT7-7, encoding the sequence of Cam minus the 34-amino acid N-terminal secretory signal peptide was used as the starting plasmid for all site-directed mutagenesis experiments [16]. Mutations were introduced at positions encoding for amino acid residues 73, 75, and 202 using the site-directed mutagenesis kit, QuickChange by Stratagene (La Jolla, California). Mutations were confirmed by DNA sequencing of the plasmids. *Escherichia coli* strain BL21 (DE3) was transformed with the Cam variant plasmids which were then used to inoculate Luria-Bertani broth containing 100 μg/mL ampicillin.

Cells were grown at 37º C to an A_{600} of 0.6-0.8, and induced to overproduce Cam variants with the addition of 500 μM $ZnSO_4$ and isopropyl thiogalactopyranoside (IPTG) to a final concentration of 0.8 mM, followed by continued growth at 37º C for 4 h. Cells were harvested by centrifugation and stored frozen at -80ºC until lysis.

Purification and Reconstitution. Frozen cells were thawed and resuspended in 50 mM MOPS pH 7.5 buffer followed by two passes through a chilled French press at a pressure of 1000 lb/in.^{2} (1 lb/in.^{2} = 6.9 kPa). Cell lysate was centrifuged at 29000g for 45 min, followed by filtration of the supernatant through a 0.45 μm filter. This filtrate solution was then loaded onto a Q-Sepharose Fast Flow column (Amersham Pharmacia Biotech, Piscataway, New Jersey) and then washed with several column volumes of 50 mM MOPS pH 7.5 buffer. A gradient elution of 0 to 1.0 M NaCl was then applied over 6 column volumes. Cam variants typically eluted between 0.35-0.45 M NaCl. These fractions were pooled and diluted 2-fold with 3.0 M $(NH_4)_2SO_4$ in 50mM MOPS pH 7.5 buffer to give a final $(NH_4)_2SO_4$ concentration of 1.5 M. This solution was loaded onto a Phenyl Sepharose high-performance column (Amersham Pharmacia Biotech, Piscataway, New Jersey) previously equilibrated with 1.5 M $(NH_4)_2SO_4$ in 50 mM MOPS pH 7.5 buffer. The column was washed with several bed volumes of equilibration buffer. Using a decreasing salt gradient of 1.5 to 0 M $(NH_4)_2SO_4$ buffer, the Cam protein was eluted. Cam fractions were then pooled, desalted using a PD-10 desalting column (Amersham Pharmacia Biotech, Piscataway, New Jersey). Wild-type Cam and Cam variants were denatured then refolded in a series of metal free 25mM MOPS pH 7.5, 150mM KCL buffer exchanges. The refolded apo-enzyme was then reconstituted with either a cobalt or zinc ion, exclusively [24].

Gel Filtration Chromatography. A Superdex 75 high-resolution gel filtration column (Amersham Pharmacia Biotech, Piscataway, New Jersey) was equilibrated with 150 mM KCl, 50 mM MOPS pH 7.5 buffer. Each metal reconstituted Cam variant was loaded onto the size exclusion column and eluted using a flow rate of 1.0-mL/min. The eluting holoenzyme was detected by measuring the UV absorbance at a wavelength of 280 nm. The trimeric Cam fractions were pooled, concentrated, frozen in liquid nitrogen, and stored at -80º C. ICP analysis was conducted on all Cam variants to determine metal content (The Chemical Analysis Laboratory, University of Georgia, Athens, GA).

Steady-State Kinetic Measurements. Wild-type Cam and Cam variants were assayed for carbonic anhydrase activity by stopped-flow spectroscopy [31], using a model SF-2001 KinTek stopped-flow instrument (KinTek Corp., Austin, TX). The Cam variants protein concentration were determined by first measuring A_{280} of these protein solutions then using a theoretical extinction coefficient, 15990 M^{-1} cm^{-1} with a computed monomer molecular mass of 22 873 Da. Protein concentrations for wild type and variants are given based on the extinction coefficient of the Cam monomer. Enzyme monomer concentrations ranged from 400 nM to 6 μM. Buffer-indicator dye pairs used were MES and chlorophenol red (at pH 5.7-6.9) measured at a wavelength of 574 nm, MOPS and 4-nitrophenol (at pH 6.5-7.7) measured at a wavelength of 400 nm, and TAPS and m-cresol purple (at pH 7.7-9.1) measured at a wavelength of 578 nm. Buffer concentrations were 50 mM, the total ionic strength was adjusted to 50 mM with Na_2SO_4, and final pH indicator concentrations were 50 μM. Saturated solutions of CO_2 (32.9 mM in H_2O) were prepared by bubbling CO_2 gas into deionized water at 25º C. The experimental final CO2 concentrations were varied from 4.7 to 24mM. The initial 5-

10% of the total absorbance changes were used to calculate initial steady-state kinetic data used for kinetic analysis, using the average of 10-15 reaction traces per experiment. The initial rate data were fit to the Michaelis-Menten equation to obtain experimental values for k_{cat} and K_m. The pH-independent values of k_{cat} and pK_a for CO_2 hydration reaction were determined by fitting the experimental pH-dependent Michaelis-Menten parameter k_{cat} to Equ 4. The pH-independent values for k_{cat}/K_m and pK_a of the Gln 75 variants were also fit to Eq. **2.6**.

$$k_{cat}^{obs} = k_{cat}/(1+10^{(pK_a - pH)}) \qquad \text{(Equation 2.6)}$$

The pH-independent values for k_{cat}/K_m and pK_a for CO_2 hydration reaction of the Cam variants were determined by fitting the pH-dependent Michaelis-Menten parameter k_{cat}/K_m to Equ 5. Eq. **2.7**

$$k_{cat}/K_m^{obs} = (k_{cat}/K_m \times 10^{(pK_a^{II} - pH)} + k_{cat}/K_m^{II})/(1 + 10^{(pK_a^{II} + pK_a^{I} - 2pH)} + 10^{(pK_a^{I} - pH)} + 10^{(pK_a^{II} - pH)}) \qquad \text{(Equation 2.7)}$$

All fits described were done using Kaleidagraph (Synergy Software, Reading, PA). All kinetic parameters were adjusted to account for metal incorporation of each variant determined by ICP analysis.

UV/Visible Absorption Spectroscopy. Optical absorption spectra were obtained for wild-type Zn-Cam and Co-Cam as well as all generated variants at 25º C using a Beckman DU640 spectrophotometer (Beckman Instruments, Inc., Fullerton, California). All samples were desalted with a PD-10 desalting column (Amersham Pharmacia Biotech, Piscataway, NJ) and placed in 20mM MOPS buffer pH 7.0. All samples were assayed at a protein concentration of 1.1 mM. Difference spectra of wild-type and

variant proteins were generated by subtracting the absorbance spectra of the Zn-Cam and Zn-Cam variants from the absorbance spectra of the respective cobalt substituted protein.

2.7 References

1. Bottoni, A., et al., *New model for a theoretical density functional theory investigation of the mechanism of the carbonic anhydrase: How does the internal bicarbonate rearrangement occur?* Journal of the American Chemical Society, 2004. **126**(5): p. 1542-1550.
2. Tautermann, C.S., et al., *About the kinetic feasibility of the Lipscomb mechanism in human carbonic anhydrase II.* Journal of Physical Chemistry B, 2003. **107**(43): p. 12013-12020.
3. Liang, Z.W., et al., *Importance of the Conserved Active-Site Residues Tyr7, Glu106 and Thr199 for the Catalytic Function of Human Carbonic Anhydrase-Ii.* European Journal of Biochemistry, 1993. **211**(3): p. 821-827.
4. Krebs, J.F., et al., *Structural And Functional Importance Of A Conserved Hydrogen-Bond Network In Human Carbonic Anhydrase-Ii.* Journal of Biological Chemistry, 1993. **268**(36): p. 27458-27466.
5. Krebs, J.F. and C.A. Fierke, *Determinants Of Catalytic Activity And Stability Of Carbonic Anhydrase-Ii As Revealed By Random Mutagenesis.* Journal of Biological Chemistry, 1993. **268**(2): p. 948-954.

6. Kimber, M.S., and Emil F.Pai, *The active site architecture of Pisum sativum β–carbonic anhydrase is a mirror image of that of a-carbonic anhydrases.* EMBO Journal, 2000. **19**(7): p. 1407-1418.

7. Rowlett, R.S., et al., *Kinetic And Structural Characterization Of Spinach Carbonic-Anhydrase.* Biochemistry, 1994. **33**(47): p. 13967-13976.

8. Rowlett, R.S., et al., *Examination of the role of Gln-158 in the mechanism of CO2 hydration catalyzed by beta-carbonic anhydrase from Arabidopsis thaliana.* Archives of biochemistry and biophysics, 2004. **425**(1): p. 25-32.

9. Campbell, I.D., and Raymond A. Dwek, *Biological Spectroscopy*, in *Biological Spectroscopy*, P. Elias, Editor. 1984, The Bengamin/Cummings Publishing Company, Inc. p. 61-73.

10. Alber, B.E. and J.G. Ferry, *A Carbonic-Anhydrase From The Archaeon Methanosarcina-Thermophila.* Proceedings of the National Academy of Sciences, 1994. **91**(15): p. 6909-6913.

11. Iverson, T.M., Birgit E. Alber, Caroline Kisker, James G. Ferry, and Douglas C. Rees, *A Closer Look at the Active Site of y-class Carbonic anhydrases: High-Resoluation Crystallographic STudies of the Carbonic Anhydrase from Methanosarcina thermophila.* Biochemistry, 2000. **39**: p. 9222-9231.

12. Tripp, B.C. and J.G. Ferry, *A structure-function study of a proton transport pathway in the gamma-class carbonic anhydrase from Methanosarcina thermophila.* Biochemistry, 2000. **39**(31): p. 9232-9240.

13. Merz, K.M., *Insights into the function of the zinc hydroxide-Thr199-Glu106 hydrogen bonding network in carbonic anhydrases.* Journal of Molecular Biology, 1990. **214**: p. 799-802.

14. Kim, Y.M. and S. Han, *Peroxynitrite inactivates carbonic anhydrase II by releasing active site zinc ion.* Bulletin of the Korean Chemical Society, 2004. **25**(5): p. 711-714.

15. Mauksch, M., et al., *New insights into the mechanistic details of the carbonic anhydrase cycle as derived from the model system (NH3)(3)Zn(OH) (+)/CO2: How does the H_2O/HCO_3^- replacement step occur?* Chembiochem, 2001. **2**(3): p. 190-198.

16. Alber, B.E. and J.G. Ferry, *Characterization of heterologously produced carbonic anhydrase from Methanosarcina thermophila.* Journal of Bacteriology, 1996. **178**(11): p. 3270-3274.

17. Cronk JD, E.J., Cronk MR, O'Neill JW, Zhang KY., *Crystal structure of E. coli beta-carbonic anhydrase, an enzyme with an unusual pH-dependent activity.* Protein Science, 2001. **5**: p. 911-22.

18. Huang S, X.Y., Sauer-Eriksson E, Chirica L, Lindskog S, Jonsson BH., *Crystal structure of Carbonic Anhydrase from Neisseria gonorrhoeae and its complex with inhibitor acetozolamide.* Journal of Molecular Biology, 1998. **283**(1): p. 301-10.

19. Krebs JF, R.F., Dluhy RA, Fierke CA., *Kinetic and spectroscopic studies of hydrophilic amino acid substitutions in the hydrophobic pocket of human carbonic anhydrase II.* Biochemistry, 1993. **32**(17): p. 4496-505.

20. Mitsuhashi S, M.T., Yamashita E, Yamamoto M, Kumasaka T, Moriyama H, and M.S. Ueki T, Tsukihara T., *X-ray structure of beta-carbonic anhydrase from the red alga, Porphyridium purpureum, reveals a novel catalytic site for CO_2 hydration.* journal of Biological Chemistry, 2000. **275**(8): p. 5521-6.

21. Nair SK, C.D., *Crystallographic studies of azide binding to human carbonic anhydrase II.* European Journal of Biochemistry, 1993. **213**(1): p. 507-15.

22. Saito, R., et al., *Structure of bovine carbonic anhydrase II at 1.95 angstrom resolution.* Acta crystallographica. Section D, Biological crystallography, 2004. **60**: p. 792-795.

23. Strop, P., et al., *Crystal structure of the "cab"-type beta class carbonic anhydrase from the archaeon Methanobacterium thermoautotrophicum.* Journal of Biological Chemistry, 2001. **276**(13): p. 10299-10305.

24. Alber, B.E., et al., *Kinetic and spectroscopic characterization of the gamma-carbonic anhydrase from the methanoarchaeon Methanosarcina thermophila.* Biochemistry, 1999. **38**(40): p. 13119-13128.

25. Håkansson, K., Carlsson, M., Svensson, L. A., and A. Liljas, *Structure of native and apo carbonic anhydrase II and structure of some of its anion-ligand complexes.* Journal of Molecular Biology, 1992. **227**: p. 4.

26. Lindskog, S. and A. Liljas, *Carbonic-Anhydrase and the Role of Orientation in Catalysis.* Current Opinion in Structural Biology, 1993. **3**(6): p. 915-920.

27. Thoms, S., *Hydrogen bonds and the catalytic mechanism of human carbonic anhydrase II.* Journal of Theoretical Biology, 2002. **215**(4): p. 399-404.

28. Park, H., B. Song, and F.M.M. Morel, *Diversity of the cadmium-containing carbonic anhydrase in marine diatoms and natural waters.* Environmental Microbiology, 2007. **9**(2): p. 403-413.

29. Lane, T.W., et al., *Isolation and Characterization of a Cadmium Carbonic Anhydrase from a Marine Diatom.* Nature, 2005. **42**.

30. Lane, T.W. and F.M.M. Morel, *A biological function for cadmium in marine diatoms.* Proceedings of the National Academy of Sciences, 2000. **97**(9): p. 4627-4631.

31. Khalifah, R.G., *The carbon dioxide hydration activity of carbonic anhydrase I. Stop-flow kinetic studies on the native human isoenzymes B and C.* Journal of Biological Chemistry, 1971. **246**(8): p. 2561-2573.

Chapter 3

CamH a γ-class isozyme with properties distinct from the prototypic member, Cam

3.1 Summary

Although many putative γ-class CA homologs have been identified throughout all three domains of life, the prototypic member (Cam) still remains the only γ-class CA shown to possess CA activity. Now, a second γ-class homolog, CamH, found in *Methanosarcina thermophila* has begun to be characterized and shown to possess CA activity albeit to a much lower extent compared with the first characterized γ-class member. CamH lacks the N-terminal 34 amino acid leader peptide present in Cam, suggesting CamH remains in cytosol. The significantly lower turnover number exhibited by CamH may be due to absence of the acidic loop and Glu84, which has been identified in Cam to play a key role in proton transfer. At this initial stage, it is not readily known whether a proton shuttle residue exists in CamH.

3.2 Introduction

Carbonic anhydrases (CAs) are metalloenzymes that catalyze the reversible hydration of carbon dioxide (CO_2) to bicarbonate (HCO_3^-) [1, 2]. Currently there are five independently evolved classes (α, β, γ, δ, and ζ) of CAs. The prototypic γ-class CA (Cam) is the only characterized member shown to have CA activity. Putative γ-class

homologs have been identified throughout the three domains of life [3-5]. A handful of γ-class homologs have been purified; however, none have been shown to exhibit any in detectable CA activity [5, 6]. The *M. thermophila* genome was recently sequenced identifying a second putative γ-class homolog, termed *camH*, bearing 96% similarity to the *cam* gene (Figure **3.1**). Preliminary characterization of heterologously produced CamH reveals that CamH possesses CA activity albeit significantly less activity than Cam. Thus, CamH is the first γ-class homolog shown to possess CA activity. Here, I present the initial biochemical characterization and kinetic analysis of CamH. Also, I compare the characteristics of Cam and CamH to which increase the biochemical and physiological understanding of the γ-class and CAs in general.

3.3 Results

3.3.1 Sequence Comparison and Model of CamH

Genomic analysis of *M. thermophila* revealed two CA genes are encoded that are related but distinct from one another [7, 8]. One CA has been characterized, representing the prototypic γ-class CA, Cam. The second gene encodes for a putative γ-class CA that is 96% similar to Cam, termed CamH or Cam Homolog. No apparent signal peptide is present in the CamH sequence, suggesting CamH is cytosolic. Amino acid sequence comparison of CamH *vs*. Cam revealed that CamH possess the heptapeptide repeat

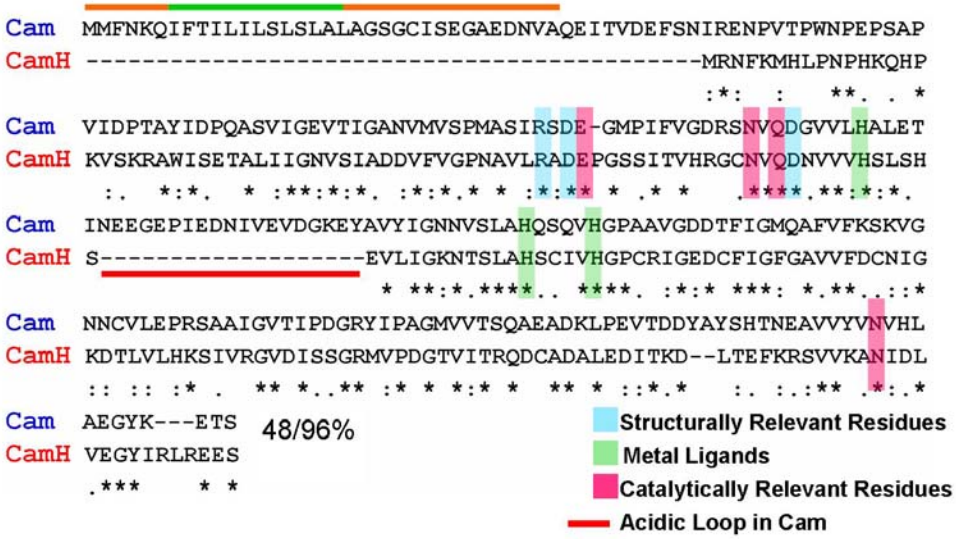

Figure 3.1**: Amino Acid Sequence Alignment of Cam vs. CamH using CLUSTAL X (1.83) multiple sequence alignment.**

CamH is aligned against Cam amino acid sequence including the N-terminal 34 amino acid signal peptide [3] depicted by the orange/green line. The orange regions are hydrophilic whereas the green region represents the hydrophobic area. The red highlighted residues represent the conserved catalytically relevant residues. The green highlighted residues represent the conserved metal ligands. The blue highlighted residues denote those residues proposed to be structurally relevant in Cam. The red line reflects the acidic loop that houses the proton shuttle residue Glu84 present in Cam.

characteristic of a left-handed β-helical fold as well as residues Arg59, Asp61 and Asp76 (Figure **3.1**) that were previously shown to be structurally relevant in Cam [9]. In addition, the three histidines (His81, His117, and His122), which ligate the catalytic metal cofactor in Cam. The presence of these histidines in CamH suggests a metal is ligated in a similar fashion in CamH. Even residues shown to be catalytically relevant in Cam (Gln75, Asn202, Asn73, and Glu62) are conserved in CamH (Figure **3.1**) [10, 11]. However, CamH does lack the acidic loop (denoted by dashes in Figure **3.1**) that houses the proton shuttle residue (PSR), Glu84, in Cam.

A CamH model was constructed (Figure **3.2**) by threading the CamH sequence onto the solved crystal structure of a Cam monomer [12, 13]. The oligomerzation state of a handful of identified γ-class homologs [5, 6] is not currently known; however the prototypic γ-class CA, Cam is trimeric and initial biochemical analysis (Figure **3.4**) suggests CamH is also trimeric [3, 14]. Superimposition of the Cam structure and the CamH model active sites are consistent with one another with the exception of Cam residue Glu84. CamH lacks the acidic loop containing the PSR, Glu84, characterized in Cam [10]. The similarities between Cam and the model of CamH indicate CamH may have CA activity although the catalytic mechanism may differ between Cam and CamH. Further structural investigations of CamH will expand the understanding of the entire γ-class.

3.4 Expression and Characterization of Heterologously Produced CamH

Western blot analysis of *M. thermophila* cell extract grown on acetate revealed two bands that cross reacted with the *anti*-Cam antibody [14]. The higher molecular weight band is Cam while it is unknown what protein is responsible for the second band. The most intriguing proposal suggested this second lower molecular band represented a second CA in *M. thermophila* [14]. Subsequent genomic analysis confirmed the presence of two distinct but related CA genes [8]. One CA gene represents Cam while the second CA gene encodes for a putative γ-class CA, *camH*, which bears 96% similarity to Cam.

The *camH* gene encodes codons not recognized in *Escherichia coli*; therefore, *camH* was cloned from the *M. thermophila* genome into a protein expression vector and

transformed into *E. coli* strain Rosetta (DE3) pLysS, which contains a plasmid that encodes tRNAs that recognize these rare codons. CamH was solubly produced with final yields of 20 mg of purified CamH/L of cell culture. N-terminal analysis of

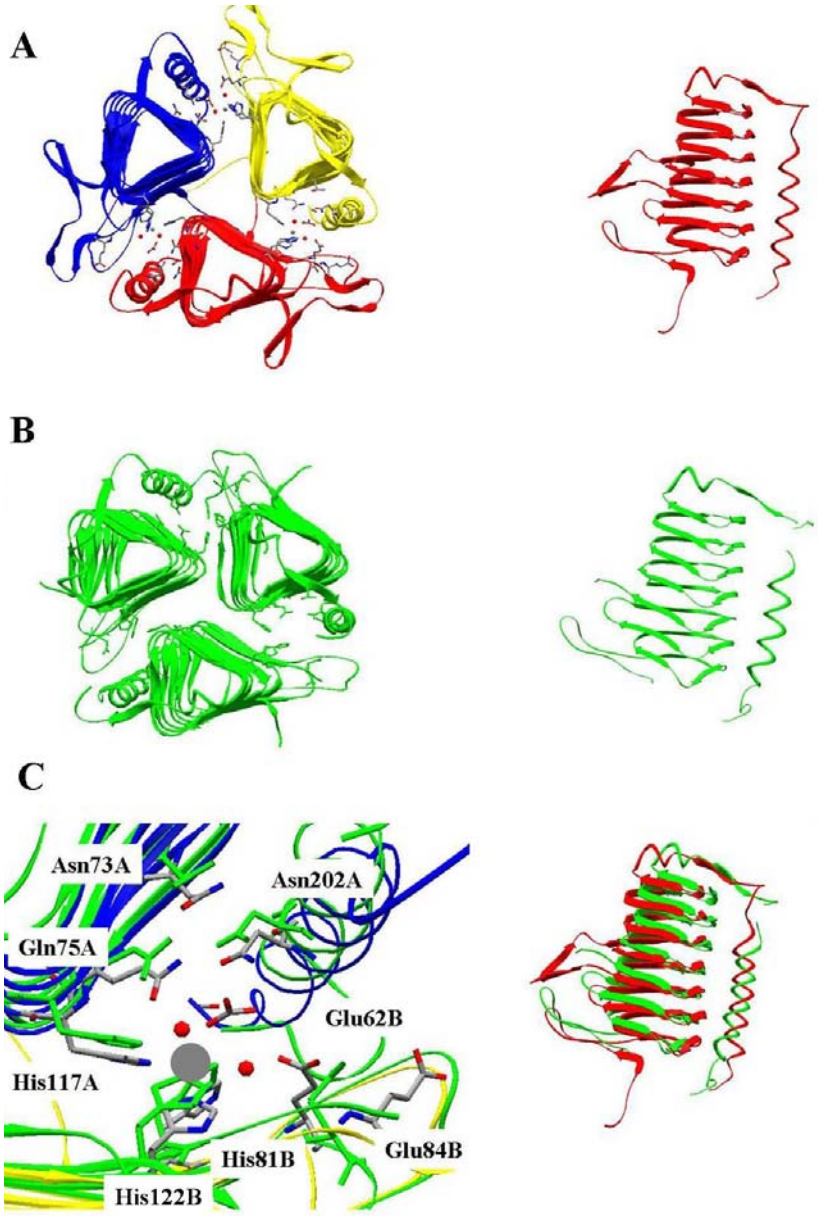

Figure 3.2**: Structural Comparison of Cam vs. CamH model.**

A) Cam holoenzyme shown as a trimer and a single subunit. B) A model of CamH was produced by threading the CamH sequence onto the solved Co-Cam structure. CamH is shown as a trimer based on CamH size-exclusion chromatogram data as well as a subunit of CamH model monomer. C) Cam and CamH superimposed active site. Blue refers to Cam monomer A while yellow refers to Cam monomer B. Green depicts the CamH model. CamH residues are also modeled in green while Cam residues are in gray. Superimposed Cam and CamH monomers. Cam is represented in red and CamH is represented in green. All structures and models were produced using DeepView/Swiss-PdbViewer v3.7.

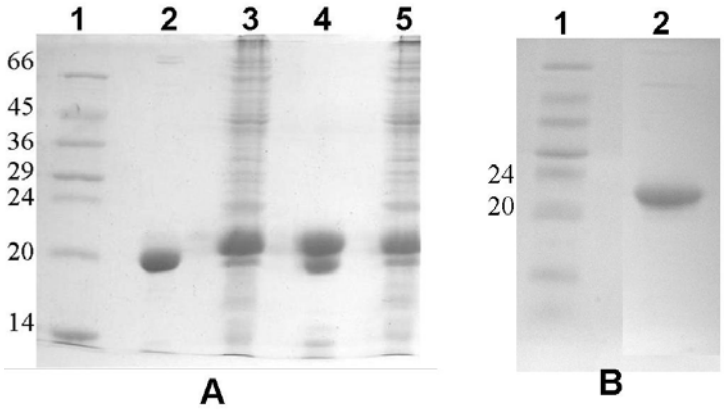

Figure 3.3**: Zn-sup CamH and Fe-sup CamH**

15% SDS-PAGE separating CamH protein preparations. Roughly 10 μg of sample were loaded into each lane. (Panel A) Lane 1) Low-weight Molecular Markers (Sigma). Lane 2) Anaerobically purified Fe-sup CamH in the presence of 1 mM DTT. Lane 3) CamH induced for 16h at 16ºC with 1 mM IPTG and supplemented with 200μM $FeSO_4$. Lane 4) Purified Zn-sup CamH in the absence of 1 mM DTT. Lane 5) CamH induced for 16h at 16º C with 1 mM IPTG and supplemented with 200μM $ZnSO_4$. (Panel B) Lane 1) Low-weight Molecular Markers (Sigma). Lane 2) Zn-sup CamH aerobically purified in the presence of 1 mM DTT.

heterologously-produced CamH (Met-Lys-Arg-Asn-Phe-Lys-Met-His-Leu-Pro-Asn-Asn-His-Lys-Gln-His-Pro) was identical to the first fifteen amino acid residues of the *M. thermophila* CamH sequence.

CamH was produced under two conditions. At induction, the cell cultures were either exclusively supplemented with 500 μM $ZnSO_4$ or 200 μM $FeSO_4$ to result in a Zn-sup CamH or Fe-sup CamH preparation, respectively. Regardless of metal supplement, similar amounts of soluble protein were produced (Panel A, Lane 3 and 4, Figure **3.3**).

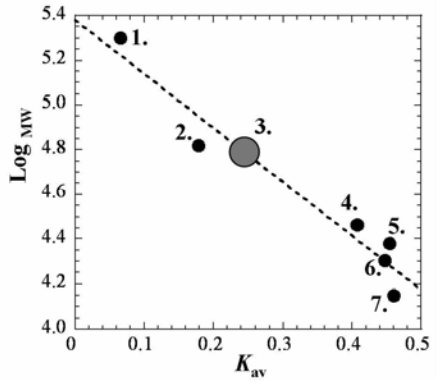

	Protein	MW (kDa)
1.	Blue Dextran	200
2.	Bovine Serum Albumin	66
3.	CamH	62.1
4.	Bovine Carbonic Anhydrase	29
5.	Chymotrypsin	24
6.	Trypsin Inhibitor (Soybean)	20.1
7.	α-Lactalbumin	14.2

Figure 3.4**: Size determination of CamH using standards separated on a Superdex 75 size exclusion column**.

Size-exclusion chromatography (SEC) was conducted at 25º C in 50 mM TAPS, pH 8.5 and 1 mM DTT. Both metal supplements resulted in similar elution values. An average of four SEC experiments using Zn-and Fe-sup CamH is presented here.

Both heterologously produced enzymes were purified to apparent homogeneity (Panel A, Lane 2 and 4, Figure **3.3**). Zn-sup CamH was aerobically purified in the absence of thiol reductant 1 mM dithiothreitol (DTT) migrating as a doublet in a 15% SDS-PAGE gel (Panel A, Lane 4, Figure **3.3**). Fe-sup CamH was purified under strict anaerobic conditions in the presence of 1 mM DTT, migrating as a single band in a 15% SDS-PAGE gel (Panel A, Lane 2, Figure **3.3**). The Zn-sup CamH preparation was aerobically re-purified in the presence of 1 mM DTT. This Zn-sup CamH preparation migrated as a single band in 15% SDS-PAGE gel (Panel B, Lane 2, Figure **3.3**) and is the preparation used for further biochemical assays.

The estimated subunit molecular mass (~22 kDa) from a 15% SDS-PAGE gel of both purified CamH preparations correlated well to the calculated CamH subunit mass of

Table **3.1**: Summary of the Metals Analysis and Free Thiols for CamH Preparations

CamH Preparation	Metal supplementation	Metal Content[a]		Thiol Quantification[a]	
		ICP-Analysis			
		molar ratio/monomer		# of Cysteines/Monomer	
		Fe	Zn	As purified	Unfolded
Anaerobic Purification	$FeSO_4$	0.13 ± 0.01	0.009 ± 0.001	1.7 ± 0.30	6.2 ± 0.6
Aerobic Purification	$ZnSO_4$	0.15 ± 0.05	0.71 ± 0.2	1.9 ± 0.2	5.9 ± 0.3

[a] Presented values are the averages of three separate trials

20.3 kDa. Size exclusion chromatography (SEC) was conducted on both metal preparations of CamH. Elution volumes of Zn- and Fe-sup CamH from a SEC column estimated a molecular mass of ~62 kDa, suggesting the CamH holoenzyme is trimeric (Figure **3.4**).

Sequence comparisons between Cam and CamH reveal that six cysteines present in CamH that are distinct from the one cysteine present in Cam (Figure **3.1**). The CamH cysteines were quantified using the DTNB (5,5'-dithio-*bis*-(2-nitrobenzoic acid)) assay (Table **3.1**) to ascertain if any of these cysteines exists as free thiols. In as-purified Zn- and Fe-sup CamH, only 2 cysteines appear accessible to DTNB (Table **3.1**). Upon denaturation in the presence of 4M guanidine hydrochloride, all six cysteines interacted with DTNB, indicating that all six cysteines exist in the reduced state in CamH albeit four cysteines appear inaccessible in the CamH holoenzyme.

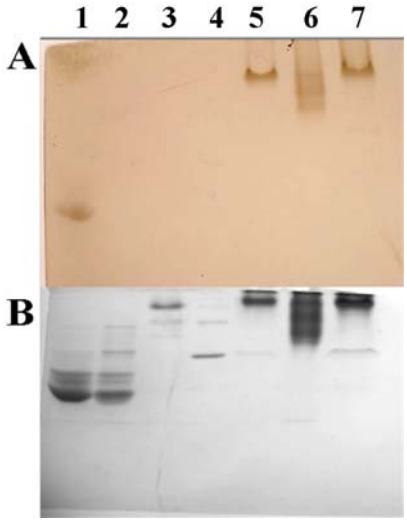

Figure 3.5**: Qualitative determination of iron in CamH.**

10% non-denaturing PAGE gel A) Iron stained with 3,5-Diaminobenzoic acid, hydrogen peroxide, 50 mM Na-acetate, pH 5.0, B) Coomaisse Brilliant Blue stained. Although a smaller molecular weight than Cam, CamH exhibits retarded migration due it is highly basic nature. Iron detection limit using this technique is 5ng/mL [15]. Lane 1, 20 μg Fe-reconstituted Cam [16]. Lane 2, 20 μg Zn-reconstituted Cam [11]. Lane 3, 10 μg α-class bovine CAII. Lane 4, 10 μg bovine serum albumin (Sigma). Lane 5, 20 μg anaerobically purified Fe-sup CamH. Lane 6, 20 μg aerobically purified Zn-sup CamH. Lane 7, 20 μg anaerobically purified Fe-sup Cam exposed to air for 30 min.

Cam was shown to be an iron enzyme [16] suggesting that at least some of the γ-class CAs may be iron enzymes. Therefore, CamH was analyzed for metal content. Metal content of the Zn-and Fe sup CamH was quantitatively determined by inductively coupled plasma (ICP) atomic emission spectroscopy (Table **3.1**). ICP analysis revealed that Zn-sup CamH possessed 0.7 Zn molar ratio/monomer and 0.15 Fe molar ratio/monomer. Anaerobically purified Fe-sup CamH possessed a 0.13 Fe molar ratio/monomer and 8.8 x 10^{-3} Zn molar ratio/monomer. More experiments are needed to conclude whether CamH is an iron enzyme like Cam. Though, the presence of similar

iron amounts, regardless of metal supplementation or purification conditions, is consistent with an iron preference in CamH.

Fe-content was also investigated using an in-gel iron stain (Figure **3.5**) [15]. A gel-staining technique was conducted to determine if the iron present in CamH was directly associated with the enzyme [15]. Iron was shown to be directly associated with both the Fe- and Zn-sup CamH (Panel A, Figure **3.5**) and not residual as a result of purification protocols. Although Zn-sup CamH appears to aggregate in the gel, (Lane 6, Figure **3.5**) Zn-sup CamH remains soluble over long exposure times on ice and at room temperature in air. In addition, Zn-sup CamH also remains soluble upon one freeze/thaw cycle. Conversely, Fe-sup CamH readily precipitates upon exposure small amounts of oxygen, room temperature and freeze/thawing.

3.4.1 Initial Characterization of CamH CA activity

Preliminary biochemical characterization revealed many similar characteristics between Cam and CamH. However, the main question remained: does CamH possess CA activity? CA activity was first qualitatively assayed using a simple in-gel method [17]. Samples of the Zn- and Fe-sup CamH were separated by mass and charge on 10% non-denaturing gels and then stained with 0.1% thymol blue, a pH indicator dye. After a ten minute exposure to CO_2 (g), both Zn- and Fe-sup CamH exhibited CA activity, indicated by a green/yellow clearing on the gel associated with the protein band (Panel A, Figure **3.6)**. The lack of resolution of the clearing on the gel is due to diffusion of the protons through the polyacrylamide gel, interacting with the 0.1% thymol blue pH indicator.

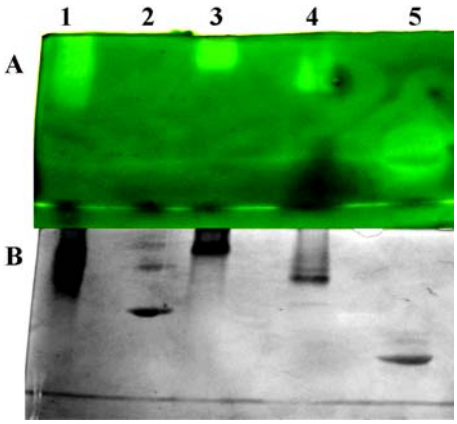

Figure 3.6**: Qualitative Determination of Carbonic Anhydrase Activity.**

10% non-denaturing gel A) stained with 0.1% thymol blue and exposed to CO_2 (g), B) the same gel stained with Coomaisse Brilliant Blue. The light green/yellow clearing seen in Panel A is a result of H^+ accumulation from the hydration of CO_2 to HCO_3^- and H^+. 10 μg of protein was added to each lane. Lane 1, Aerobically purified Zn-sup CamH. Lane 2, Bovine serum albumin (Sigma). Lane 3, Anaerobically purified Fe-sup CamH. Lane 4, Bovine α-class CAII [16]. Lane 5, Fe-Cam.

To date, CAs were shown to bind the universal CA inhibitor, 5-dimethylaminonaphthalene-1-sulfonamide (DNSA) [18]. In the α-class CAs, the sulfonamide moiety directly binds to the metal, replacing the metal bound hydroxide. The oxygens on the sulfonamide group are further stabilized by active site residues, Thr199 and Glu106 [19]. Free DNSA does not possess any inherent fluorescence; however, bound DNSA exhibits fluorescence when excited in the UV range [20]. In the α-class CAs, the fluorescence intensity correlates with the amount of bound DNSA to the enzyme's metal cofactor, in a 1:1 ratio [18]. DNSA may behave in a similar manner in the γ-class in which the DNSA replaces the metal bound hydroxide, directly binding to the γ-class metal cofactor.

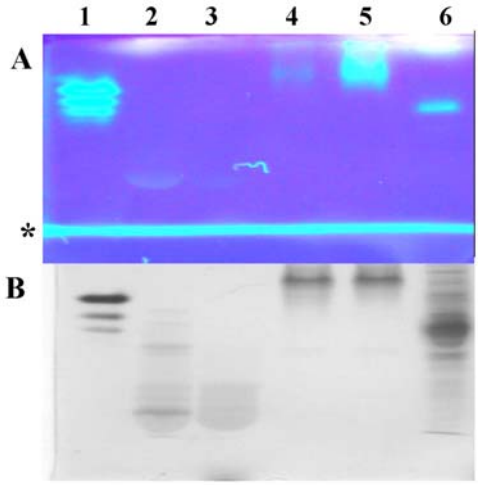

Figure 3.7**: Determining if Fluorescent inhibitor, dansylamide (DNSA), binds to γ-CAs.**

10% non-denaturing gel. *The bright line in Panel A is the dye front. (A) UV illuminated (B) Coomaisse stained. DNSA (6mM) was incubated at 37 ºC for 1 hour with 40μg of protein with the exception of α- class bovine CAII where 60μM DNSA was used. Lane 4, the incubation was done at RT in an anaerobic glove bag. . Lane 1, α-class bovine CAII. Lane 2, Zn-Cam. Lane 3, Fe-Cam. Lane 4, anaerobically purified Fe-sup CamH incubated with DNSA *AEROBICALLY*. Lane 5, anaerobically purified Fe-sup CamH incubated with DNSA A*NAEROBICALLY*. Lane 6, aerobically purified Zn-sup CamH.

DNSA binds weakly to both Zn-and Fe-Cam indicated by the weak fluorescence (Panel A, Lane 2 and 3, Figure **3.7**). Conversely, DNSA bound to CamH exhibits a much higher fluorescence (Panel A, Lane5 and 6, Figure **3.7**). Increased fluorescent intensity was observed when DNSA was anaerobically incubated with the Fe-sup CamH compared to the fluorescent intensity when DNSA was aerobically incubated with Fe-sup CamH. Similar to what occurs in α-class CAs [18], DNSA may directly bind to the catalytic metal in CamH and may not have access to oxidized iron once Fe-Sup CamH once the Fe is exposed to air (Lane 4 and 5, Figure **3.7**). The fluorescence intensity of DNSA incubated Zn-sup CamH is comparable (Panel A, Lane 6, Figure **3.7**) to that of

anaerobically incubated DNSA with Fe-sup CamH further supporting that DNSA may directly bind to the metal. More detailed characterization of DNSA inhibition is needed in Cam and CamH to better understand the mechanism of inhibition. DNSA inhibition may differ in Cam than CamH as suggested by the different DNSA fluorescent characteristics between the two enzymes.

3.4.2 Initial Kinetic Analysis of CamH

Catalytically relevant residuesGln75, Asn73, Glu62 and Asn202 are conserved in the CamH amino acid sequence (Figure **3.1**.) However, Glu84, the PSR in Cam, is absent in the CamH sequence. No apparent nearby residue in the amino acid sequence alignment appears able to substitute as the PSR suggesting that CamH may exhibit a turnover $\leq 10^3$ s^{-1} [10, 21-23]. The CA activity of CamH was shown qualitatively assayed using stopped flow spectroscopy [24]. Steady-state parameters of CamH are shown in Table **3.2**. The subscript ***eff*** denotes kinetic parameters adjusted for the actual amount of metal incorporation in the enzyme.

Compared to Zn- or Fe-Cam, both Zn- or Fe-sup CamH exhibited drastically lower kinetic parameters (Table **3.2**). Zn-sup CamH, according to ICP analysis (Table **3.1**), can be considered the most "reconstituted" CamH preparations; however, Zn-sup CamH exhibited the least amount of CA activity (Table **3.2**). The less "reconstituted" Fe-sup CamH only had 0.13 Fe ratio/monomer associated with the enzyme, but exhibited a ten-fold increase in k_{cat} and k_{cat}/K_m (Table **3.2**).

Table **3.2**: Michaelis-Menten Steady-State Kinetic Parameters for Wild-type Cam and CamH. Assays were Performed using Stopped-Flow Spectroscopy at 25° C

	K_m (mM)	k_{cat} (ms^{-1})	k_{cat}/K_m ($M^{-1}\ s^{-1}$)	k_{cat}^{eff} (ms^{-1})	k_{cat}/K_m^{eff} ($M^{-1}\ s^{-1}$)	Metal/ monomer
WT Zn-Cam[a]	15.6 ± 0.8	116.4 ± 3.0	7.5± 0.6	70.2 ± 7.8	4.4 ± 0.5	1.2
WT Fe-Cam[a]	44.8 ± 7.4	231.4 ± 20.4	40.9 ± 2.1	235.1 ± 22.8	54.4 ± 15.5	0.97
Zn-sup CamH[b]	3.1 ± 0.1	0.493 ± 0.002	0.16 ± 0.03			0.7 (Zn) 0.15 (Fe)
Fe-sup CamH[c]	1.6 ± 0.4	7.1 ± 0.2	4.6 ± 0.6	54.4 ± 1.8	35.2 ± 4.8	0.13 (Fe)
Fe-sup CamH[d] Imid. (50mM)	8.0 ± 1.7	24.2 ± 1.9	3.0 ± 0.9	151.4 ± 11.6	19.0 ± 5.5	0.13 (Fe)

[a] Previously published (Zimmerman et. al, 2006)
[b] Zn-sup CamH aerobically purified and aerobically assayed in 50mM HEPES, pH 7.5
[c] Fe-sup CamH anaerobically purified and anaerobically assayed in 50 MM HEPES, pH 7.5
[d] Fe-sup CamH anaerobically purified and anaerobically assayed in 50 mM Imidazole, Ph 7.5

When the Fe-sup CamH kinetic parameters were adjusted for the amount of Fe incorporated, the catalytic efficiency of Fe-sup CamH was comparable to the catalytic efficiency of wild-type Fe-Cam (Table **3.2**), although the turnover number was still four-fold lower in Fe-sup CamH than in wild-type Fe-Cam. One possible reason for the lower k_{cat} in Fe-sup CamH may be attributed to the absence of the acidic loop that includes the PSR, Glu84, shown to enhance turnover number in Cam [10]. In fact, when Fe-sup CamH is assayed in the presence of the exogenous proton acceptor, imidazole, less than a fold difference is observed between k_{cat} of Fe-sup CamH and wild-type Fe-Cam (Table **3.2**.).

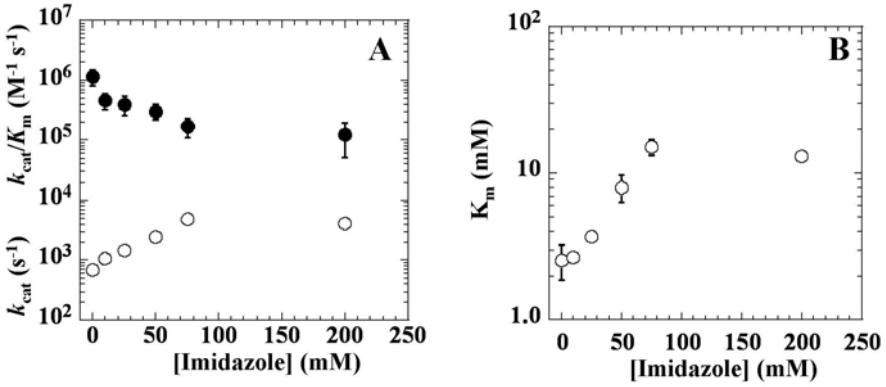

Figure 3.8**: Plot of imidazole dependence of steady-state kinetic parameters for Fe-sup CamH.**

A) k_{cat} and k_{cat}/K_m. B) K_m. The imidazole concentration was varied from 0 to 200 mM. At each imidazole concentration; samples were assayed at 25º C at pH 7.5.

In Cam, lower activity was also observed when the enzyme was reconstituted with Zn compared to the observed activity with Fe-Cam (Table **3.2**) [16]. The higher activity observed with Fe coupled with the apparent strong preference for Fe in Cam demonstrated that Fe is most likely the physiological metal for Cam [16]. In CamH, lower activity when Zn is present is consistent with Zn as the least efficient metal in CamH. Like Cam, similar amounts of Fe were detected in CamH preparations regardless of metal supplementation or purification conditions is consistent with an Fe preference in CamH. In addition, the higher activity observed with Fe supports Fe as the physiological metal for CamH.

Imidazole is a chemically reactive (pK_a ~6.8) buffer molecule that is used to rescue proton transfer, *in vitro*, in CAs that lack a PSR or in situations where the PSR is compromised by site-directed mutagenesis [10, 25-29]. The relatively small imidazole

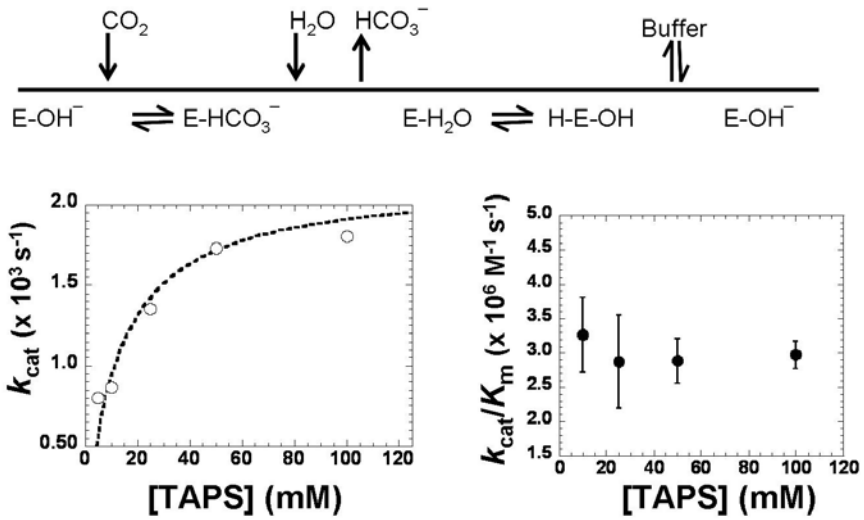

Figure 3.9**: The buffer dependence of CO_2 hydration catalysis of Fe-sup CamH.**

The Cleland diagram at the top of figure describes the ping-pong mechanism. Fe-sup CamH (1μM final concentration) was anaerobically assayed, via stopped-flow spectroscopy, at pH 8.2, 25º C. CO_2 concentration was varied from 4.7 to 24 mM and TAPS concentration was varied from 5 to 100 mM. K_m(TAPS) = 10.3 ± 0.2 mM and k_{cat} (max) = 1.9 x 10^3 ± 0.01 s^{-1}. Both kinetic parameters were determined by fitting the observed initial rates to the Michaelis-Menten equation.

buffer molecule enters CAs' active site to act as an exogenous proton acceptor. If imidazole is able to enhance k_{cat} of CAs, this is considered strong evidence that proton transfer is rate-limiting [23, 28, 30]. Fe-sup CamH was assayed under increasing amounts of imidazole (Figure **3.8**). As the imidazole concentration increases, the Fe-sup CamH turnover number also increased. The Fe-sup CamH k_{cat} is only dependent on imidazole concentration up 75 mM (Figure **3.8**), suggesting at saturating imidazole conditions (>75 mM) (Figure **3.8**) intermolecular proton transfer may no longer be rate limiting. The decrease in Fe-sup CamH k_{cat}/K_m most likely is due to the increase in the Michaelis-Menten constant (K_m) (Figure **3.8**). Inhibition of k_{cat}/K_m by

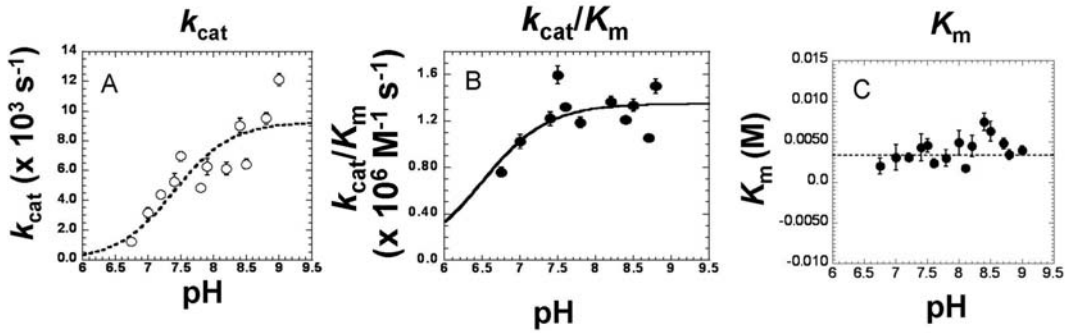

Figure 3.10**: pH profile of steady-state parameters for anaerobically purified Fe-sup CamH.**

All assays were conducted anaerobically. A) k_{cat}. B) k_{cat}/K_m. C) K_m.

imidazole has been observed in similar experiments with other CAs [10, 23, 25-28]. It is thought that most likely imidazole is binding near the metal or in the vicinity of CO_2 binding, thus impeding CO_2 hydration.

The dependence of CO_2 hydration on buffer substantiates the ping-pong mechanism (Figure **3.9**). The Fe-sup CamH steady-state parameter, k_{cat}, is dependent on the concentration of TAPS in a saturating manner at pH 8.2 (Panel A, Figure **3.9**). An apparent K_m(TAPS) was determined to be 10.3 ± 0.2 mM. This result strongly suggests CO_2 hydration is facilitated by a ping-pong mechanism in which buffer acts as the second substrate, accepting a proton from Fe-sup CamH. In addition, k_{cat}/K_m was not dependent on buffer (Panel B, Figure **3.9**), consistent with CamH participating in a two-step isomechanism in which the interconversion of CO_2 to HCO_3^-, represented by k_{cat}/K_m, is independent from the second proton transfer step.

The pH dependence of catalysis was determined for Fe-sup CamH in the pH range of 6.75 to 9.0 (Figure **3.10**). At pH < 6.75, Fe-sup CamH was not assayed as a

Table **3.3**: pH-Independent Michaelis-Menten Kinetic Parameters Obtained from the pH Dependence of CO_2 Hydration Catalyzed by Wild-Type Cam, and CamH.

[a] Parameters	Cam		Fe-sup CamH
	Zn-Cam[#]	Co-Cam[#]	
k_{cat} (ms^{-1})	61.2 ± 0.1	104.3 ± 0.2	7.4 ± 0.1
pK_a (k_{cat})	6.8 ± 0.1	6.5 ± 0.1	7.3 ± 0.02
pK_a^{I} (k_{cat}/K_m^{I})	6.9 ± 0.1	6.7 ± 0.1	6.6 ± 0.4
pK_a^{II} (k_{cat}/K_m^{II})	8.2 ± 0.3	8.4 ± 0.2	NA[b]
k_{cat}/K_m^{I} (mM^{-1} s^{-1})	3.3 ± 0.5	5.3 ± 0.5	1.3 ± 0.01
k_{cat}/K_m^{II} (mM^{-1} s^{-1})	6.1 ± 0.5	15.1 ± 1.4	NA[b]

[a] pH-independent kinetic parameters and pK_a values for CO_2 hydration were determined by fitting pH-dependent k_{cat} and k_{cat}/K_m data obtained over the pH range of 6.75-8.8 as described in Materials and Methods.
[b] The kinetic parameter, k_{cat}/K_m, of CamH is dependent on a single pK_a, whereas, in Cam, k_{cat}/K_m is dependent on two pK_a's. NA- Not Applicable
[#] Values from (Alber et. al,1999)

result of protein precipitation. The steady-state parameter k_{cat} for CO_2 hydration for Fe-sup CamH was dependent on a single ionization with a pK_a of 7.3 (Table **3.3**). No significant change in the Michaelis-Menten constant (K_m) for CO_2 (Panel C, Figure **3.10**) was observed. The steady-state parameter k_{cat}/K_m is also dependent on a single ionization in Fe-sup CamH with an extrapolated pK_a of 6.6 (Table **3.3**). The pH dependency of Fe-sup CamH differs from that of the prototypic γ-class CA, Cam, in which k_{cat}/K_m is dependent on two ionizations [27].

3.4.3 Effect of Oxidation on Fe-sup CamH vs. Zn-sup CamH Activity

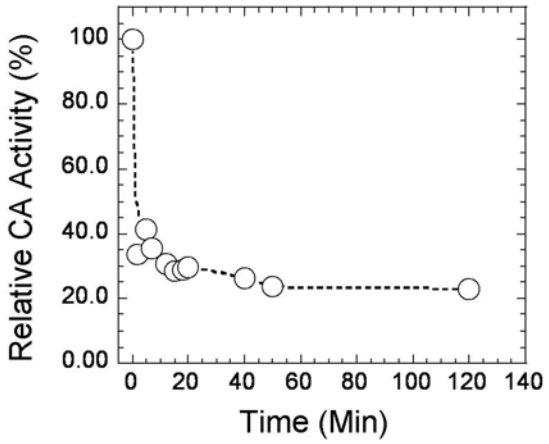

Figure 3.11**: Inactivation of anaerobically purified Fe-sup CamH upon exposure to air.**

Anaerobically purified Fe-sup CamH was exposed to 1 Atm air and samples were assayed at the times indicated via the stopped-flow method at 25º C in 50 mM HEPES, pH 7.5. Relative CA activity refers to the turnover rate (k_{cat}). Each point is referenced to the turnover number of Fe-sup CamH anaerobically assayed. Presented here is the average of three experiments.

Metal supplementation, Zn or Fe, during induction of CamH production resulted in purified CamH enzymes that had different magnitudes of the steady-state parameters k_{cat} and k_{cat}/Km; however, the Michaelis-Menten constant, K_m, remained comparable (Table **3.2**). To determine if the iron associated with CamH was catalytically relevant, Fe-CamH was exposed to oxidation by ambient air and hydrogen peroxide (Figure **3.11-3.12**). Fe-sup CamH rapidly lost activity during exposure to air, retaining only ~30% after five minutes (Figure **3.11**). After two hours exposure to air, Fe-CamH retained 20-25% of the original activity, similar to the activity exhibited by aerobically assayed Zn-CamH.

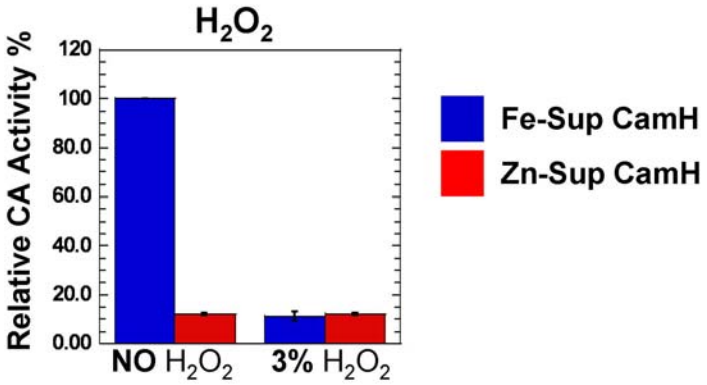

Figure 3.12**: Effect of hydrogen peroxide on Fe- and Zn-sup CamH**.
Hydrogen peroxide (3% final concentration) was incubated with either Fe- or Zn-sup CamH (1 μM final concentration) for 10 min, then assayed immediately.
***** All CA activities are relative to the observable activity of anaerobically purified Fe-CamH assayed anaerobically.

Zn- and Fe-sup CamH were also incubated with 3% H_2O_2 for ten minutes, and then assayed. Addition of 3% H_2O_2 caused a small amount of Fe-sup CamH to precipitate; however, the remaining soluble Fe-sup CamH (0.26 μM) was assayed for CA activity. Unlike Fe-sup CamH, no precipitate was observed upon addition of 3% H_2O_2 to Zn-sup CamH. Incubation with 3% H_2O_2 resulted in near abolition of CA activity in Fe-sup CamH but had no significant effect on Zn-sup CamH (Figure **3.12**). Fe-sup CamH incubated with 3% H_2O_2 resulted in less than 20% retention of observed activity of Fe-sup CamH not incubated with 3% H_2O_2 (Figure **3.12**).

In Fe-Cam, it was demonstrated that upon exposure to an oxidant, the CA active ferrous iron was oxidized to the CA inactive ferric iron which then fell out of the Cam active site [10]. Exposure of oxidants to Fe-Cam in buffers that were treated with chelex to remove metals, Cam was completely inactive [10]. However, if Fe-Cam was exposed to oxidants in buffers not treated with chelex, Cam retained activity suggesting that once

the ferric iron left the active site, advantageous CA active metals, like Zn, entered [10, 31]. Similarly, Fe-sup CamH upon exposure oxidants, either air or 3% H_2O_2, exhibited activity roughly equal to that observed from Zn-sup CamH exposed to similar conditions (Figure **3.12**). These experiments were conducted in buffers not treated with chelex. The data are consistent with a Zn ion entering the active site in oxidant treated Fe-sup CamH. Thus, the CA activity observed in Fe-sup CamH incubated with H_2O_2 may be due to unaffected holoenzyme containing zinc.

3.5 Discussion

The results presented here document the preliminary characterization of the second identified γ-class CA found in *M. thermophila* that exhibits CA activity. A few identified γ-class homologs have been purified but shown not to possess CA activity under conditions assayed. This chapter provides the first documentation of a CA active γ-class isozyme. A few biochemical and kinetic differences exist between CamH and the prototypic γ-class CA, Cam. This investigation represents the beginning of comparative analysis of the γ-class to begin to elucidate the general characteristics of the γ-class. The differences between CamH and Cam may direct research on other identified γ-class CAs, especially those previously shown not to exhibit CA activity.

3.5.1 Comparisons of Biochemical Characteristics of CamH to Cam and the α-Class CAs

Possible roles of the cysteines in CamH. Each monomer of the prototypic γ-class CA (Cam) possesses a single cysteine residue. Unlike Cam, six cysteines are present per CamH monomer, with none at the same position as the cysteine in Cam. Thiol groups in CamH were assayed using DTNB reagent. Two cysteines did react with DTNB suggesting accessible these cysteines are more "exposed." Under denaturing conditions, all six cysteines interacted with DTNB suggesting steric hinderance may prevent DTNB access to four of the six cysteines. CamH does migrate differently on a SDS-PAGE gel depending on whether CamH was purified in the absence or presence of dithiothreitol (DTT) (Figure **3.3**). These differences may be the result of modification of the cysteines reusing in alternate forms of CamH.

Possible roles for the cysteines present in CamH may be involved in protein-protein interactions or post-translational modification. Cysteines have been shown to be involved in post-translational modification in the α-class CAs. The α-class isozyme, CAIII possesses five cysteines whereas α-class CAII possesses only one cysteine [32, 33] analogous to γ-class CamH and Cam. Two exposed cysteines in isozyme CAIII are post-translationally modified by S-glutathionylation [34, 35], which regulates CAIII activity under oxidative stress in muscle tissue [33, 36]. Unmodified isozyme CAIII exhibits greater CA activity than glutathionylated CAIII, thus minimizing CA activity during oxidizing conditions [36]. S-thiolation of cytosolic CamH may regulate CA activity in a similar fashion. Further investigation of S-thiolation in Archaea may increase the understanding of post-translational regulation on the protein level in Archaea.

3.5.2 CamH: An Iron Enzyme?

Prototypic γ-class Cam is an iron enzyme *in vivo* [16]. Thus, at least some γ-class CAs may be iron enzymes, especially those putative γ-class CAs functioning in a reduced iron-rich environment [16]. Unlike Cam, CamH lacks a signal peptide indicative that CamH most likely functions in the cytosol in the strict anaerobic methanogen, *M. thermophila*. CamH possesses similar amounts of iron whether supplemented with zinc or iron during overexpression in *E. coli*. Unsupplemented CamH preparations that are aerobically purified contained less than one zinc ion per monomer and no appreciable amount of any other metal. Lack of metal incorporation may be due to Fe limitation resulting in the formation of apo-CamH which is consistent with an iron preference for CamH.

In Cam, metal binding to the monomeric subunits provides $\geq$ 45 kcal/trimer of stabilization energy to the holoenzyme whereas the sole assembly of apo-trimeric Cam only provides only ~ 25 kcal/trimer of energy, indicating that metal binding contributes the most to the stability to trimerization of Cam [37, 38]. Even though Zn- and Fe-sup CamH possess similar amounts of iron regardless of metal supplementation or purification conditions, Zn-sup CamH did have a higher metal incorporation than Fe-sup CamH. Based on empirical observations, Zn-sup CamH appeared significantly more stable at room temperature and/or in the presence of oxygen than Fe-sup CamH. Further, the instability of CamH may be a direct result of low metal incorporation.

Low metal incorporation in CamH may be compounded by the requirement for the incorporation of a preferred metal, such as Fe, by an accessory protein. When Cam

was expressed under Fe supplementation and anaerobically purified, Fe was fully incorporated in Cam [16]. Under these same conditions, CamH incorporates very little Fe and even less Zn. Several attempts to reconstitute CamH with zinc, cobalt, or iron failed due to the inability to refold CamH once it had been denatured, even in the presence of metal. An accessory protein or chaperonin may be required that incorporates Fe *in vivo*. Accessory proteins have been shown to be required for the metal incorporation of a Fe-hydrogenases in *Chlamydomonas reinhardtii* and strictly anaerobic organisms from the genus *Clostridium* and *Desulfovibrio* [39]. Low metal incorporation in CamH *in vitro* may be due to the absence of a metallo-chaperone that is not present in *E. coli in vivo*.

3.5.3 Kinetic analysis of CamH

CamH is the first γ-class homolog to exhibit detectable activity. The turnover number for CamH is significant lower than that of Cam. The best explanation for this difference is the apparent absence in the CamH amino acid sequence of the acidic loop shown to play an important role in proton transfer in Cam. The CamH model does not obviously identify possible residue(s) in the active site that may act in proton transfer. In addition, low metal incorporation of CamH may underestimate the *in vivo* turnover number. The observed k_{cat}^{eff} (54.4 ms^{-1}) Fe-sup CamH is four-fold lower than the k_{cat}^{eff} of Fe-Cam (231.4 ms^{-1}). However, when Fe-sup CamH was assayed in the presence of the exogenous proton acceptor, imidazole, the specific activity increased to 142.3 ms^{-1} which is comparable to that of Fe-Cam. The observed kinetic parameters, k_{cat} and k_{cat}/K_m, of Fe-

sup CamH may be underestimates of the actual rates of CamH *in vivo*. Alternatively, the low CA activity determined *in vitro* may be important for an unknown role CamH *in vivo*.

An exogenous proton acceptor was able to enhance proton transfer in CamH, indicating proton transfer is rate-limiting. No apparent PSR candidate is identified in the amino acid sequence of CamH. However, a protein present in *M. thermophila* may act as an exogenous proton acceptor by associating with CamH *via* a tight protein-protein interaction possibly through the aforementioned cysteines. In *C. reinhardtii*, an extracellular CA was shown to oligomerize with 4 kDa protein via disulfide bonds *in vivo* [40]. The absence of the 4 kDa protein did not affect binding of the CA specific inhibitor, dansylamide, suggesting the accessory protein did not interfere with the first step of CO_2 catalysis, CO_2 hydration [40]. However, the turnover number (k_{cat}), reflecting proton transfer in CAs, was reduced by 85% in the absence of this small subunit. This result suggests the 4 kDa accessory protein may play a substantial role in proton transfer [40]. Thus, it is enticing to propose that the exposed cysteines in the heterologously-produced CamH may function to oligomerize with an accessory protein *via* disulfide bonds that may enhance catalysis by the associated protein acting as a proton acceptor.

Alternatively, the low k_{cat} exhibited by CamH may be intrinsic. The α-class enzyme, CAIII, also exhibits a turnover number of 10^3 s^{-1} [35], the lowest activity of all characterized CA active α-class isozymes. CAIII possesses a leucine at PSR position 64 whereas all other CA active α-class isozymes possess a histidine at this position [23, 35]. CAIII is distributed primarily in the muscle tissues and its role is still unknown.

Therefore, at this stage, these lower active CAs, like α-class CAIII and γ-class CamH, may play an unknown physiological role that requires low-levels of CA activity.

Despite overall structural and general active site differences, the α-, β-, and γ-class (Cam) CAs have been shown to share the same two-step isomechanism for CO_2 catalysis [10, 11, 24-27, 29, 35, 41-52]. These two steps have been shown to be kinetically distinct indicated by accumulating evidence from chemical equilibrium and steady-state kinetics [21-25, 27-29, 36, 37, 42-45, 48, 50, 52-57]. The low CA activity exhibited by CamH prompted investigation to determine if CamH participates in a similar two-step isomechanism previously described for other CAs. The kinetic parameter, k_{cat}, was shown to be buffer dependent in CamH. This result is consistent with a buffer molecule acting as a second substrate in the ping-pong mechanism. Buffer dependency on k_{cat}/K_m was not observed suggesting that buffer does not directly contribute to the nucleophilic attack of the metal bound hydroxide on CO_2. This result provides support that CO_2 hydration is separate from the second step, proton transfer [21, 28, 54, 58] in CamH, correlating well with previous α-, β-, and γ-class kinetic investigations [10, 26, 27, 36, 50-52, 59].

The values of k_{cat}/K_m and k_{cat} observed for Fe-sup CamH increases with increasing pH, suggesting that deprotonation of residue(s) within the active site is required for catalytic competency. In Cam, CO_2 hydration (k_{cat}/K_m) is dependent on two ionizations (pK_a = ~6.8, ~8.3) [27]. One pK_a reflects the catalytic metal bound hydroxide (~6.8), while the other has been postulated to represent Glu62's influence on the nearby coordinating water (~8.3) [11, 27]. The second ionization is not apparent in the current CamH pH *vs*. k_{cat}/K_m profile. If a second ionization does exist in CamH, this second pK_a

may exist outside the pH range (6.75-9.0) examined. The calculated pK_a values for water coordinated to Zn ion in the absence of an enzyme is ~9.3 [60]. Therefore, the pK_a of the coordinating water in CamH may be higher than pH 9.0 possibly due to the absence of the acidic loop and its subsequent influence on the coordinating water which may lower the p*K*a to 8.3 in Cam [27].

The pH dependency of k_{cat} in CamH differs from pH dependency of k_{cat} observed in Cam [27] . This is not surprising since the Cam PSR, Glu84 [10], is not present in the CamH sequence. In CamH, the kinetic parameter, k_{cat}, was also dependent on a single pK_a value (7.3) apparently distinct from the ionization observed for k_{cat}/K_m (Table **3.3**). Many speculations can be made in regards to what groups is responsible for this ionization. In CamH, this pK_a may reflect a deprotonation of active site group Glu62. Alternatively, this pK_a could reflect a proton wire in which the extracted proton travels during proton transfer [29]. The proton wire in CamH most likely has many different properties than the proton wire involved in proton transfer in Cam. In Cam, the acidic loop containing five glutamates including PSR, Glu84. These glutamates most likely have a strong influence on nascent waters; thus, exerting more control on the overall structure of a proton wire that extends from the active site to buffer. Conversely, in CamH, the waters involved may be less ordered with more inherent entropy due to the absence of this acidic loop.

3.5.4 Conclusions

CamH is an active CA with significant homology to Cam shown participate in a two-step isomechanism; thus qualifying CamH as a γ-class isozyme. In addition, initial characterization suggests CamH is an iron enzyme. Future characterization of the similarities and differences between Cam and CamH will provide insight to the general characteristics of the γ-class, possibly aiding research of other identified γ-class CAs not yet shown to possess CA activity. For example, lack of observable CA activity in those characterized γ-class homologs in *A. thaliana* [5, 6] and *C. reinhardtii* [61] may be due to inactivation of the catalytic iron or iron deficiency. Reinvestigation of these γ-class homologs will increase the understanding of metal preference in the γ-class CAs. On the other hand, any γ-class homologs that do not possess one or more of the metal ligands or catalytic relevant residues may represent γ-class Carbonic Anhydrase-Related Proteins (CA-RPs) [62]. If CA-RPs do exist in the γ-class, this is another example of the similarities that exist between the independently evolved α- and γ-class.

3.6 Materials and Methods

Cloning the *camH* gene encoding CamH from *Methanosarcina thermophila* and heterologous expression of the enzyme. One 31-mer oligonucleotide (primer1 5`-GGTGGTCATATGAAGAGGAATTTTAAAATGC-3` , partially corresponds to nucleotides encoding amino acids 1 to 7 of CamH; primer II , the second 27-mer oligonucleotide (5`-ACCACCAAGCTTTCATCAACTCTCTTC-3`), partially

corresponding to nucleotides 551 to 570 downstream of the *camH* gene, 100 ng of chromosomal *M. thermophila* DNA, the Expanded High Fidelity PCR System (Roche Applied Sciences, Germany) were used to amplify the 570 bp region of *M. thermophila* containing the *camH* gene. This amplification generated *Nde*I and *Hin*dIII (New England Biolabs) restriction sites on either end of the *camH* product. The PCR product was blunt ended with Expanded High Fidelity polymerase mix (Roche Applied Sciences, Germany), digested with *Nde*I and *Hin*dIII and cloned into the digested pet22b vector (Novagen, San Diego, CA) to yield pCamHT13A. This plasmid was transformed into the chemically competent *Escherichia coli* strain Rosetta (DE3) *pLys*I (Novagen, San Diego, CA) which were then used to inoculate Luria-Bertani broth containing 100μg/mL ampicillin and 34μg/mL chlorophenicol. Cells were grown at 37º C to an A_{600} of 0.6-0.8, then chilled to 16º C. The chilled cultures were induced to overproduce CamH with the addition of isopropyl thiogalactopyranoside (IPTG) to a final concentration of 1 mM. Simultaneously, 500 μM $ZnSO_4$ or 200 μM ferric ammonium citrate was added to supplement the media. Induced cultures were allowed to continuing growing at 16º C for 16-20h. Cells were harvested by centrifugation and stored frozen at -80º C until lysis.

Purification. Fe-supplemented CamH cells were anaerobically purified employing an inert atmosphere glove bag (Coy Laboratory Products, Ann Arbor, MI). All buffers used for anaerobic purifications were filtered and made anaerobic by vacuum degassing and replacement with nitrogen. All steps are conducted in the glove bag with the exception of lysis and centrifugation. Frozen cells were thawed in the glove bag on ice and resuspended in chilled 50 mM TAPS pH 8.5 buffer, 1 mM DTT, 1 μM DNase I (Sigma) followed by two passes through a chilled French press at a pressure of 1000

lb/in.^{2} (1 lb/in.^{2} = 6.9 kPa). Cell lysate was collected via a 18 gauge needle in a stoppered serum bottle to ensure lysate was kept under anaerobic conditions. Crude lysate was then centrifuged at 29000g for 60 min, followed by filtration of the supernatant through a 0.45 µm filter. Syringes and filters were placed into the glove bag 24 hours prior to purification to allow equilibration with the glove bag atmosphere.

This filtrated solution was then loaded onto a 66 mL the cation exchanger SP-Sepharose Fast Flow column (Amersham Pharmacia Biotech, Piscataway, New Jersey) and then washed with one column volume of 50 mM TAPS, pH 8.5, 1 mM DTT buffer to remove unbound proteins. Weakly bound proteins were removed by washing the column with 1.5 column volumes of 0.11 M NaCl, 50 mM TAPS, pH 8.5, 1 mM DTT. A gradient elution of 0.13 to 0.55 M NaCl was then applied over 6 column volumes. CamH variants typically eluted between 0.15-0.30 M NaCl. These fractions were pooled and immediately diluted to avoid aggregation. CamH precipitates at high concentrations (greater than 12 mg/mL) which can be avoided by diluting the protein to concentrations beneath this threshold. Diluted and pooled CamH is stored in a 100-mL stoppered serum bottle on packed ice. Freeze/Thaw causes aggregation; however, CamH is stable kept anaerobic on ice. Zn-supplemented CamH purification is the same except buffers are not anaerobic and purification occurs in normal room conditions.

Gel Filtration Chromatography. A Superdex 75 high-resolution gel filtration column (Amersham Pharmacia Biotech, Piscataway, New Jersey) was equilibrated with 150 mM KCl, 50 mM TAPS pH 8.5 buffer, 1 mM DTT. Zn- or Fe-supplement CamH was loaded onto the size exclusion column and eluted using a flow rate of 1.0-mL/min.

The eluting holoenzyme was detected by measuring the UV absorbance at a wavelength of 280 nm.

N-terminal analysis. The N-terminal sequence of the heterologous expressed CamH was determined by an Applied Biosystems Procise 491 (Macro Core Facility, College of Medicine, Pennsylvania State University, Hershey, Pennsylvania).

Metals analysis. A comprehensive metals analysis of CamH preparations were conducted using inductively coupled plasma (ICP) atomic emission spectroscopy (The Chemical Analysis Laboratory, University of Georgia, Athens, GA). Protein concentration of each CamH preparation sample was determined. An aliquot of each preparation was diluted in metal-free water and used for ICP analysis.

CamH preparations were also qualitatively assayed for iron by an in gel iron stain [15]. Aliquots (10 μg/μL) of CamH preparations were run on 10% non-denaturing gels. Gels were soak in 50 mM Na-Acetate, pH 5.0 for five minutes. Once equilibrated, 3,5-Diaminobenzoic acid (final concentration of 80 mM) and hydrogen peroxide (final concentration of 40 mM) was added to a to the soaking gel. The iron present in the protein stained brown within five to ten minutes.

Iron content was also determined using the Ferene S Fe assay [63]. Both Zn- and Fe-supplemented CamH preparations were assayed in triplicate.

Thiol Quantification. Thiols were quantified via reaction with Ellman's reagent (5, 5'-Dithio-bis(2-nitrobenzoic acid), DTNB) as described previously [64]. Free thiols were measured at pH 8.5 by the addition of 200 μM DTNB in the presence and absence of 4M guanidine hydrochloride. Free thiols were detected by monitoring the concentration of TNB produced at 412 nm using a Beckman DU640 spectrophotometer

(Beckman Instruments, Inc., Fullerton, California). The concentration of TNB was calculated using 13600 cm^{-1} M^{-1}. The spectrophotometer was blanked using the CamH storage buffer.

Carbonic Anhydrase In-Gel Assay. The carbonic anhydrase in gel activity assay was performed in a similar matter as previously published [65]. CamH samples were run on a 12.5% non-denaturing gel and then soaked in 0.1% bromothymol blue (Sigma) solution until the gel was stained deeply blue. Residual liquid was blotted away. A stream of CO_2 gas was blown over the gel for 5-10 min until a yellow band appeared against the dark blue background. Once the yellow spots were recorded, the same gel was Coomaissed stained. The detection limit for this assay was 0.56 μg/μL CamH purified protein.

Steady-State Kinetic Measurements. Zn-supplemented and Fe-supplemented CamH protein preparations were assayed for carbonic anhydrase activity by stopped-flow spectroscopy [24], using a model SF-2001 KinTek stopped-flow instrument (KinTek Corp., Austin, TX). The CamH protein concentration were determined by first measuring A_{280} of these protein solutions then using a theoretical extinction coefficient, 6990 cm^{-1} M^{-1} with a computed monomer molecular mass of 20 335 Da. Protein concentrations for CamH are given based on the extinction coefficient of the CamH monomer. Enzyme monomer concentrations ranged from 400 nM to 1 μM. Buffer-indicator dye pairs used were MES and chlorophenol red (at pH 5.7-6.9) measured at a wavelength of 574 nm, MOPS or imidazole and 4-nitrophenol (at pH 6.5-7.7) measured at a wavelength of 400 nm, and TAPS and m-cresol purple (at pH 7.7-9.1) measured at a wavelength of 578 nm. Buffer concentrations were 50 mM, the total ionic strength was adjusted to 50 mM with

Na_2SO_4, and final pH indicator concentrations were 50 μM. Saturated solutions of CO_2 (32.9 mM in H_2O) were prepared by bubbling CO_2 gas into deionized water at 25º C. The experimental final CO_2 concentrations were varied from 4.7 to 24mM. The initial 5-10% of the total absorbance changes were used to calculate initial steady-state kinetic data used for kinetic analysis, using the average of 10-15 reaction traces per experiment. The initial rate data were fit to the Michaelis-Menten equation to obtain experimental values for k_{cat} and K_m. The pH-independent values of k_{cat} and k_{cat}/K_m and pK_a for CO_2 hydration reaction were determined by fitting the experimental pH-dependent Michaelis-Menten parameter k_{cat} and k_{cat}/K_m to Eq. **2.6- 2.7**.

$$k_{cat}^{obs} = k_{cat}/(1+10^{(pKa\ pH)}) \qquad \text{(Equation } \mathbf{3.1}\text{)}$$

$$k_{cat}/K_m^{obs} = (k_{cat}/K_m \times 10^{(pKaII\ pH)} + k_{cat}/K_m^{II})/(1 + 10^{(pKaII\ pKaI - 2pH)} + 10^{(pKaI\ pH)} + 10^{(pKaII\ pH)}) \qquad \text{(Equation } \mathbf{3.2}\text{)}$$

Solvent hydrogen isotope effect (SHIE) studies were performed at pD 6.75, 50 mM MES; pD 7.6, 50 mM HEPES; pD 8.8, 50 mM TAPS buffers. All pD values are uncorrected pH electrode readings. The ionic strength was adjusted to 0.2 M $NaSO_4$. D_2O solutions had a final concentration of 99%. Substrate was prepared by bubbling D_2O water with CO_2 at 25º C. The CO_2 concentrations were varied from 4.7 to 24 mM. All fits described were done using Kaleidagraph (Synergy Software, Reading, PA).

Constructing the CamH Model. The model of CamH was constructed using Swiss PDBViewer version 3.7. The CamH sequence was threaded on the solved crystal coordinates of the Cam monomer (PDB ID 1THJ). The structural alignment was

manipulated to remain faithful to alignment conducted previously in CLUSTAL X (v1.83).

3.7 References

1. Meldrum, N.N. and F.J.W. Roughton, *Carbonic anhydrase. Its preparation and properties.* Journal of Physiology, 1933. **80**: p. 113-141.
2. Stadie, W.C. and H. O'Brien, *The Catalysis of the Hydration of Carbon Dioxide and Dehydration of Carbonic Acid by an Enzyme Isolated from Red Blood Cells.* Journal of Biological Chemistry, 1933. **103**(2): p. 521-529.
3. Alber, B.E. and J.G. Ferry, *A carbonic anhydrase from the archaeon Methanosarcina thermophila.* Proceedings of the National Academy of Sciences, 1994. **91**(15): p. 6909-6913.
4. Parisi, G., M. Fornasari, and J. Echave, *Evolutionary Analysis of γ-Carbonic Anhydrase and Structurally Related Proteins.* Molecular Phylogenetics and Evolution, 2000. **14**(3): p. 323-334.
5. Parisi, G., et al., *Gamma Carbonic Anhydrases in Plant Mitochondria.* Plant Molecular Biology, 2004. **55**: p. 193-207.
6. Perales, M., et al., *Disruption of a Nuclear Gene Encoding a Mitochondrial Gamma Carbonic Anhydrase Reduces Complex I and Supercomplex I+III_2 Levels and Alters Mitochondrial Physiology in Arabidopsis.* Journal of Molecular Biology, 2005. **350**: p. 263-277.

7. Galagan, J.E., et al., *The genome of M. acetivorans reveals extensive metabolic and physiological diversity.* Genome Research, 2002. **4**: p. 532-42.

8. Tomb, J.F., *DuPont*.

9. Tripp, B.C., C. Tu, and J.G. Ferry, *Role of Arginine 59 in the γ-Class Carbonic Anhydrase.* Biochemistry, 2002. **41**: p. 669-678.

10. Tripp, B.C. and J.G. Ferry, *A structure-function study of a proton transport pathway in the gamma-class carbonic anhydrase from Methanosarcina thermophila.* Biochemistry, 2000. **39**(31): p. 9232-9240.

11. Zimmerman, S.A. and J.G. Ferry, *Proposal for a Hydrogen Bond Network in the Active Site of the Prototypic Gamma-Class Carbonic Anhydrase.* Biochemistry, 2006. **45**(16): p. 5149-57.

12. Iverson, T., et al., *A closer look at the active site of γ-class carbonic anhydrases: High-Resolution crystallographic studies of the carbonic anhydrase from Methanosarcina thermophila.* Biochemistry, 2000. **39**: p. 9222-9231.

13. Kisker, C., et al., *A left-handed beta-helix revealed by the crystal structure of a carbonic anhydrase from the archaeon Methanosarcina thermophila.* EMBO Journal, 1996. **15**(10): p. 2323-2330.

14. Alber, B.E. and J. G. Ferry, *Characterization of heterologously produced carbonic anhydrase from Methanosarcina thermophila.* Journal of Bacteriology, 1996. **178**(11): p. 3270-3274.

15. Kuo, C. and I. Fridovich, *A stain for iron-containing proteins sensitive to nanogram levels of iron.* Analytical Biochemistry, 1988. **170**: p. 183-185.

16. Tripp, B.C., et al., *A role for Iron in an Ancient Carbonic Anhydrase.* Journal of Biological Chemistry, 2004. **279**(8): p. 6683-6687.

17. Lane, T., et al., *Biochemistry: A cadmium enzyme from a marine diatom.* Nature, 2005. **435**(5 May 2005): p. 42.

18. Chen, R.F. and J.C. Kernohan, *Combination of Bovine Carbonic Anhydrase with a Fluorescent Sulfonamide.* The Journal of Biological Chemistry, 1967. **242**(24): p. 5813-5823.

19. Nair, S.K., et al., *Structural basis of inhibitor affinity to variants of human carbonic anhydrase II.* Biochemistry, 1995. **34**(12): p. 3981-9.

20. Yu, Z., et al., *A novel carbonic anhydrase from the mantle of the pearl oyster (Pinctada fucata).* Comparative Biochemistry and Physiology. Part B, Biochemistry and Molecular Biology, 2006. **143**: p. 190-194.

21. Lindskog, S., *Structure and mechanism of carbonic anhydrase.* Pharmacol. Ther, 1997. **74**(1): p. 1-20.

22. Lindskog, S. and J.E. Coleman, *The Catalytic Mechanism of Carbonic Anhydrase.* Proceedings of the National Academy of Sciences, 1973. **70**(9): p. 2505-2508.

23. Tu, C.K., et al., *Chemical rescue of proton transfer in catalysis by carbonic anhydrases in the β- and γ-class.* Biochemistry, 2002. **41**(51): p. 15429-15435.

24. Khalifah, R.G., *The carbon dioxide hydration activity of carbonic anhydrase I. Stop-flow kinetic studies on the native human isoenzymes B and C.* Journal of Biological Chemistry, 1971. **246**(8): p. 2561-2573.

25. Fisher, Z., et al., *Structural and kinetic characterization of active-site histidine as a proton shuttle in catalysis by human carbonic anhydrase II.* Biochemistry, 2005. **44**(4): p. 1097-105.

26. Rowlett, R.S., et al., *Kinetic characterization of wild-type and proton transfer-impaired variants of beta-carbonic anhydrase from Arabidopsis thaliana.* Arch Biochem Biophys, 2002. **404**(2): p. 197-209.

27. Alber, B.E., et al., *Kinetic and spectroscopic characterization of the γ-class carbonic anhydrase from the methanoarchaeon Methanosarcina thermophila.* Biochemistry, 1999. **38**(40): p. 13119-13128.

28. Silverman D. N. and S.H. Vincent, *Proton transfer in the catalytic mechanism of carbonic anhydrase.* CRC Crit. Rev. Biochem, 1984. **14**: p. 207-255.

29. Dodgson, S., et al., *The Carbonic Anhydrases*. 1991, New York: Plenum Press. 379.

30. Zheng, Y.J. and K.M. Merz, *Mechanism of the Human Carbonic Anhydrase-II Catalyzed Hydration of Carbon-Dioxide.* Journal of the American Chemical Society, 1992. **114**(26): p. 10498-10507.

31. Bell III, C.B.

32. Duda, D., et al., *Crystallization and preliminary X-ray analysis of human carbonic anhydrase III.* Acta crystallographica. Section D, Biological crystallography, 2002. **58**: p. 849-852.

33. Mallis, R.J., et al., *Crystal structure of S-glutathionylated carbonic anhydrase III.* FEBS Letters, 2000. **482**: p. 237-241.

34. Kim, G. and R.L. Levine, *Molecular Determinants of S-Glutathionylation of Carbonic Anhydrase 3.* Antioxidants and Redox Signaling, 2005. **7**(7-8): p. 849-854.

35. Carter, N., et al., *Characterization of human carbonic anhydrase III from skeletal muscle.* Biochemical Genetics, 1979. **17**(9-10): p. 837-854.

36. Tu, C., et al., *The pH dependence of the hydration of CO_2 catalyzed by carbonic anhydrase III from skeletal muscle of the cat.* Journal of Biological Chemistry, 1983. **258**(14): p. 8867-8871.

37. McCall, K.A., C.C. Huang, and C. A. Fierke, *Function and mechanism of zinc metalloenzymes.* Journal of Nutrition, 2000. **130**(5): p. 1437S-1446S.

38. Simler, B.R., B.L. Doyle, and C.R. Matthews, *Zinc binding drives the folding and association of the homo-trimeric γ-carbonic anhydrase from Methanosarcina thermophila.* Protein Engineering, Design, and Selection, 2004. **17**(3): p. 285-291.

39. Posewitz, M.C., et al., *Discovery of two novel radical S-adenosylmethionine protiens required for the assembly of an active [Fe] hydrogenase.* Journal of Biological Chemistry, 2004. **279**(24): p. 25711-25720.

40. Husic, H.D., S. Hsieh, and A.L. Berrier, *Effect of dithiothreitol on the catalytic activity, quaternary structure and sulfonamide-binding properties of an extracellular carbonic anhydrase from Chlamydomonas reinhardtii.* Biochimica et biophysica acta, 1991. **1078**(1): p. 35-42.

41. Bracey, M.H., et al., *Spinach carbonic anhydrase: Investigation of the zinc-binding ligands by site-directed mutagenesis, elemental analysis, and EXAFS.* Biochemistry, 1994. **33**(44): p. 13126-13131.

42. Covarrubias, A.S., et al., *Structure and function of carbonic anhydrase from Mycobacterium tuberculosis.* The Journal of Biological Chemistry, 2005. **280**(19): p. 18782-18789.

43. Davenport, H.W., *The early days of research on carbonic anhydrase.* Annals of NY Academic Science, 1984. **429**: p. 4-9.

44. Elleby, B., et al., *Characterization of carbonic anhydrase from Neisseria gonorrhoeaea.* European Journal of Biochemistry, 2001. **268**: p. 1613-1619.

45. Johansson, I. and C. Forsman, *Kinetic studies of pea carbonic anhydrase.* European Journal of Biochemistry, 1993. **218**: p. 439-446.

46. Kiefer, L.L., S.A. Paterno, and C.A. Fierke, *Hydrogen-Bond Network In The Metal-Binding Site Of Carbonic Anhydrase Enhances Zinc Affinity And Catalytic Efficiency.* Biochemistry, 1995. **117**(26): p. 6831-6837.

47. Kimber, M. and E. Pai, *The active site architecture of Pisum sativum β-carbonic anhydrase is a mirror image of that of α-carbonic anhydrases.* The EMBO Journal, 2000. **19**(7): p. 14-7-1418.

48. Krebs JF, et al., *Kinetic and spectroscopic studies of hydrophilic amino acid substitutions in the hydrophobic pocket of human carbonic anhydrase II.* Biochemistry, 1993. **32**(17): p. 4496-505.

49. Krebs, J.F., et al., *Structural And Functional Importance Of A Conserved Hydrogen-Bond Network In Human Carbonic Anhydrase II.* Journal of Biological Chemistry, 1993. **268**(36): p. 27458-27466.

50. Rowlett, R.S., et al., *Kinetic And Structural Characterization Of Spinach Carbonic Anhydrase.* Biochemistry, 1994. **33**(47): p. 13967-13976.

51. Rowlett, R.S., et al., *Examination of the role of Gln-158 in the mechanism of CO_2 hydration catalyzed by β-carbonic anhydrase from Arabidopsis thaliana.* Archives of biochemistry and biophysics, 2004. **425**(1): p. 25-32.

52. Smith, K.S., et al., *Structural and kinetic characterization of an archaeal beta-class carbonic anhydrase.* Journal of Bacteriology, 2000. **182**(23): p. 6605-6613.

53. Chegwidden, W.R., N. Carter, and Y.H. Edwards, *The Carbonic Anhydrases: New Horizons*. 200, Basel: Birkhäuser Verlag.

54. Lindskog, S. and A. Liljas, *Carbonic Anhydrase and the Role of Orientation in Catalysis.* Current Opinion in Structural Biology, 1993. **3**(6): p. 915-920.

55. Ren, X. and S. Lindskog, *Kinetics And Mechanism Of Cobalt-Substituted Bovine Muscle Carbonic Anhydrase.* European Journal of Biochemistry, 1987. **106**(6-7): p. 430-430.

56. Silverman, D.N. and S. Lindskog, *The Catalytic Mechanism Of Carbonic Anhydrase. Implications Of A Rate-Limiting Proteolysis Of Water.* Accounts of Chemical Research, 1988. **21**(1): p. 30-36.

57. Tu, C., et al., *Bicarbonate as a Proton Donor in Catalysis by Zn(II)- and Co(II)-Containing Carbonic Anhydrases.* Journal of American Chemical Society, 2001. **123**: p. 5861-5866.

58. Liljas, A. and M. Laurberg, *A wheel invented three times: The molecular structures of the three carbonic anhydrases.* EMBO Reports, 2000. **1**(1): p. 16-17.

59. Lipton, A.S., R.W. Heck, and P.D. Ellis, *Zinc solid-state NMR spectroscopy of human carbonic anhydrase: Implications for the enzymatic mechanism.* Journal of the American Chemical Society, 2004. **126**(14): p. 4735-4739.

60. Bergquist, C., et al., *Protonation and reactivity towards carbon dioxide of the mononuclear tetrahedral zinc and cobalt hydroxide complexes, Tp(But,Me) ZnOH and Tp(But,Me) CoOH: Comparison of the reactivity of the metal hydroxide function in synthetic analogues of carbonic anhydrase.* Journal of the American Chemical Society, 2003. **125**(20): p. 6189-6199.

61. Mitra, M. 2002.

62. Tashian, R.F., et al., *Carbonic anhydrase (CA)-related proteins (CA-RPs), and transmembrane proteins with CA or CA-RP domains.* EXS, 2000. **90**: p. 105-20.

63. Zabinski, R., et al., *Kinetic and Mossbauer studies on the mechanism of protocatechuic acid 4,5-oxygenase.* Biochemistry, 1972. **11**(17): p. 3212-3219.

64. Bulaj, G., T. Kortemme, and D.P. Goldenberg, *Ionization-reactivity relationships for cysteine thiols in polypeptides.* Biochemistry, 1998. **37**(25): p. 8965-8972.

65. Lane, T.W., et al., *Isolation and Characterization of a Cadmium Carbonic Anhydrase from a Marine Diatom.* Nature, 2005. **42**.

Chapter 4

Implications for the role of γ-class carbonic anhydrases in aceticlastic methanogenesis in *Methanosarcina acetivorans*

4.1 Summary

To date, CA activity in methanogens has only been observed in cell lysate of *Methanosarcina* spp. grown on acetate. This phenomenon suggests CA(s) play a role during aceticlastic methanogenesis. In fact, the prototypic γ-class CA, Cam, was isolated from *Methanosarcina thermophila* cultures grown on acetate. A Δ*cam* strain of *Methanosarcina acetivorans* exhibited impaired growth on acetate supporting a role for Cam role in aceticlastic methanogenesis. In addition, two γ-class isozymes, Cam and the newly characterized CamH, were shown to be up-regulated during acetate growth. The gene expression profiles of both γ-class CAs implicate them in aceticlastic methanogenesis. A proposed model is presented based on present and previous results depicting a role for Cam and CamH in importing acetate into the cell.

4.2 Introduction

Methanogenesis is the metabolic process of converting simple carbon compounds to methane (CH_4) gas accomplished by a group of microorganisms in *Archaea* termed methanogens [1]. Methanogens play a key role in the global carbon cycle (Figure **4.1**).

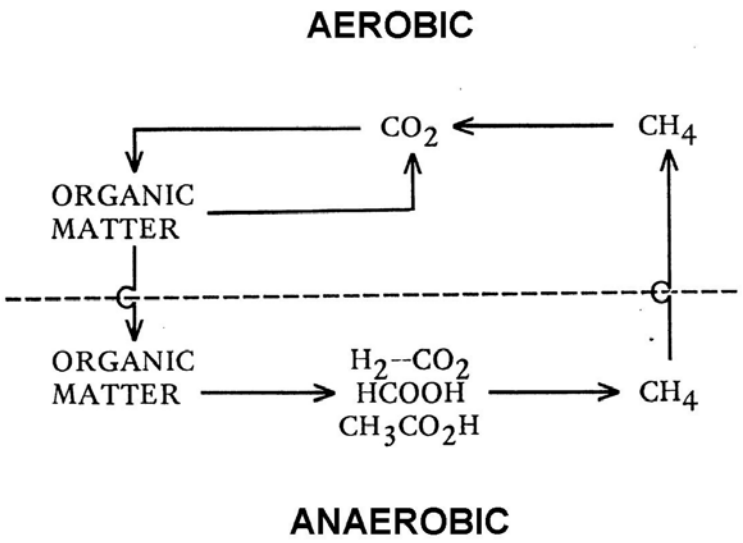

Figure 4.1**: The Global Carbon Cycle.**

This schematic provides a simple representation of how carbon is cycled between the aerobic environment and the anaerobic environment on Earth.

CO_2 is fixed into complex organic material in the aerobic environment. Ultimately a small percentage of this organic matter becomes sequestered in the anaerobic environment. Fermentative bacteria break the complex material in the anaerobic environment into simple one or two carbon compounds. Methanogens further metabolizing these simple carbon compounds into CH_4 gas which can freely recycle back into the aerobic environment. In the absence of methanogens, eventually all the organic carbon would be trapped at this point demonstrating the methanogens' role in the global carbon cycle.

Methane can be produced from either the reduction of CO_2, the dismutation of methyl groups on methanol or methylated amines, or fermentation of acetate (Table **4.1**)

Table **4.1**: Main methanogenic chemical reactions. The acetate reaction is in bold.

Reaction			***ΔG°` (kJ/mol CH_4)***
$4\ H_2 + CO_2$	$\rightleftarrows$	$CH_4 + 2\ H_2O$	131
$4\ CH_3OH$	$\rightleftarrows$	$H_4 + CO_2 + 2\ H_2O$	-106
$4\ CH_3NH_2 + 2H_2O$	$\rightleftarrows$	$3\ CH_4 + CO_2 + 4\ NH_3$	-76.7
$CH_3COO^- + H^+$	$\rightleftarrows$	**$CH_4 + CO_2$**	**-36.0**

[1]. Indeed, the majority of the biologically produced CH_4 is a result of the breakdown of acetate into CH_4 gas [2]. During aceticlastic methanogenesis (Table **4.1**), the acetate is brought into the cell by an unknown method [1, 3]. Once in the cell, acetate is activated by the addition of coenzyme A (CoA) by two enzymes, acetate kinase and phosphotransacetylase [1]. The acetyl-CoA is cleaved by CO dehydrogenase (CODH) producing a methyl group and a carbonyl group. The carbonyl group is further oxidized by CODH to CO_2 and the electrons from that oxidation are used to reduce ferredoxin. The methyl group is transferred onto tetrahydrosarcinapterin to be further transferred to coenzyme M (HS-CoM). Then the methyl group of the CH_3-S-CoM complex is reduced to CH_4 using the electrons originally from the oxidation of the carbonyl to CO_2 as the now reduced methyl group is simultaneously cleaved from the coenzyme M [1].

A handful of methanogens are capable of metabolizing acetate to CH_4 (Table **4.1**). To date, only two genera are known to perform aceticlastic methanogenesis, the *Methanosarcina* and *Methanosaeta* (formerly the *Methanothrix*). CA activity was

observed in cellular lysate from *Methanosarcina barkeri* and *Methanosarcina thermophila* cultures grown on acetate [3, 4]. DNA microarray analysis of *Methanosarcina mazei* Gö1 also revealed elevated expression of an uncharacterized CA in acetate-grown cultures *vs.* methanol-grown cultures [5]. Therefore, CAs most likely play a role during aceticlastic methanogenesis in many *Methanosarcina* spp. The prototypic γ-CAs (Cam) was isolated from *M. thermophila* cells grown on acetate [4]. Immunoblotting, proteomics and DNA microarrays confirmed that Cam is up-regulated during aceticlastic methanogenesis in *M. thermophila* and *M. acetivorans* [6-8]. As a result, Cam has been hypothesized to play a key role in acetate metabolism by either *i*) removing the CO_2 product to improve the thermodynamics of acetate fermentation or *ii*) functioning in conjunction with an antiporter that includes a second cytosolic CA to simultaneously remove the CO_2 by-product and import acetate into the cell [3, 4, 6] (Table **4.1**). The identification and characterization of the γ-class CA, CamH, also expressed in *M. thermophila* and *M. acetivorans* provides support for the latter hypothesis (see **Chapter 3**). Here, I present preliminary data investigating the role of γ-class CAs, Cam and CamH, during aceticlastic methanogenesis. Based on these results a model of the physiological function of these γ-class isozymes is provided.

4.3 Results

4.3.1 *In vivo* characterization of *cam* and *camH*

Cell lysate from *M. thermophila* cultures grown exclusive on trimethylamine (TMA), methanol (MetOH), or acetate (HAC) were probed with anti-Cam antibody. Cam was only present in detectable amounts in those cultures grown on HAC [6]. In addition to Cam, a second lower molecular weight protein cross reacted with the anti-Cam antibody [6]. It was postulated that this "second" protein was either degradation or processing product of Cam or a second γ-class CA [6]. Further, the genome sequence of *M. thermophila* revealed genes encoding two related but distinct CAs [9]. One CA gene was 100% identical to the gene of the prototypic γ-class member, Cam, that was previously isolated from *M. thermophila* [4]. The other CA gene was 96% similar to *cam* from *M thermophila*. It was annotated as *camH*. The related species, *M. acetivorans* was also shown to possess two putative CAs; one gene was 92% identical to *cam* while the other was 96% identical to *camH* [10].

Taqman quantitative RT-PCR was used to determine if *cam* and *camH* from *M. acetivorans* were expressed and under what metabolic condition; HAC, TMA, or MetOH. Since the dismutation of the methyl group on TMA and MetOH occur by a similar metabolic pathway, *cam* and *camH* abundances were not anticipated to differ significantly during growth on either of these substances [1]. Internal primers were constructed for the *M. acetivorans cam* and *camH* homologs. These primers

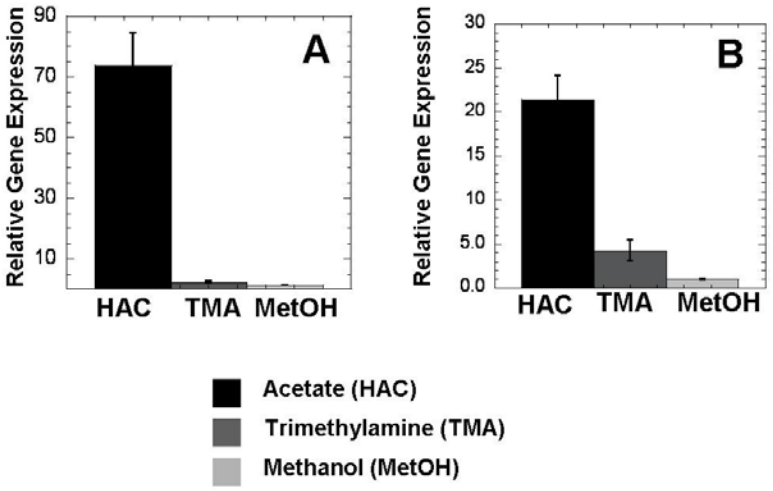

Figure 4.2**: Relative *cam* and *camH* genes amount of RNA transcript determined by Quantitative RT-PCR.**

RNA was extracted from *M. acetivorans* cultures grown exclusively on acetate (HAC), trimethylamine (TMA), or methanol (MetOH) during exponential growth of an OD_{600} of 0.4-0.5. Relative Gene Expression refers to the amount of transcript observed on HAC or TMA relative to the amount observed in MetOH. A) *cam* transcript expression. B) *camH* transcript expression.

were used to probe for the presence of *cam* or *camH* transcripts in total cellular RNA harvested at mid-exponential phase from *M. acetivorans* grown on TMA, MetOH, and HAC (Figure **4.2**). *cam* is up-regulated during growth on HAC compared MetOH and TMA (Panel A, Figure **4.2)**. This result correlated well with the immunoblotting results conducted in *M. thermophila* [6] as well as the proteomic expression profile of Cam during growth on HAC vs. MetOH in *M. acetivorans* [7]. In addition, *camH* was expressed in *M. acetivorans*, and up-regulated in cell cultures grown on HAC (Panel B, Figure **4.2)**. These results suggest that Cam and CamH may play important roles during aceticlastic methanogenesis.

4.3.2 Characterization of the Δ*cam* Strain of *M. acetivorans*

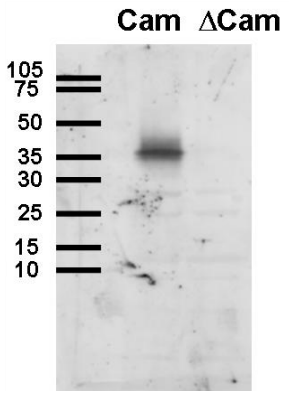

Figure 4.3**: Determining the presence of Cam in wild-type *M. acetivorans* and the Δ*cam* knockout strain grown on HAC.**

A 20 ng of cell lysate from wild-type *M. acetivorans* and Δ*cam* strain of *M. acetivorans* grown on HAC were separated on a 12.5% SDS-PAGE gel and transferred onto a PVDF membrane. The membrane was probed with 1:20,000 dilution of anti-Cam antibody.

Using the genetic tools available for *M. acetivorans*, [11], a *cam* knockout (Δ*cam*) strain of *M. acetivorans* was constructed in Dr. Kevin Sower's laboratory at the Center of Marine Biotechnology at University of Maryland Biotechnology Institute by Ethel Apolinario-Smith (not yet published). The characterization of the Δ*cam* strain is presented here. The cellular lysate from wild-type and Δ*cam* strains grown on HAC were probed with anti-Cam antibody. No Cam protein was detected in the cellular lysate of Δ*cam*, confirming that Cam protein is not being produced in the knockout strain (Figure **4.3**).

Proteomics [7] and western blot analysis [6] have shown Cam is up-regulated only in HAC-grown *M. acetivorans* cultures. In addition, CA activity was not observed in cellular lysate from *M. thermophila* grown on MetOH or TMA, but was detected

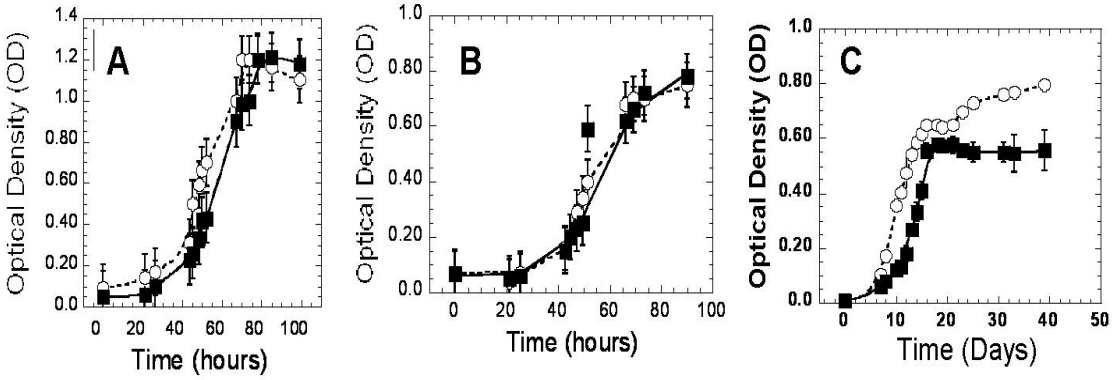

Figure 4.4**: Growth curves of the wild-type and the Δ*cam M. acetivorans* strains grown on TMA** (A)**, MetOH** (B) **or HAC** (C).

Optical density (OD) refers to the absorbance of a culture at 600 nm. The open circles (○) refer to the wild-type strain and the closed squares (■) refer to the Δ*cam* strain.

during growth on HAC [3, 4]. If Cam is important during growth on HAC, then no difference in growth will be observed between the wild-type strain and the Δ*cam* strain when grown on MetOH or TMA. Growth characteristics of the wild-type and Δ*cam* strains were determined for MetOH and TMA-grown cells (Figure **4.4**). Both strains grew equally in terms of the generation time, lag phase upon transfer to fresh media, or the maximum optical (Table **4.2**).

Differences in growth parameters were observed between the wild-type and Δ*cam* strains grown on HAC (Panel C, Figure **4.4**, Table **4.2**). The wild-type strain grown on HAC demonstrated a "biphasic" growth pattern. Growth appeared to cease after the exponential growth phase for several days and then resumed at a 35-fold slower rate than observed during exponential growth (Panel C, Figure **4.4**). The Δ*cam* strain does not

Table **4.2**: Growth of wild-type and Δ*cam* strain on MetOH, TMA, and HAC

	Generation time (Hours)	Lag time[a] (Hours)	Maximum Optical Density (OD)
WT MetOH	6.1 ± 1.5	55 ± 5.2	0.75 ± 0.05*
Δ*cam* MetOH	8.9 ± 2.1	57 ± 3.4	0.78 ± 0.08*
WT TMA	11.9 ± 2.4	50 ± 2.1	1.2 ± 0.1
Δ*cam* TMA	13.8 ± 4.1	59.5 ± 4.8	1.2 ± 0.2
WT HAC	49.6 ± 13.7	264 ± 5.6	0.80 ± 0.02
Δ*cam* HAC	85.7 ± 8.6	312 ± 4.8	0.56 ± 0.07

***Cultures were not monitored well into stationary phase.**

[a] Lag time represents the time required to reach one-half of the maximum optical density.

achieve the maximum optical density observed for the wild-type and the second growth phase is not apparent (Panel C, Figure **4.4**). The Δ*cam* cells demonstrated a lag phase that was ~3 days longer than wild-type cells (Table **4.2**). The Δ*cam* strain has an exponential phase generation time that is two-fold slower than the wild-type (Table **4.2**). These data reveal that Cam is required for wild-type growth on HAC. Also, the growth observed by the Δ*cam* strain maybe due to the presence of second γ-class isozyme, CamH. It is possible that CamH may have perform a redundant role or function in concert with Cam during aceticlastic methanogenesis.

4.4 Discussion

CAs are involved in many key physiological roles in nature [12-23]. CA activity has been observed in cell lysate from many anaerobic methanogens and bacteria that are capable of metabolizing acetate [3]; thus, implicating a role for CAs in acetate metabolism [3]. The isolation and characterization of the prototypic γ-class CA, Cam, suggest that the γ-class CAs were responsible in at least some of these organisms [4, 6]. Although the broad distribution of γ-class CA homologs across the three domains of life suggested that γ-class CAs must perform other physiological functions not limited to aceticlastic methanogenesis. However, two functions for γ-CA, Cam, in acetate metabolism were proposed. One proposal suggested that Cam promptly removes CO_2 by-product to increase the thermodynamics of aceticlastic methanogenesis [3, 6]. Alternatively, the second proposal suggests two γ-class CAs are involved in acetate uptake in conjunction with an antiporter protein similar to the HCO_3^-/Cl^- characterized in erythrocytes that involves α-class CAs CAIV and CAII [23]. The latter proposal was contingent on the presence of two CAs and an HAC transporter which has not been evident until now. The discovery and subsequent characterization of the second γ-class CA, CamH, (see **Chapter 3**) has increased support for the latter hypothesis.

4.4.1 A Physiological Model of the Aceticlastic Methanogenesis involving γ-class Carbonic Anhydrases

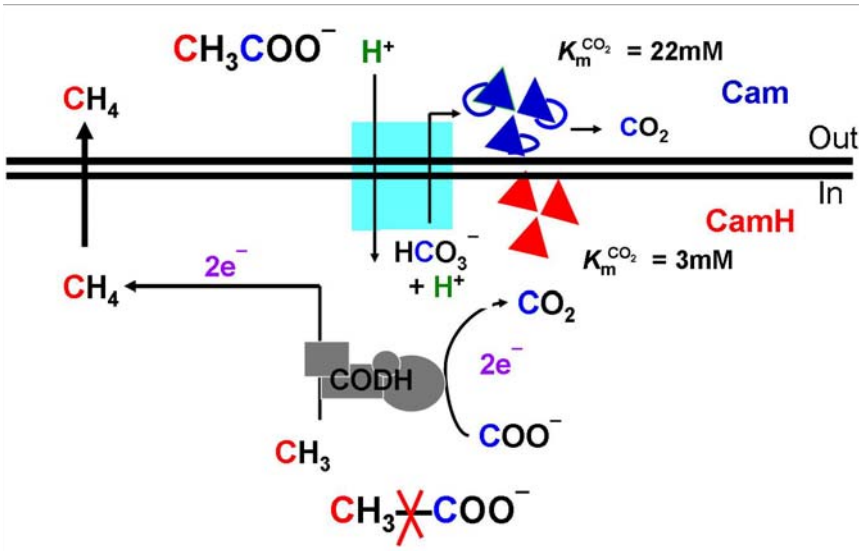

Figure 4.5**: A proposed physiological model of how Cam and CamH function in HAC uptake during aceticlastic methanogenesis in *Methanosarcina* spp.**

This simple schematic proposes an antiport anion exchanger is involved with two CAs to transport HAC into the cell and effectively remove the by-products of HAC fermentation; also improving the thermodynamics of the reaction. The model proposes that the CO_2 by-product is hydrated to HCO_3^- by cytosolic CamH. The HCO_3^- is exported out of the cell, as HAC is imported. The extracellular HCO_3^- is dehydrated by membrane associated Cam. At temperatures where these organisms flourish (50ºC and 37ºC) the solubility of the resulting CO_2 would be low; thus most likely the gas readily escapes from the liquid environment.

As much as two-thirds of the biologically produced CH_4 is the result of the fermentation of HAC by anaerobic methanogens [2]. Only two genera of the methanogens are capable of utilizing HAC for the production of methane [1, 24]; the *Methanosarcina* and the *Methanosaeta* (formerly known as *Methanothrix*). Unlike *Methanosarcina* which can also utilize methylated amines and, in some cases, reduce CO_2, the *Methanosaeta* genera only utilize acetate for methanogenesis [24]. More

attention has been given investigation the physiology of *Methanosarcina* than *Methanosaeta* during aceticlastic methanogenesis. However, it is unknown how organisms in these two genera transport HAC into the cell.

The discovery that γ-class isozymes, *cam* and *camH* are up-regulated during aceticlastic methanogenesis support their involvement in aceticlastic methanogenesis. The Δ*cam* strain also showed differences in growth trends from that of wild-type ***M. acetivorans***, demonstrating that Cam is required for wild-type growth on acetate. I propose a model (Figure **4.5**) based on the anion antiporter that has been characterized in the α-class with the extracellular CAIV and cytosolic CAII in erythrocytes [23]. In erythrocytes, the presence of an extracellular CAIV and cytosolic CAII provides the HCO_3^-/CL^- a push-pull mechanism to transport HCO_3^- in and out of the cell. This anion transport is used maximize the removal of the CO_2 waste from muscles [23].

Dr. Birgit Alber showed that Cam localized to the membrane in ***M. thermophila*** using immuno-gold labeling conducted with anti-Cam antibody that is most likely due to the 34 N-terminal amino acid leader peptide (unpublished). The lack of this leader peptide in CamH and the ability to solubly express the recombinant CamH in ***E. coli*** strongly supports that CamH is cytosolic. In the proposed model, Cam is externally tethered to the membrane while CamH resides in the cytosol. The carbon-carbon bond of HAC is cleaved and the resulting carbonyl is oxidized to CO_2 and two electrons. The electrons are then used to reduce the methyl group to methane, which eventually diffuses out of the cell.

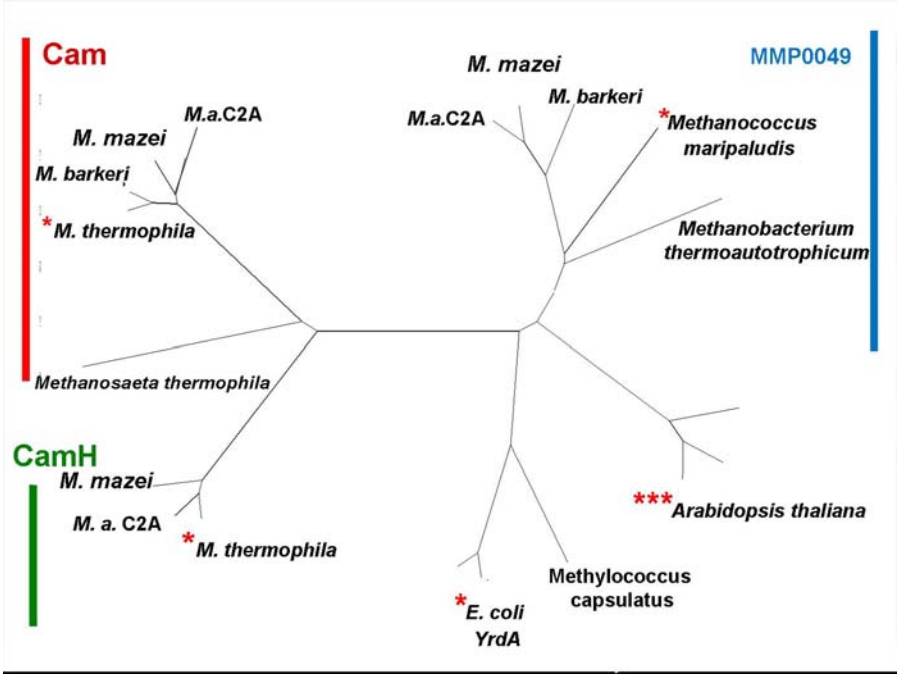

Figure 4.6**: A phylogenetic tree produced by MEGA v 3.83 displaying the relatedness of the Cam homologs in methanogens with a few examples from the *Bacteria* and *Eukarya.***

The red line denotes the Cam homologs that are most similar to the Cam from M. thermophila. The green line denotes those Cam homologs that are most like CamH from M. thermophila. The blue line denotes those Cam homologs that clade into a separate group that are most similar to a Cam homolog MMP0049 from *M. maripaludis*. The red stars refer to those homologs that have been isolated and assayed for activity. *M.* = *Methanosarcina*. *M. a.* C2A = *M. acetivorans* strain C2A

CamH hydrates theCO_2 to HCO_3^-. The HCO_3^- is exported *via* a transmembrane antiporter protein as an acetate molecule is imported into the cytosol. Once the HCO_3^- is on the outside of the cell, Cam dehydrates HCO_3^- to CO_2 (Figure **4.5**).

A strong candidate for the antiporter transmembrane protein is uncharacterized homologs, termed Ady2, found in *Methanosaeta* spp. and *Methanosarcina* spp. [24] that bear similarity to the characterized Ady2p HAC transporter found in *Saccharomyces cerevisiae* [25]. Upon disruption of the *ady2p* gene in *S. cerevisiae*, growth on HAC

ceases [25]. BLAST search using the amino acid sequence of the yeast Ady2p revealed homologs with > 50% similarity in *M. mazei*, *M. barkeri*, *M. acetivorans*, *M. thermophila* and the *Methanosaeta thermophila* PT1. These homologs were previously annotated as transcription factors although they possess several putative transmembrane domains. I propose that the Ady2 homologs in *M. acetivorans* or *M. thermophila* are reasonable candidates as the putative acetate transporter outlined in the model (Figure **4.5**). In addition, both Cam and CamH homologs (Figure **4.6**) were identified in other *Methanosarcina* spp., with the exception of *M. barkeri*, suggesting that this model may extend to other species in the *Methanosarcina* genera. Only one γ-class homolog is found in *Methanosaeta thermophila* and *M. barkeri* that bears > 90% similarity to both Cam and CamH which suggests that the mechanism of aceticlastic methanogenesis differs in these species from that of *M. acetivorans*, *M. thermophila*, and *M. mazei*.

4.5 Materials and Methods

Construct of *M. acetivorans* Δ*cam* knockout strain. (A gift from Dr. Sowers laboratory prepared by Ethel Apolinario-Smith.) Polymerase chain reaction (PCR) was used to clone cam +/- approx. 300bp upstream and downstream of gene from *M. acetivorans* with primers #234 (5'-CCCTAGTGTCTCGTCAATTCTTAAA) and #235(5'-CCTACAAATTAGTCTGCTTGAACGA). The PCR product was inserted into *PCR4.0 cloning vector* (Invitrogen TOPO cloning kit) resulting in the construction of the plasmid termed pEA156. Plasmid pEA156 was then digested with restriction enzymes *Mfe*I and *BstB*I. These two sites are internal restriction sites in the *cam* gene, resulting in

the removal of an internal section of 442bp of the *cam* gene. The $serC_P$::proC cassette, which contains the pur gene that corresponds to puromycin resistance, was cloned from pJK88 [11] using primers #251 (CCACCTTTTTTCCTCAATTGGTGAACTC) (*Mfe*I site) and #252 (CGTAACCGCTTCGAAGTGGCGGCC) (*BstB*I site). The $serC_P$::proC PCR was digested with restriction enzymes *Mfe*I and *BstB*I. The restriction digested $serC_P$::proC product was then ligated into the digested pEA156. The ligated plasmid containing pEA156 and $serC_P$::proC was named plasmid pEA162.

Cam+/- primers # 234 and #235 was used to clone and amplify the *cam*::$serC_P$::proC product from pEA156. The amplified DNA product, 4 μg, was used to transform competent *M. acetivorans* strain WWM24, which is auxotrophic for proline using the liposome-mediated transformation protocol [11]. The transformed cultures were then grown on high salt media with the addition of 100mM TMA and proline. Transformants were screened for the ability to grow in the presence and absence of proline. Those transformants that grew in the absence of proline were considered cam mutant candidates. A *cam* mutant was confirmed by PCR screening the extracted genomic DNA from mutant candidates using primers #251 and #252.

Adapting Wild-type and Δ*cam* Mutant to growth substrates. In parallel experiements, trimethylamine (TMA) adapted wild-type *M. acetivorans* and the Δ*cam* strain were innoculated into high salt media containing 100mM MetOH. After several serial transfers to fresh media, the wild-type and Δ*cam* strains were considered adapted to MetOH. Adaptation to growth on HAC requires significantly more passages to ensure all residual substrate and enzymes involved in growth from the previous substrate. Wild-

type cells, previously grown on MetOH were adapted to HAC by serially diluting stationary phase cultures (1:100) into fresh medium containing 75 mM MetOH and 25 mM HAC. On each subsequent passage, the concentration of HAC was increased and the concentration of MetOH was decreased until growth on 100 mM HAC was achieved. The wild-type strain was considered adapted after 10 passages on 100 mM HAC. The Δ*cam* strain required a more stringent adaptation protocol. The Δ*cam* strain previously grown on MetOH was HAC adapted by serially diluting stationary phase cells into fresh media containing 10mM HAC and 90 mM MetOH. On each subsequent passage, the concentration of HAC was increased by 10 mM and the concentration of MetOH was decreased by 10 mM until growth on 100 mM HAC was achieved. Again, the Δ*cam* strain was considered adapted onto HAC after 10 passages on 100 mM HAC.

Immunoblotting. Western Blot analysis was performed on cell extracts from *M. acetivorans* grown on 100 mM acetate, methanol or trimethylamine. Cell extracts were prepared by resuspending pellet in 1.5 mL 50mM TAPS, pH 8.5, 1 mM DTT, 1 μM DNase I. The resuspended pellets were lysed using sonication. Cell extracts were separated by SDS-PAGE on 15% gels and electro-transferred and 50 volts at room temperature to a polyvinylidene difluoride membrane (Sequi-Blot PVDF; BioRad) in Mini Trans-Blot Cell (BioRad) in the presence of 1mM CAPS, pH 11, 10% methanol for 45 minutes. Additional protein binding sites were blocked by incubating membrane in 10mM Tris-HCl, pH 8.0, 150 mM NaCl, 0.05% Tween 20, 0.1% casein, and 0.1% gelatin (Buffer D). A 1:20,000 dilution of anti-Cam antiserum raised in New Zealand white rabbits (Cocalica Biological Corp., Reamstown, PA) and 1:7,500 anti-rabbit immunoglobulin G-horseradish peroxidase in Buffer D. The antibody-antigen complex

was detected with the ECL Western blotting detection system (Amersham Biosciences, Piscataway, NJ).

Growth Studies. Growth of wild-type and Δ*cam* in high salt media containing 100 mM TMA or MetOH was monitored by measuring changes in optical density at 600 nm using a Spectronic 20 spectrophotometer (Bausch and Lomb). TMA and MetOH growth curves of wild-type and the Δ*cam* knockout are shown in this chapter as an average of three growth trials on those respective carbon sources. Wild-type and the Δ*cam* knockout growth on HAC was conducted in serum bottles in high salt media plus 100 mM HAC. Optical density was monitored at wavelength of 600 nm using a Beckman DU 630 spectrophotometer. In order to maintain a relatively constant HAC concentration of 100 mM, HAC cultures were fed once the cultures reached an optical density of 0.1 using the feeding formula 10 mL of gas produced = 20 μL of 10 M Acetic Acid from sterile anaerobic stocks. pH was monitored for all cultures throughout the growth study using pH paper. All carbon sources used for feeding are anaerobic.

The generation time is defined as the time required for the cell number, as a function of optical density, to double. Generations times were determined by plotting the log of optical density (OD) vs. time. The slope, K, of the exponential phase of plotted

$$K= (\log(N) - \log(N_o))/(T-T_o) \qquad \text{(Equation } \mathbf{4.1}\text{)}$$

growth was determined using Eq. **4.1**. After the slope has been determined, the time, *T*, it takes for the culture to double, *a.k.a* the generation time, is represented by Eq. **4.2**.

$$T = \log 2/K \qquad \text{(Equation 4.2)}$$

Quantitative RT-PCR. Total RNA was extracted from M. acetivorans cultures grown on MetOH, TMA, or HAC using a modified protocol from the RNeasy Mini Kit (Qiagen, Valencia, CA) that involves 2 additional DNase I steps. Quantitative RT-PCR was performed at the Nucleic Acid Facility in Huck Institute for Life Science (Pennsylvania State University, PA).

Constructing the Phylogenetic Tree. A BLAST search using the Cam amino acid sequence that retained the 34-amino acid leader peptide as a reference and a second BLAST search using the CamH sequence as a reference in order to identify putative Cam and CamH homologs in methanogens that had previously shown growth on acetate or by CO_2 reduction. Those identified Cam and CamH homologs chosen showed high similarity (58%-98%). These sequences were then aligned using ClustWal X version 1.83 and Molecular Evolutionary Genetics Analysis (MEGA) v.3.83 [26]. The phylogenetic tree was bootstrapped using the maximum parsimony in the MEGA program. The resulting tree is displayed as a radial branch style.

4.6 References

1. Ferry, J.G., *Methanogenesis: Ecology, Physiology, Biochemistry and Genetics*. 1 ed. Chapman and Hall Microbiology Series, ed. C.A. Reddy, et al. 1993, New York: Chapman and Hall. 536.

2. Jones, W.J., *Microbial prodiction and consumption of greenhouse gases: Methane, Nitrogen Oxides, and halomethanes*, ed. J.E. Rogers and W.B. Whitman. 1991: American Society for Microbiology.

3. Karrasch, M., M. Bott, and R.K. Thauer, *Carbonic anhydrase activity in acetate grown Methanosarcina barkeri.* Archives of microbiology, 1989. **151**(2): p. 137-142.

4. Alber, B.E. and J.G. Ferry, *A carbonic anhydrase from the archaeon Methanosarcina thermophila.* Proceedings of the National Academy of Sciences, 1994. **91**(15): p. 6909-6913.

5. Hovey, R., et al., *DNA microarray analysis of Methanosarcina mazei Gö1 reveals adaptation to different methanogenic substrates.* Molecular Genetics and genomics, 2005. **273**: p. 225-239.

6. Alber, B.E. and J. G. Ferry, *Characterization of heterologously produced carbonic anhydrase from Methanosarcina thermophila.* Journal of Bacteriology, 1996. **178**(11): p. 3270-3274.

7. Li, L., et al., *Quantitative proteomic and microarray analysis of the archaeon Methanosarcina acetivorans grown with acetate versus methanol.* Journal of Proteome Research, 2007. **2**: p. 759-71.

8. Ding, Y.H., et al., *Genomic and proteomic analyses reveal multiple homologs of genes encoding enzymes of the methanol:coenzyme M methyltransferase system that are differentially expressed in methanol- and acetate-grown Methanosarcina thermophila.* FEMS Microbiology Letters, 2002. **215**(1): p. 127-132.

9. Tomb, J.F., *DuPont*.

10. Galagan, J.E., et al., *The genome of M. acetivorans reveals extensive metabolic and physiological diversity.* Genome Research, 2002. **4**: p. 532-42.

11. Metcalf, W., et al., *A genetic systerm for Archaea of the genus Methanosarcina: lipsome-mediated transformation and construction of shuttle vectors.* Proceedings of the National Academy of Sciences, 1997. **94**(6): p. 262-2631.

12. Bataller, L., et al., *Carbonic anhydrase-related protein VIII: autoantigen in paraneoplastic cerebellar degeneration.* Annals of Neurology, 2004. **56**(4): p. 575-9.

13. Chegwidden, W.R., N. Carter, and Y.H. Edwards, *The Carbonic Anhydrases: New Horizons*. 200, Basel: Birkhäuser Verlag.

14. Chesler, M., *Regulation and modulation of pH in the brain.* Physiological Reviews, 2003. **83**(4): p. 1183-1221.

15. Covarrubias, A.S., et al., *Structure and function of carbonic anhydrase from Mycobacterium tuberculosis.* The Journal of Biological Chemistry, 2005. **280**(19): p. 18782-18789.

16. Cullen, J., et al., *Modulation of Cadmium uptake in phytoplankton by seawater CO_2 concentration.* Nature, 1999. **402**: p. 165-167.

17. Davenport, H.W., *The early days of research on carbonic anhydrase.* Annals of NY Academic Science, 1984. **429**: p. 4-9.

18. Dodgson, S., et al., *The Carbonic Anhydrases*. 1991, New York: Plenum Press. 379.

19. Lane, T.W. and F.M.M. Morel, *Regulation of carbonic anhydrase expression by zinc, cobalt, and carbon dioxide in the marine diatom Thalassiosira weissflogii.* Plant Physiology, 2000. **123**(1): p. 345-352.

20. Marcus, E.A., et al., *The periplasmic alpha-carbonic anhydrase activity of Helicobacter pylori is essential for acid acclimation.* Journal of Bacteriology, 2005. **187**(2): p. 729-738.

21. Meldrum, N.N. and F.J.W. Roughton, *Carbonic anhydrase. Its preparation and properties.* Journal of Physiology, 1933. **80**: p. 113-141.

22. Potter C. and A. Harris, *Hypoxia inducible carbonic anhydrase IX marker of tumor hypoxia, survival pathway and therapy target.* Cell Cycle, 2004. **3**(2): p. 164-167.

23. Sterling D, Alvarez V, and J. Casey, *The extracellular component of a transport metabolon.* The Journal of Biological Chemistry, 2002. **277**(28): p. 25239-25246.

24. Smith, K. and C. Ingram-Smith, *Methanosaeta, the forgotten methanogen?* TRENDS in Microbiology, 2007. **30**(10).

25. Pavia, S., et al., *Ady2p is essential for the acetate permease activity in the yeast Saccharomyces cerevisiae.* Yeast, 2004. **21**(3): p. 201-210.

26. Kumar, S., T. Tamura, and M. Nei, *MEGA3: Integrated software for Molecular Evolutionary Genetics Analysis and sequence alignment.* Briefings in Bioinformatics, 2004. **5**: p. 150-163.

Chapter 5

Discussion and Conclusions

5.1 Summary of study

Carbonic anhydrases (CAs) are excellent examples of convergent evolution of catalytic function. Since the discovery of the first CA, the majority of biochemical and kinetic investigation has been conducted on the α-class. The CA field is only recently beginning to understand the characteristics of the relatively newly identified CA classes (β, γ, δ, and ζ). As a result, the importance of these CA classes in biology still remains unclear, although the broad distribution of CAs in Nature comments to their importance.

The general understanding of the γ-class is in its infancy. Only the prototypic member, Cam, has been characterized [1-5]. Until now, no other γ-class CA had been confirmed although many putative homologs were identified by [6-8]. One of the major findings of this thesis is the documentation of the second characterized γ-class CA, CamH. The characterization of CamH begins to contribute to a general understanding of the γ-class CAs which previously was not possible. In addition, for the first time, this thesis shows Cam plays an important role for in aceticlastic methanogenesis. This thesis further proposes γ-CAs, Cam and CamH, may play a key role in acetate uptake during aceticlastic methanogenesis, thus, increasing the awareness physiological processes that involve CAs.

5.2 A Catalytic Hydrogen Bond Network may be Universal in CAs

Although, the α-, β-, and γ- CA, Cam, differ in overall structure and active site architecture, these three classes were shown to participate in the same two-step ping-pong mechanism. However, the lack of homology amongst the active sites of these three independently evolved classes inferred that differences existed in their respective catalytic mechanisms. Chapter 2 presents the kinetic analysis of three Cam active site residues that were proposed to play a role in catalysis. Two residues, Gln75 and Asn202 were shown to be essential while the third, Asn 73, appeared to enhance the catalytic efficiency of Cam [9]. Further a catalytic mechanism was proposed using these kinetic analyses [9] and previous structural analyses [10, 11] suggesting roles for Gln75, Asn73, Asn202, and Glu62. Indeed, the catalytic mechanism of Cam differs from proposed catalytic mechanisms of the α- and β-class CAs; however, the catalytic roles of the Cam residues seem to provide the same function as in the other CA classes [9, 12, 13].

Cam residue Gln75 and Asn73 were proposed to act in a hydrogen bond network analogously as α-class residues Thr199 and Glu106. Superimposition of the α-class HCAII active site onto the Cam active site showed that the metal ligands and the bidentate-bound HCO_3^- overlap while the O (ε) atom of Gln75 and the hydroxyl of Thr199 are similarly situated relative to the respective metal-bound HCO_3^-, providing support to the hydrogen bond theory. Now, evidence exists of showing support for an essential hydrogen bond network that in the α-, β-, and, γ-class CAs [9, 13-16] suggesting that although the active sites may differ, similarities do exist in the catalytic mechanism of the independently evolved CA classes.

5.3 CamH is a γ-class CA Isozyme

Until now, no putative γ-class CA homolog was shown to possess CA activity. Chapter 3 presents the first biochemical and kinetic data of an archaeal γ-class isozyme (CamH) with detectable CA activity. Preliminary data suggest CamH has properties significantly different from Cam, which can be used to direct future work as a valuable comparative tool towards understanding the biochemistry and physiology of the γ-class while also contributing to the general understanding of CAs as a whole. There were kinetic differences between CamH and Cam suggesting that catalytic mechanism may also differ between the two enzymes. However, much like Cam, CamH was shown to possess higher CA activity when anaerobically assayed with iron associated with CamH which is consistent with iron as the physiological relevant metal. Therefore the preference for iron may be a general characteristic of the γ-class CAs. The lack of CA activity for other putative γ-class CAs may be the result of exposure the preferred metal to oxidizing conditions, thus inactivating that homolog in the process.

5.4 Two γ-class CAs may Contribute to Acetate Uptake during Aceticlastic Methanogenesis

CAs were first implicated to play a part in aceticlastic methanogenesis when CA activity was detected from the cell lysate of methanogens grown on acetate. In fact, Cam, the prototypic γ-class CA, was originally isolated from *Methanosarcina thermophila* cultures grown on acetate [2]. Proteomic and microarray analysis also showed Cam up-regulated during growth on acetate in *M. acetivorans*, a close relative to *M. thermophila*

[17]. A Δ*cam* knockout strain of *M. acetivorans* exhibited impaired growth further supporting that Cam plays an important role in acetate metabolism. Initially, Cam was proposed to remove the CO_2 by-product during aceticlastic methanogenesis to increase the thermodynamics of the overall reaction. However, with quantitative RT-PCR revealed that both γ-class isozymes, Cam and CamH, are up-regulated during acetate growth in *M. acetivorans* cultures in Chapter 4. The presence of both γ-class CAs during growth on acetate provides support for the proposal that these γ-class CAs participate in concert with an anion antiporter to facilitate the acetate uptake. The presence of homologs of both Cam and CamH in other methanogens capable of aceticlastic methanogenesis is consistent with this proposal.

5.5 Future Directions

The work presented in this thesis substantial increases the overall understanding of γ-class CAs, in particular that of the archaeal CAs. Nonetheless, much remains to be understood about the apparent differences of CamH and Cam as well as whether these differences and similarities are specific to the γ-class CAs or can be applied to CA classes in the *Archaea, Bacteria* or *Eukarya* domains. First, the γ-class homologs that have been previously purified and assayed need to be reinvestigated to determine if γ-class CAs are Fe-enzymes. The extent of Fe preference most likely varies between putative γ-class isozymes. If these homologs still posses no CA activity after thorough investigation of their metal preference, these homologs may represent the first examples of γ-class CA-

RPs. The presence of CA-RPs in both the α- and γ-class suggests that these CA look-a-likes may be essential in life. Therefore, the role of CA-RPs will need to be further explored.

Although CamH is a γ-class isozyme, CamH possess many different properties than previously observed for the prototypic γ-CA, Cam. These differences may indicate that the catalytic mechanism differs between these two γ-class CAs. One of the more interesting differences is the presence of six cysteines in CamH that are distinct from the one cysteine identified in Cam. The presence of these cysteines poses many questions such as: what roles do these cysteines play in catalysis in CamH? Are these cysteines involved in protein-protein interactions? Is CamH post-translationally modified *via* one or more of these cysteines? And do any of these cysteines influence what metal cofactor is preferred in the active site of CamH?

The CamH amino acid sequence does not readily identify a PSR that may play a key role in catalysis. Lack of a PSR generally results in the low turnover number similar to the observed k_{cat} of CamH. Although CamH does not possess an inherent PSR, an accessory protein present *in vivo* may associate with CamH in order to enhance the turnover number. In α-class CAs, a small accessory protein have been shown to enhance k_{cat}, setting precedence for such an occurrence [18].

From a global perspective, Cam and CamH may play a significant role in acetate uptake. Chapter 4 provides data demonstrating both γ-class CAs are up-regulated during aceticlastic methanogenesis as well as Cam is important for growth on acetate in *M. acetivorans*. Homologs of these γ-class CAs are found distributed in those methanogens

that are capable of aceticlastic methanogenesis. Also found equally distributed are homologs to the characterized acetate transporter, Ady2p, from *Saccharomyces cerevisiae* [19]. The method of acetate uptake has largely remained unknown. Characterizing the Ady2 homolog in *M. acetivorans* as well as creating a double knockout of Cam and CamH may begin to finally shed light on this question.

5.6 References

1. Alber, B.E., et al., *Kinetic and spectroscopic characterization of the γ-class carbonic anhydrase from the methanoarchaeon Methanosarcina thermophila.* Biochemistry, 1999. **38**(40): p. 13119-13128.
2. Alber, B.E. and J.G. Ferry, *A carbonic anhydrase from the archaeon Methanosarcina thermophila.* Proceedings of the National Academy of Sciences, 1994. **91**(15): p. 6909-6913.
3. Alber, B.E. and J. G. Ferry, *Characterization of heterologously produced carbonic anhydrase from Methanosarcina thermophila.* Journal of Bacteriology, 1996. **178**(11): p. 3270-3274.
4. Tripp, B.C. and J.G. Ferry, *A structure-function study of a proton transport pathway in the gamma-class carbonic anhydrase from Methanosarcina thermophila.* Biochemistry, 2000. **39**(31): p. 9232-9240.
5. Tripp, B.C., C. Tu, and J.G. Ferry, *Role of Arginine 59 in the γ-Class Carbonic Anhydrase.* Biochemistry, 2002. **41**: p. 669-678.

6. Parisi, G., M. Fornasari, and J. Echave, *Evolutionary Analysis of γ-Carbonic Anhydrase and Structurally Related Proteins.* Molecular Phylogenetics and Evolution, 2000. **14**(3): p. 323-334.

7. Smith, K.S., et al., *Carbonic anhydrases is an ancient enzyme widespread in prokaryotes.* Proceedings of the National Academy of Sciences, 1999. **96**(26): p. 15184-15189.

8. Tripp, B., K. Smith, and J.G. Ferry, *Carbonic anhydrase: New insights for an ancient enzyme.* The Journal of Biological Chemistry, 2001. **276**(52): p. 48615-48618.

9. Zimmerman, S.A. and J.G. Ferry, *Proposal for a Hydrogen Bond Network in the Active Site of the Prototypic Gamma-Class Carbonic Anhydrase.* Biochemistry, 2006. **45**(16): p. 5149-57.

10. Iverson, T., et al., *A closer look at the active site of γ-class carbonic anhydrases: High-Resolution crystallographic studies of the carbonic anhydrase from Methanosarcina thermophila.* Biochemistry, 2000. **39**: p. 9222-9231.

11. Kisker, C., et al., *A left-handed beta-helix revealed by the crystal structure of a carbonic anhydrase from the archaeon Methanosarcina thermophila.* EMBO Journal, 1996. **15**(10): p. 2323-2330.

12. Liang, Z.W., et al., *Importance of the Conserved Active-Site Residues Tyr7, Glu106 and Thr199 for the Catalytic Function of Human Carbonic Anhydrase II.* European Journal of Biochemistry, 1993. **211**(3): p. 821-827.

13. Rowlett, R.S., et al., *Examination of the role of Gln-158 in the mechanism of CO_2 hydration catalyzed by β-carbonic anhydrase from Arabidopsis thaliana.* Archives of biochemistry and biophysics, 2004. **425**(1): p. 25-32.

14. Alvarez-Santos, S., A. Gonzalez-Lafont, and J.M. Lluch, *Effect of the hydrogen bond network in carbonic anhydrase II zinc binding site. A theoretical study.* Canadian Journal of Chemistry-Revue Canadienne De Chimie, 1998. **76**(7): p. 1027-1032.

15. Kiefer, L.L., S.A. Paterno, and C.A. Fierke, *Hydrogen-Bond Network In The Metal-Binding Site Of Carbonic Anhydrase Enhances Zinc Affinity And Catalytic Efficiency.* Biochemistry, 1995. **117**(26): p. 6831-6837.

16. Thoms, S., *Hydrogen bonds and the catalytic mechanism of human carbonic anhydrase II.* Journal of Theoretical Biology, 2002. **215**(4): p. 399-404.

17. Li, L., et al., *Quantitative proteomic and microarray analysis of the archaeon Methanosarcina acetivorans grown with acetate versus methanol.* Journal of Proteome Research, 2007. **2**: p. 759-71.

18. Husic, H.D., S. Hsieh, and A.L. Berrier, *Effect of dithiothreitol on the catalytic activity, quaternary structure and sulfonamide-binding properties of an extracellular carbonic anhydrase from Chlamydomonas reinhardtii.* Biochimica et biophysica acta, 1991. **1078**(1): p. 35-42.

19. Pavia, S., et al., *Ady2p is essential for the acetate permease activity in the yeast Saccharomyces cerevisiae.* Yeast, 2004. **21**(3): p. 201-210.

Appendix A

Derivation of kinetic parameters of carbonic anhydrases

A.1 CO_2 Catalysis by Carbonic Anhydrases

Carbonic anhydrases (CA) catalyze the reversible hydration of CO_2 to HCO_3^- [1, 2]. Subsequently, it was discovered [3-7] that CAs employ a two-step ping-pong mechanism. The first step describes the nucleophilic attack of the catalytic moiety, the metal-bound hydroxide, on the incoming CO_2 resulting in a metal bound HCO_3^-, which is displace from the active site by H_2O [4, 8, 9]. This step is commonly referred to as CO_2 hydration. The second step describes the regeneration of the metal-bound hydroxide by transferring a proton from the metal bound H_2O molecule to a buffer molecule[5-7]. In fact, this step is the rate-limiting step and is simply referred to as proton transfer. The CA mechanism was first realized through chemical equilibrium studies with α-class CA isozymes I, II, and some extent with III [3-8, 10-17]. It was latter found that the kinetic parameters determined with these techniques were consistent with kinetic parameters obtained by steady-state experiments determined by stopped-flow spectroscopy [9, 15]. This correlation has been shown to extend to other α-class isozymes and CAs from the other independently evolved CA classes [18-20]. Empirical data has determined that CO_2 hydration is reflected by k_{cat}/K_m and proton transfer, since it is the rate-limiting step in CO_2 catalysis is described by k_{cat}. The evidence for which is discussed below.

A.1.1 The Kinetic Mechanism of Carbonic Anhydrases

Chemical equilibrium studies using ^{18}O exchange were instrumental in investigating the two half reactions of the reversible hydration of CO_2 to HCO_3^- [6]. Using this technique, the CO_2 hydration step, or the interconversion of CO_2 to HCO_3, was able to be examined separately from the second step, the transfer of a proton from the metal bound hydroxide to a buffer molecule (proton transfer) in the absence and presence of buffers unlike the steady-state experiments which require the presence of buffer and a pH-indicator dye.

$$CO^{18}O + H_2O \longrightarrow HCOO^{18}O^- + H^+ \longrightarrow COO + H_2{}^{18}O \qquad \text{(Equation 1.1)}$$

$$\begin{aligned} HCOO^{18}O + EOH_2 &\longrightarrow E^{18}OH + CO_2 + H_2O \\ E^{18}OH + {}^{13}CO_2 + H_2O &\longrightarrow EOH_2 + H^{13}COO^{18}O^- \end{aligned} \qquad \text{(Equation 1.2)}$$

The rate constants for two types of ^{18}O exchange are monitored (Eq. **1.1** and Eq. **1.2**). The first type is the exchange of ^{18}O between CO_2 and H_2O due to the cycle of reversible hydration while at chemical equilibrium (Eq. **1.1**). The first order rate constant θ reflects the rate of decrease of ^{18}O in CO_2 resulting in the appearance of ^{18}O in the H_2O. The second type of monitors the exchange of ^{18}O between CO_2 and $^{13}CO_2$ as a result of a transiently labeled active site, which can be described by the first order rate constant ϕ (Eq. **1.2**). Using these rate constants θ and ϕ, two rates, $R_1$and R_{H2O}, are calculated that are consistent with the steady state parameters k_{cat}/K_m and k_{cat}. The rate, R_1, represents the catalyzed rate of exchange of CO_2 and HCO_3^- at chemical equilibrium. The rate R_1 is proportional to $k_{cat}^{(exch)}/K_{eff}^{(CO2)}$ in which $k_{cat}^{(exch)}$ is the maximal rate constant at

equilibrium and $K_{eff}^{(CO2)}$ is the apparent binding constant for the substrate. Although the individual rate constants in $k_{cat}^{(exch)}/K_{eff}^{(CO2)}$ have different meanings than the steady-state parameters, k_{cat} and K_m, the subsequent second-order rate constants, k_{cat}/K_m and $k_{cat}^{(exch)}/K_{eff}^{(CO2)}$ are comparable [15, 21].

The second rate, R_{H2O}, describes the rate of release from the enzyme of water bearing the labeled oxygen substrate. The release of labeled water from the active site involves a proton transfer from the proton transfer group to the labeled active site. This proton transfer is rate-limiting; thus, R_{H2O} can be described as k_{cat}. Varying the buffer concentration did not affect R_1 whereas R_{H2O} proportionally increased with increasing concentration of buffer until buffer was in sufficient excess. Although, solvent hydrogen isotope effects (SHIE) were not observed with R_1, strong SHIE were observed on R_{H2O} even in excess buffer conditions. These SHIE provided direct evidence that a rate-limiting proton transfer event was involved those kinetic steps involving the release of H_2O from the active site but not during the interconversion of CO_2 to HCO_3^-.

Scheme 1 outlines the kinetic mechanism of CAs (Figure **1.1**). The reversible hydration of CO_2 to HCO_3^- is shown in Steps 1-3 (Figure **1.1**). Intermolecular proton transfer is portrayed in Step 5 while intramolecular proton transfer is shown in Step 4. The interconversion of CO_2 to HCO_3^- occurs in Step 2 which involves the catalytic metal bound hydroxide or water depending on the direction of the catalyzed reaction. At chemical equilibrium, the rate of exchange between CO_2 and HCO_3^- could be limited by any one of the rate constants k_{-1}, k_{+2}, k_{-2}, and k_{+3}. At high buffer concentrations, the maximal rate of CO_2 hydration during steady-state conditions may be limited by k_{+2}, k_{+3}

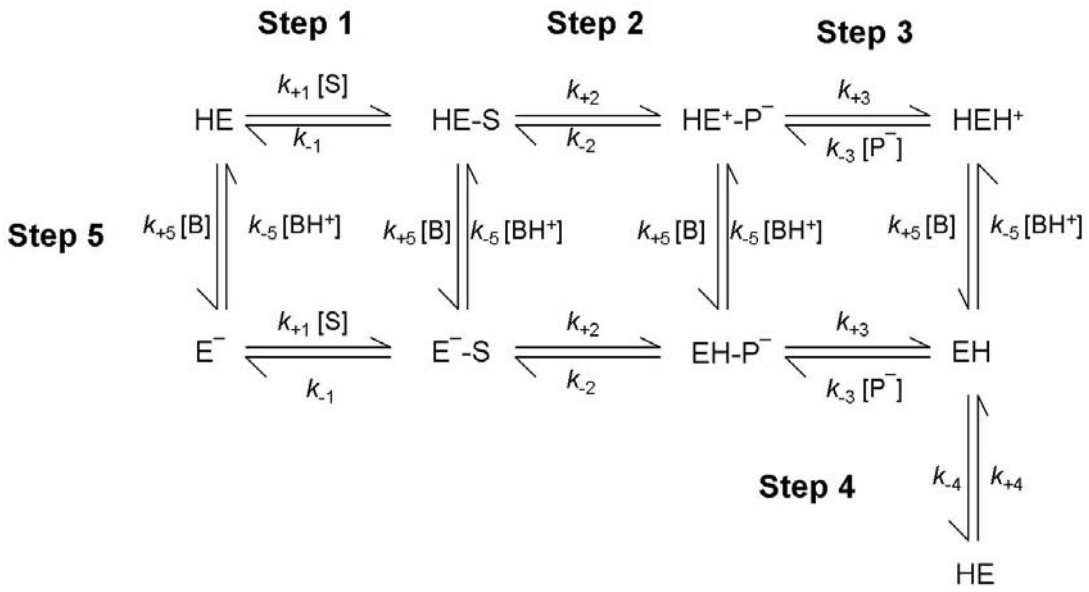

Figure 1.1**: General kinetic mechanism of Carbonic Anhydrase.**

HE refers to a protonated proton transfer group (i.e. the proton shuttle residue) while EH refers to the catalytic form of the enzyme (i.e. M-OH$^-$). S refers to CO_2 and P refers to HCO_3^-. The interconversion of CO_2 to HCO_3^- is described in STEP 1-3. *Intermolecular* proton transfer is described by STEP 5 and *intramolecular* proton transfer is described by STEP 4. STEP 5 is rate-limiting at low buffer concentrations. Recreated from [9].

or k_{+4}. The maximal velocity of the dehydration of HCO_3^- during steady-state conditions, conversely, may be limited by k_{-2}, k_{-3}, or k_{-4}. Empirical data obtained for $k_{cat}^{(exch)}$ at chemical equilibrium is greater than the steady-state determined k_{cat} for either direction of catalysis determined under steady state conditions lending evidence that the rate-limiting rate constant describes a step outside those steps involved in CO_2 hydration (Figure **1.1**). Observed isotope effects seen on steady-state parameters must also affect steps outside the exchange of CO_2 and HCO_3^- seen during chemical equilibrium. In addition the absence of a SHIE on $k_{cat}^{(exch)}$ suggests that a proton transfer step is not involved during the CO_2-HCO_3^- interconversion. There was also no effect observed on $k_{cat}^{(exch)}$ in the absence or presence of buffer. However, a strong affect is observed on k_{cat} during steady-

state conditions. Therefore, it seems that the buffer depenndent step(s) are occur outside the pathway of CO_2-HCO_3 exchange. Also, k_{cat} must include all rate constants during the CO_2 hydration step and the proton transfer step.

A.1.2 Rate Constants and Rate Equations for Chemical Equilibrium and Steady State

The corresponding rate constants and rate equations for the ^{18}O exchange between CO_2 and HCO_3^- and for CO_2 catalysis during steady-state conditions are provided in this section. Also provided is the comparison of kinetic parameters obtained by ^{18}O exchange experiments at chemical equilibrium with those obtained by stopped-flow spectroscopy at steady-state. Only the constants for the hydration of CO_2 to HCO_3^- are shown. The rate constant, K_{E1}, represents the acid dissociation constant for the catalytic group (EH, Figure **1.1**) whereas the rate constant, K_{E2}, is the acid dissociation constant for the proton transfer group (HE, Figure **1.1).**

R_1 represents the rate of interconversion between CO_2 and HCO_3^- at chemical equilibrium. Only the rate constants in Step1-3 are involved because it was empirically determined that the exchange of ^{18}O between CO_2 and HCO_3^- was not dependent on buffer (omit Step 5) and no SHIE was observed (omit Step 4) (Figure **1.1).** The steady-state rate, ν_{ss}, is a dependent on buffer and a proton transfer event. However, at high buffer concentrations the rate constants in Step 5 can be omitted, which simplifies the rate equations (Eq. **1.4).** The rate constant in Step 4 cancels out in k_{cat}/K_m during steady-

state conditions and Step 5 becomes inconsequential at high buffer conditions (Eq. **1.5**). Notice that $k_{cat}^{(exch)}/K_{eff}^{(S)}$ (Eq. **1.3**) is comparable (Eq. **1.45**) to the steady-state (Eq. **1.4**) parameter k_{cat}/K_m at high buffer concentrations.

$$\frac{R_1}{[E_t]} = \frac{\upsilon_{exch}}{[E_t]} = \frac{k_{cat}^{(exch)}[S]}{K_{eff}^{(S)} + [S]} = \frac{k_{cat}^{(exch)}[P^-]}{K_{eff}^{(P)} + [P^-]}$$

$$k_{cat}^{(exch)} = \frac{k_{-1}k_{-2}k_{+2}k_{+3}}{(k_{+1}k_{-2} + k_{-1}k_{+3} + k_{+2}k_{+3})(k_{+2} + k_{-2})} \qquad \text{(Equation 1.3)}$$

$$K_{eff}^{(S)} = \frac{k_{-1}k_{-2}(1 + [H^+]/K_{E1})}{(k_{+1}(k_{+2} + k_{-2})}$$

$$\frac{\upsilon_{ss}}{[E_t]} = \frac{k_{cat}^{(S)}/K_m^{(S)}[S] - (k_{cat}^{(P)}/K_m^{(P)})[P]}{1 + [S]/K_m^{(S)} + [P]/K_m^{(P)} + [S][P]/K_{sp}}$$

$$k_{cat}^{(S)} = \frac{k_{+2}k_{+3}k_{+4}}{k_{+2}k_{+3}(1 + [H^+]/K_{E2}) + k_{+4}(k_{+2} + k_{-2} + k_{+3})} \qquad \text{(Equation 1.4)}$$

$$K_m^{(S)} = \frac{(1 + [H^+]/K_{E1})k_{+4}(k_{-1}k_{-2} + k_{-1}k_{+3} + k_{+2}k_{+3})}{k_{+1}\{k_{+2}k_{+3}(1 + [H^+]/K_{E2}) + k_{+4}(k_{+2} + k_{-2} + k_{+3})\}}$$

$$\frac{k_{cat}^{(S)}}{K_m^{(S)}} = \frac{k_{cat}^{(exch)}}{K_{eff}^{(S)}}$$

$$\frac{k_{cat}^{(exch)}}{K_{eff}^{(S)}} = \frac{\cancel{k_{-1}k_{-2}}k_{+2}k_{+3}}{(k_{-1}k_{-2} + k_{-1}k_{+3} + k_{+2}k_{+3})\cancel{(k_{+2} + k_{-2})}} \bullet \frac{k_{+1}\cancel{(k_{+2} + k_{-2})}}{\cancel{k_{-1}k_{-2}}(1 + [H^+]/K_{E1})} \qquad \text{(Equation 1.5)}$$

$$\frac{k_{cat}^{(S)}}{K_m^{(S)}} = \frac{k_{+2}k_{+3}\cancel{k_{+4}}}{\cancel{(k_{+2}k_{+3}(1 + [H^+]/K_{E2} + k_{+4}(k_{+2} + k_{-2} + k_{+3})}} \bullet \frac{k_{+1}\cancel{[k_{+2}k_{+3}(1 + [H^+]/K_{E2}) + k_{+4}(k_{+2} + k_{-2} + k_{+3}}}{(1 + [H^+]/K_{E1})\cancel{k_{+4}}(k_{-1}k_{-2} + k_{-1}k_{+3} + k_{+2}k_{+3})}$$

A.2 Reference

1. Meldrum, N.N. and F.J.W. Roughton, *Carbonic anhydrase. Its preparation and properties.* Journal of Physiology, 1933. **80**: p. 113-141.
2. Stadie, W.C. and H. O'Brien, *The Catalysis of the Hydration of Carbon Dioxide and Dehydration of Carbonic Acid by an Enzyme Isolated from Red Blood Cells.* Journal of Biological Chemistry, 1933. **103**(2): p. 521-529.
3. Lindskog, S., *Structure and mechanism of carbonic anhydrase.* Pharmacol. Ther, 1997. **74**(1): p. 1-20.
4. Lindskog, S. and J.E. Coleman, *The Catalytic Mechanism of Carbonic Anhydrase.* Proceedings of the National Academy of Sciences, 1973. **70**(9): p. 2505-2508.
5. Silverman D. N. and S.H. Vincent, *Proton transfer in the catalytic mechanism of carbonic anhydrase.* CRC Crit. Rev. Biochem, 1984. **14**: p. 207-255.
6. Silverman, D.N., *Carbonic Anhydrase: Oxygen-18 Exchange Catalyzed by an Enzyme with Rate-Contributing Proton-Transfer Steps.* Methods in Enzymology, 1982. **87**: p. 732-753.
7. Silverman, D.N. and S. Lindskog, *The Catalytic Mechanism Of Carbonic Anhydrase. Implications Of A Rate-Limiting Proteolysis Of Water.* Accounts of Chemical Research, 1988. **21**(1): p. 30-36.
8. Lindskog, S. and A. Liljas, *Carbonic Anhydrase and the Role of Orientation in Catalysis.* Current Opinion in Structural Biology, 1993. **3**(6): p. 915-920.

9. Simonsson, I., B. Jonsson, and S. Lindskog, *A ^{13}C Nuclear-Magnetic-Resonance Study of CO_2-HCO_3^- Exchange Catalyzed by Human Carbonic Anhydrase C at Chemical Equilibrium.* European Journal of Biochemistry, 1979. **93**: p. 409-417.

10. Alber, B.E., et al., *Kinetic and spectroscopic characterization of the γ-class carbonic anhydrase from the methanoarchaeon Methanosarcina thermophila.* Biochemistry, 1999. **38**(40): p. 13119-13128.

11. Carter, N., et al., *Characterization of human carbonic anhydrase III from skeletal muscle.* Biochemical Genetics, 1979. **17**(9-10): p. 837-854.

12. Fisher, Z., et al., *Structural and kinetic characterization of active-site histidine as a proton shuttle in catalysis by human carbonic anhydrase II.* Biochemistry, 2005. **44**(4): p. 1097-105.

13. Jewell, D.A., et al., *Enhancement of the catalytic properties of human carbonic anhydrase III by site-directed mutagenesis.* Biochemistry, 1991. **30**(6): p. 1484-1490.

14. Johansson, I. and C. Forsman, *Kinetic studies of pea carbonic anhydrase.* European Journal of Biochemistry, 1993. **218**: p. 439-446.

15. Khalifah, R.G., *The carbon dioxide hydration activity of carbonic anhydrase I. Stop-flow kinetic studies on the native human isoenzymes B and C.* Journal of Biological Chemistry, 1971. **246**(8): p. 2561-2573.

16. Lipton, A.S., R.W. Heck, and P.D. Ellis, *Zinc solid-state NMR spectroscopy of human carbonic anhydrase: Implications for the enzymatic mechanism.* Journal of the American Chemical Society, 2004. **126**(14): p. 4735-4739.

17. Ren, X.L. and S. Lindskog, *Buffer Dependence Of CO_2 Hydration Catalyzed By Human Carbonic Anhydrase I.* Biochimica et biophysica acta, 1992. **1120**(1): p. 81-86.

18. Smith, K.S., et al., *Carbonic anhydrases is an ancient enzyme widespread in prokaryotes.* Proceedings of the National Academy of Sciences, 1999. **96**(26): p. 15184-15189.

19. Tripp, B., K. Smith, and J.G. Ferry, *Carbonic anhydrase: New insights for an ancient enzyme.* The Journal of Biological Chemistry, 2001. **276**(52): p. 48615-48618.

20. Zimmerman, S., J. Ferry, and C. Supuran, *Inhibition of the archaeal beta-class (Cab) and gamma-class (Cam) carbonic anhydrases.* Current Topics in Medicinal Chemistry, 2007. **7**(9): p. 901-908.

21. Darvey, I., Journal of theoretical Biology, 1973. **41**: p. 441-450.

CURRICULUM VITA

July 2, 2007

Sabrina Anastasia Zimmerman

Education

2001-Present Ph.D., BMMB, Pennsylvania State University, University Park, PA

1999-2001 B.S *cum laude* University of Alaska-Fairbanks, Fairbanks, AK

1996-1999 Major in Microbiology Northern Arizona University, Flagstaff, AZ

1996 High School Graduation Tempe High School, Tempe, AZ

Honors Awards

2006-2007 The Thomas H. Maren Foundation Grant

2005-2006 Stanley Person Graduate Fellowship

2004-2005 NACME Alfred P. Sloan Fellowship

2002 Paul M. Althouse Teaching Assistant Award

Publications

Zimmerman, SA, Ferry JG, Supuran CT. 2007. Inhibition of the Archaeal β (Cab) and γ-Class (Cam) Carbonic Anhydrases. *Current Topics in Medicinal Chemistry* 7(9):901-8

Zimmerman SA, Ferry JG. 2006. Proposal for a Hydrogen Bond Network in the Active Site of the Prototypic Gamma-Class Carbonic Anhydrase. Biochemistry, 45: 5149-57

Zimmerman S, *Innocent A, Casini A, Ferry JG, Scozzafava A, Supuran CT.* 2004. Carbonic anhydrase inhibitors. Inhibition of the prokaryotic beta and gamma-class enzymes from Archaea with sulfonamides. *Bioorganic & medicinal chemistry letters* 24: 6001-6

Innocenti A. ***Zimmerman S****, Ferry JG, Scozzafava A, Supuran CT. 2004.* Carbonic anhydrase inhibitors. Inhibition of the beta-class enzyme from the methanoarchaeon *Methanobacterium thermoautotrophicum* (Cab) with anions. *Bioorganic & medicinal chemistry letters* 17: 4563-7

Innocenti A, ***Zimmerman S****, Ferry JG, Scozzafava A, Supuran CT.* 2004. Carbonic anhydrase inhibitors. Inhibition of the zinc and cobalt gamma-class enzyme from the archaeon *Methanosarcina thermophila* with anions. *Bioorganic & medicinal chemistry letters* 12: 3327-31

Parisi G, Perales M, Fornasari MS, Colaneri A, Gonzales-Schain N,Gomez-Casati D, ***Zimmerman S****, Brennicke A, Araya A, Ferry JG, Echave J, Zabaleta E.* 2004. Gamma carbonic anhydrases in plant mitochondria. *Plant molecular biology* 2: 193-2